Internal dynamics of a medium-sized subarctic lake: field measurements and numerical modeling

Morgane Priet-Mahéo

Faculty of Civil and Environmental Engineering
University of Iceland
2019

Internal dynamics of a medium-sized subarctic lake: field measurements and numerical modeling

Morgane Priet-Mahéo

Dissertation submitted in partial fulfillment of a
Philosophiae Doctor degree in Environmental Studies

Advisor
Hrund Ólöf Andradóttir

PhD Committee
Francisco Rueda Valdivia
Sigurður Magnús Garðarsson
Jón Ólafsson

Opponents
Ben R. Hodges
David C. Finger

Faculty of Civil and Environmental Engineering
School of Engineering and Natural Sciences
University of Iceland
Reykjavik, September 2019

Internal dynamics of a medium-sized subarctic lake: field measurements and numerical modeling

Dissertation submitted in partial fulfillment of a *Philosophiae Doctor* degree in Environmental Studies

Copyright © Morgane Priet-Mahéo 2019
All rights reserved

Faculty of Civil and Environmental Engineering
School of Engineering and Natural Sciences
University of Iceland
VRII, Hjardarhagi 2-6
107, Reykjavik
Iceland

Telephone: 525-4000

Bibliographic information:
Morgane Priet-Mahéo, 2019, *Internal dynamics of a medium-sized subarctic lake: field measurements and numerical modeling*, PhD dissertation, Faculty of Civil and Environmental Engineering, University of Iceland, 145 pp.

ISBN 978-9935-9473-6-9

Printing: Háskólaprent
Reykjavik, Iceland, September 2019

Abstract

As the Arctic Circle opens up due to the effects of global warming, the surrounding regions, and in particular the subarctic zone, experience both climatic and societal changes, which makes it imperative to understand the existing ecosystems. Lake Lagarfljót, an Icelandic fjord lake with glacial inflow, is used to evaluate processes occurring in weakly stratified water bodies in the sub-Arctic. Field observations during the summers of 2010 and 2011 show that the lake experiences a short period of stratification, with overturning occurring when the heat fluxes become negative. The internal-wave regime evolves rapidly as the stratification strengthens, higher vertical modes and Kelvin waves are identified. Glacial inflow to Lake Lagarfljót delivers large volumes of fine sediment. It is expected that most of the sediments remain in suspension and this can alter the density of the water-column, resulting in inverse thermal gradients. Additionally, the glacial river is deflected to the eastern edge of the lake by Coriolis forces, causing the inflow to remain in shallow water before entering the center of the lake. Results from the Münnich model demonstrate that the natural oscillation of the lake basin is close to the oscillation period of the wind. The 3D hydrodynamic model Si3D was adapted to account for suspended sediment, and it successfully reproduced the motions observed in the lake, showing its utility for the study of weakly stratified lakes. Results suggest that wind is the main driver of internal waves in Lake Lagarfljót, but that the river influences stratification, meaning that it cannot be ignored when considering lake circulation. The model confirms the presence of Kelvin waves in the basin. Tracking the pathways of the inflowing glacial water, it appears that the initial intrusion depth is dependent on internal waves. During summertime stratification, the river penetrates the lake as interflows or underflows. Underflows can become trapped, causing them to oscillate and becoming flushed episodically when large glacial discharges enter the lake as underflow. Water entering the lake as interflow mixes more easily and it is flushed quasi-continuously out of the basin. Because the circulation of Lake Lagarfljót is sensitive to the strength of the stratification, the internal dynamics of the lake are expected to change significantly in a warming climate.

Útdráttur

Hlýnun jarðar hefur mikil áhrif á Norðurskautssvæðinu og þar eru að opnast nýir möguleikar til samgangna og annarra athafna. Hlýnuninni fylgja miklar veðurfars- og samfélagsbreytingar á aðliggjandi svæðum, einkanlega í kaldtempraða beltinu. Áríðandi er að auka skilning á ýmsum vistkerfum á þessu belti og viðbrögðum þeirra við hlýrra loftslagi. Í ritgerð þessari er gerð grein fyrir rannsókn á lagskiptingu í stöðuvatninu Leginum, sem er jökulmyndað vatn efst í Lagarfljóti á Héraði. Vettvangsrannsóknir sem gerðar voru á Leginum sumurin 2010 og 2011 sýna skammæja lagskiptingu sem hverfur þegar hitaflæði verður neikvætt. Innri bylgjukerfi í vatnsbolnum þróast hratt þegar lagskipting styrkist, lóðrétt streymi eykst og Kelvin bylgjur eru sjáanlegar. Jökulsá í Fljótsdal ber með sér mikið magn fíngerðra setagna í Löginn. Viðbúið er að mest af setögnunum haldist í sviflausn og getur það breytt eðlisþyngd vatnssúlunnar, sem veldur viðsnúnum hitastigli. Þar að auki sveigist straumur jökulvatns að eystri bakka Lagarins vegna Coriolis kraftsins og helst því lengur á grynningum en ella áður en það rennur út á mitt stöðuvatnið. Niðurstöður úr Münnich líkaninu sýna að náttúrulegar sveiflur í vatninu eru nálægt sveiflutíma vinds. Þrívíða straumfræðilega reiknilíkanið Si3D var aðlagað til að taka tillit til svifagna. Líkanið endurspeglar innri hreyfingar sem mælast í vatninu og sýnir rannsóknin því fram á nytsemi þessa líkans við greiningu veikrar lagskiptingar í stöðuvötnum. Niðurstöður benda til þess að vindur sé helsti drifkraftur innri bylgjuhreyfinga Lagarins. Áhrif innstreymis Jökulsár á hringrásina í vatninu og þar með á lagskiptinguna eru einnig veruleg. Líkanið staðfestir tilvist Kelvin bylgna í vatninu. Þegar fylgst er með hvernig Jökulsá í Fljótsdal blandast við vatnið virðist innstreymisdýptin í vatnsbolnum vera háð innri bylgjuhreyfingum hans. Við þá lagskiptingu sem ríkir á sumrin rennur áin inn í vatnið sem innra flæði um miðbik vatnsins og eftir botninum sem undirflæði. Vatn sem rennur eftir botninum getur lokast þar af og dýpi þess sveiflast til. Innikróað vatn skolast svo út stöku sinnum þegar mikið af nýju jökulvatni rennur eftir botni vatnsins. Jökulvatn sem berst í vatnið sem innra flæði um miðbik þess blandast betur og skolast nokkuð jafnt út úr því aftur. Þar sem vatnshringrásin í Leginum er háð styrkleika lagskiptingarinnar er viðbúið að innri hrif muni breytast verulega við hækkandi vatnshita.

Dedication

À mes trois mousquetaires, Emilý Sóley, Helen Hekla and Astrid Eir.

Table of Contents

List of Figures

List of Tables

Acknowledgments

This project was initiated by Dr. Hrund Ólöf Andradóttir in 2008 and funded by the National Power Company through the Energy Research Fund. I was recruited by Dr. Andradóttir and joined the research project in spring 2010. This doctorate has been a long but fruitful learning process and I have been confronted to a whole range of challenges that have taught me new skills: from the organization of field campaigns to the use of super-computer for the running of models.

During this research, I was lucky to collaborate with great researchers, meet a lot of interesting and helpful persons and I received the support of my I would like to thank Dr. Hrund Ólöf Andradóttir for guiding me in this research. She has been a patient advisor which introduced me to physical limnology and taught me the specificity of this sphere of study, both in the books and on the field. I would also like to thank Dr. Francisco José Rueda Valdivia, member of my scientific committee which has been actively supporting me during this research. I was lucky to be welcomed in his laboratory at the Instituto Del Agua of the University of Granada at three occasions. During these visits I managed to work intensively on this research, benefiting both from his guidance and the advises of his students. I learnt a great deal about field data analysis and modeling. I would like to express my very great appreciation to from Dr. Sigurður Magnús Garðarsson and DSc. Jón Ólafsson, members of my scientific committee, for the help and advises; they have followed my work over the years and shown me support.

I would like to thank Hákon Aðalsteinsson, from the National Power Company, for his collaboration and support, allowing me to pursue the research after the funds depleted. I am particularly grateful for the assistance given by Vilhjálmur Ívar Sigurjónsson, which has kindly given me precious advises and provided me with a lot of support during the years of field campaign. Svana Hafdís Stefánsdóttir was kind to help me with laboratory work. Dr. Javier Vidal and Dr. Halldór Pálsson provided me with valuable inputs for the coding of the Münnich model. I also want to thank Óðinn Þórarinsson, Gunnar Sigurðsson at the Icelandic Meteorological Office (IMO) as well as Victor Kristinn Helgason and Egill Axelsson at the National Power Company of Iceland that assisted me with field data.

My superiors at IMO, in particular Matthew James Roberts, Jórunn Harðardóttir, Davíð Egilson, have provided me with tremendous support towards the end of this research project and helped me climb the last obstacles of this long journey; I am extremely grateful for their guidance.

My special thanks are also extended to the friends that accompanied me through this experience: my colleagues at IMO and in particular my office mates Tinna Þórarinsdóttir and Andrea-Georgio Massad, and my fellow (former) doctoral students, Warsha Singh, Astrid Lelarge, Behnood Rasti, Þorbjörg Sævarsdóttir, Marta Rós Karlsdóttir, Gunnar

Skúlason Kaldal, Lárus Þorvaldsson, Elizabeth Anne Unger and Elísabet Björney Lárusdóttir.

Finally this research project would not have been possible without the support and love of my family. Eysteinn my husband has been a constant support, helping me on the field, patiently advising me when needed and taking on him to give me time to work on the project. My children Emilý Sóley, Helen Hekla and Astrid Eir have been also very patient with their busy mum. My parents, Martine and Pierre, and siblings, Delphine and Ivan have been very supportive of my choices. My parent-in-law, Helga and Sigurður Ingi have helped me by lending me their boat for field work. Finally I would like to thank my grand parents, Gisèle, Marie-Josèphe and Ferdinand who have been an inspiration, with their thirst for knowledge and their great respect for education.

1 Introduction

Lakes around the world represent 87% of the (liquid) freshwater surface storage (Gleick, 1996) and in more recent research (Downing et al., 2006), it was estimated that more than 3% of the continental land surface was covered by water. They are nowadays an important resource for the communities living in their proximity: a source of life, recreation, transport and energy. The quality of their waters, controlled in part by the lake's hydrodynamics, can therefore have a decisive impact on the neighboring communities. Dynamic processes such as currents, mixing events and internal waves can redistribute oxygen and nutrients or, in some cases, pollutants. Physical limnologists have been working on identifying and characterizing these processes in order to assist managers in their decisions.

In the nineties, as talks about climate change intensified, it became evident that global warming was going to modify our environment and that these changes would occur with different intensities around the globe (Watson et al., 1996). The Arctic and its surroundings was pointed out as particularly vulnerable and responsive to these changes (Watson et al., 1998; Intergovernmental Panel on Climate Change, 2014) and the necessity of studying this region was emphasized in several studies (Rouse et al., 1997; Hinzman et al., 2005). In the last two decades, the Arctic has been increasingly attracting the attention of politicians and economic interests from across the world as sea ice melts and new routes open up (Larsen and Fondahl, 2015). Lakes are particularly numerous in this marginal environment, commonly resulting from glacial erosion of bedrock, the damming effect of moraines and subsidence of ground in regions of melting permafrost. Such lakes are referred to as "sentinels" of climatic change (Adrian et al., 2009; Mueller et al., 2009; Williamson et al., 2009).

This thesis investigates the internal dynamics of Lake Lagarfljót in North-east Iceland, based on a combination of field techniques and numerical models. The remainder of this chapter highlights the subarctic factors pertinent to this study, including the characteristics and sensitivity of subarctic lakes. The specific aims of the thesis are listed in section 1.3 and the overall structure of the thesis is outlined in section 1.4.

1.1 Subarctic environments

The subarctic is a sub-class of what is sometimes referred to as the arctic regions, the northern regions, the cold regions or the high-latitude regions. They are the transition zones between the Arctic and the temperate regions and are quite generally defined as the zone between 50 and 70°N latitude. The tree line is sometimes used as the limit between the Arctic and the subarctic region. Several attempts of classifications have

been made, based on the latitude, the climate and even its demography (Hamelin, 1978). The delineation of the subarctic zone changes in relation to the topics being considered; this results in several terms for the region, including sub-polar and circumpolar.

1.1.1 Climate

Climate is most often considered in order to characterize the subarctic environments. Different terms are used in the literature, including "subarctic", "boreal", "taiga" or "tundra" climate (Critchfield, 1974). Seppälä (2004) summarizes rather beautifully the climate in this transition zone by saying that it mimics the arctic climate in winter but the temperate climate in the summer.

Air temperatures and precipitation are the two main criteria used to distinguish the different variants (Kottek et al., 2006; Peel et al., 2007). However, the subarctic is a transition zone, making it difficult to delineate differences based purely on climatic factors. According to the Köppen system of climate classification (Figure 1.1), four subtypes of the humid continental climates with severe winters can be identified as subarctic (Dfc, Dwc, Dfd, Dwd). The tundra climate (ET) found among other places in Northern Iceland is categorized as a polar and alpine climate but is also sometimes classified as subarctic (Lutgens et al., 2013).

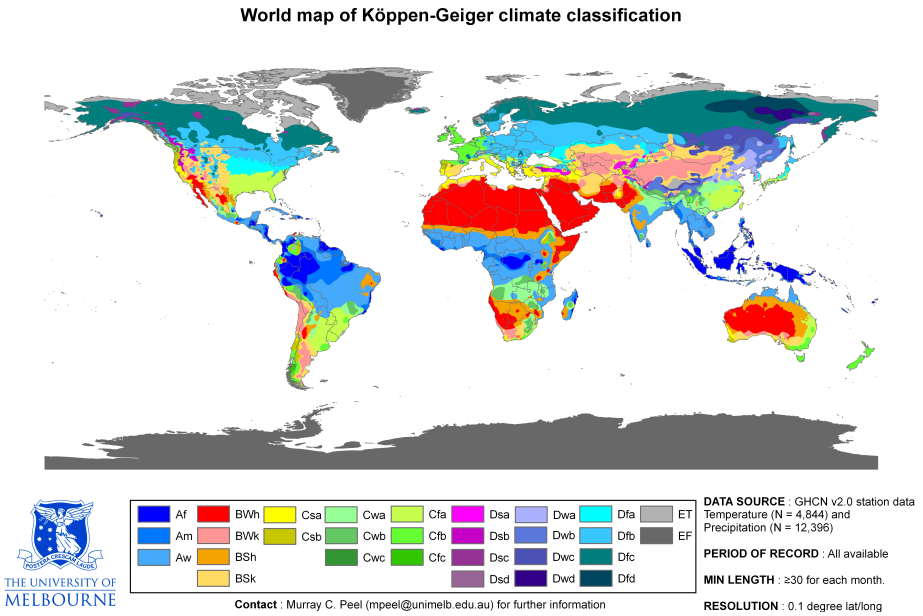

Figure 1.1. Global distribution of climate according to the Köppen-Geiger climate classification (Peel et al., 2007)

In these regions, two seasons are prominent, with short daylight periods during the long winter season and long daylight periods in the shorter summer season. Mean air temperatures are below freezing points during the coldest months and rise above

10°C no more than four months (Prowse and Ommanney, 1990). Precipitation is most important during the warm season. The annual precipitation is generally between 600 and 1200 mm (Barry and Chorley, 2009). During the cold season, precipitation occurs as snowfall and it contributes to the winter snow and ice cover. Freshwater bodies (rivers, ponds and lakes) start freezing when air temperatures drop under 0°C. The ice-cover is complete or partial according to the volume of the water body .

The weather in these regions is controlled by depressions that are weakly developed during the summer (Barry and Chorley, 2009). Winds can be very strong (Hughes and Cassano, 2015) and are considered an important ecological forcing factor (Holtmeier and Broll, 2010). Wind speeds are relatively high but the distribution is quite heterogeneous: more inland parts of this region experience lighter wind than coastal areas, Greenland experiences katabatic winds due to the presence of a large ice cap and Iceland is exposed to very strong oceanic winds associated to the oscillating Icelandic lows (Seppälä, 2004; Lutgens et al., 2013). Liu et al. (2016) find that the highest average summer wind speeds ($9.5\ \mathrm{m.s^{-1}}$) observed in the Arctic region during the last two decades are to be found in the vicinity of Iceland in the Greenland and Norwegian seas.

1.1.2 Hydrology

Lakes Glacial ice movements are one of the main contributors to the genesis of lakes in the world. In subarctic environments, glacier retreat and the melting of ice sheets are quite often relatively recent history and the resulting features are a great diversity of lakes, including : glacial ice-scour lakes, cirque lakes, paternoster lakes, fjord lakes, kettle lakes (Wetzel, 1983).

Rivers In northern regions, four regimes are often identified (Rouse et al., 1997): the arctic nival regime with the presence in areas of continuous permafrost where the main peak is associated with spring snowmelt; the subarctic nival regime where spring snowmelt dominates the signal of the river but summer runoff and precipitation can create significant peak and winter flow is apparent; the wetland regime in poorly drained catchments with high temporary storage capacities which presents attenuated peak flows but still high yields; the pro-glacial regime where the spring snowmelt peak is followed by summer peaks associated to meltwaters from upstream glaciers.

Permafrost, groundwater and wetlands In these regions, frozen ground below the surface, known as permafrost, is widespread. It can be continuous or discontinuous. The presence of permafrost results in delays of the melting of snow as heat flows from the snow to the frozen ground (Rouse et al., 1997). In addition, permafrost acts as a lid isolating deep groundwaters from the surface. Hence, when permafrosts thaws, flowpaths to deeper groundwaters are reactivated, giving rise to larger baseflows (Carey et al., 2013).

The occurrence of permafrost also controls the areal and spatial distribution of wetlands (Rouse et al., 1997) and in the subarctic region, wetland can be isolated and limited in depth by the underlying permafrost or interacting with the groundwater where the permafrost is absent (Woo and Winter, 1993).

1.2 Lakes in the subarctic zone

In their inventory of water bodies, Lehner and Döll (2004) find that the highest concentration of lakes of all size classes occurs between 50 and 70°North, in areas recently deglaciated (Figure 1.2), the largest number being located in Canada.

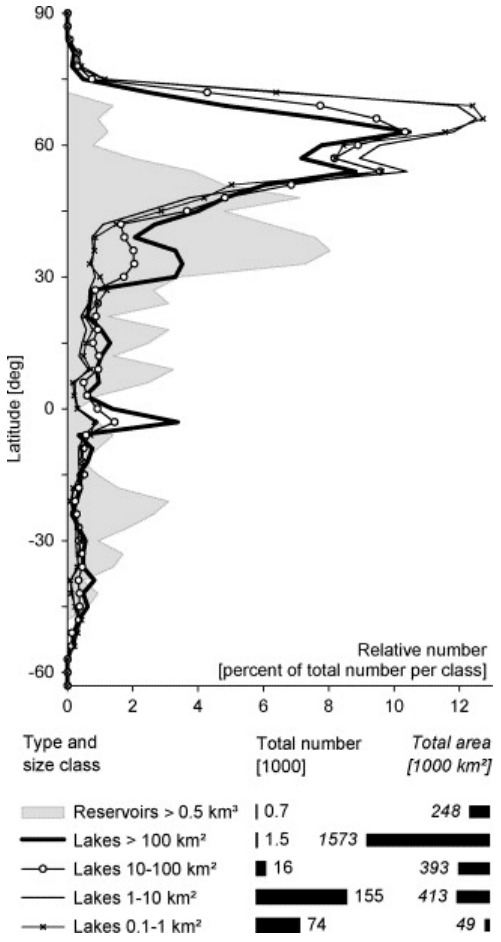

Figure 1.2. Global distribution of lakes and reservoirs across the latitudes (Lehner and Döll, 2004).

1.2.1 Characteristics of subarctic lakes

The thermal process of stratification, combined with kinetic mixing, are the key factors controlling the circulation of heat, oxygen and nutrients between the surface and deep waters. Hence, lakes are classified according to their thermal behavior, size, depth, and location (latitude, elevation). Researchers have mostly been focusing on temperate

lakes, which often show clear seasonal stratification (in summer and winter) and mixing periods (fall and spring). Lakes in the subarctic and polar regions have received much less attention to date. Yoshimura (Yoshimura, 1936) classified subpolar lakes as those with temperatures below 4°C half of the year, with a weak summer stratification. Lewis (1983) reconsidered the Hutchinson-Löffler classification (Hutchinson and Löffler, 1956) which divides the lakes into six categories : amictic, cold monomictic, dimictic, warm monomictic, oligomictic and polymictic and introduces the meromixis / holomixis dichotomy. He kept the original criteria - ice-cover, mixing and direct stratification- and added the effect of depth and fetch on mixing behavior at any latitude and altitude. Hence he divided lakes with winter ice-cover and with temperatures rising above 4°C during the summer into three categories: "Dimictic if they stratify for the whole season, discontinuous cold polymictic if they stratify for days or weeks but not the whole season, and continuous cold polymictic if they do not stratify or stratify only for hours at a time".

As mentioned earlier, lakes in temperate regions develop a thermal stratification in summer. Salinity and suspended sediments can sometimes also contribute to lake's stratification. Under stratified conditions, internal waves are developed by the action of wind. The currents associated with internal wave motions are responsible for most of the deep water movements in lakes, affecting the "vertical and horizontal transport of heat and dissolved substances" (Wetzel, 1983). In contrast, subarctic lakes have been considered to be water bodies with simple hydrodynamic behaviors, being fully mixed most of the year and only weakly stratified during the summer (Yoshimura, 1936; Touchart, 2005). Limited research has been conducted to verify these assumptions.

1.2.2 Main forcings of lakes in subarctic environments

There is a strong seasonality in the type of forcing acting on the lake. Located in high latitudes, heat fluxes are negative during the winter and positive but relatively weak during the short summer despite long hours of daylights, as solar radiation is not intense (Lutgens et al., 2013). The key input of mechanical energy during the ice-free period is the wind (MacIntyre and Melack, 2009). During this season, the strong winds are major forcing of these water bodies and the lack of vegetation increases the efficacy of the wind.

The hydrology in the subarctic environment is controlled heavily by temperatures. During the winter the water freezes, the precipitation falls as snow and the discharge of rivers reaches a low. During early summer, the snow melts leading to increased discharges; as the rain falls on still (semi-)frozen grounds, it results in a direct run-off to the river leading to spring highs. During the summer, temperature increase melts the glaciers and firn, leading to increase of discharge in dry period (no precipitation).

The ice layer forming on lakes and covering them completely or partially during the winter season prevents the wind from acting on their surface. During the ice-free season however, the strong winds are major forcing of these water bodies and the lack of vegetation increases the efficacy of the wind.

1.2.3 Vulnerability of subarctic lakes

The lack of research in polar lakes was stressed as early as 1954 by Rawson (1954), and more recently by Touchart (2005). Discontinuous field measurements interrupted by the cold season and a focus on small lakes have both led to theoretical classifications that do not describe the entire diversity of these lakes. Touchart (2005) introduced a classification of these lakes based on the ice-cover thickness and duration, but barely mentioned the subarctic lakes located at the margin between the polar and temperate environment within the category of lakes with a seasonal ice-cover. The necessity of working towards a better understanding of the lakes in the arctic and subarctic areas was emphasized by Rouse (1997), who pointed out the lack of studies on these environments and insisted on the greater vulnerability of the freshwater system in these latitudes in the context of global warming.

Global warming Climate change is expected to result in a spatially variable increase in temperature and precipitation. Global warming will have a direct on the ice cover of subarctic lakes; the ice-free season will be longer and the ice coverage might become spatially discontinuous. Callaghan et al. (2010) mention that, if the ice cover becomes thinner, this might impact the safety of inland herd migrations. In addition to this ecological impact, Assel et al. (2003) points out direct social impacts as ice fishing will become more restricted in space and time. As the ice-free period will increase, the water circulation in the lake will also be affected: the lake will be exposed to winds and the summer stratification period might lengthen. A study by O'Reilly et al. (2015) shows that seasonally ice-covered lakes have experienced faster warming that ice-free lakes over the last decades.

Indirect impacts of global warming on lakes are connected to the thawing of permafrost and the subsequent release of carbon or other sequestrated pollutants such as mercury in the water system downstream, lakes acting as new sinks (Rydberg et al., 2010; Gorham, 1991). Williamson et al. (2009) declare that lakes are sentinels and integrators of climate changes, their (physical, chemical and biological) responses to climate changes are indeed providing signals about climate change and the sediments that they store are the memory of past changes. They add that lakes act also as important regulators due to their role in the carbon cycle.

Anthropogenic pressure and stress Forbes et al. (2001) states that ecosystems in the Arctic are impacted by the increasing anthropogenic pressure associated in parts to global warming more than global warming itself. While the Russian Arctic experiences a demographic decline, most regions in the Arctic present a growth of population, associated both with a relatively high birth rate and life expectancy and increased positive migration fluxes triggered by the economic development of these regions (Larsen and Fondahl, 2015). The improved accessibility of these northern territories has given rise to a fast development of (eco)tourism (Tolvanen and Kangas, 2016) and other invasive industries. According to Schindler and Smol (2006), "(r)apid development of gas and oil pipelines, mining for diamonds and metals, increases in human populations, and the development of all-season roads, seaports, and hydroelectric dams will stress northern aquatic ecosystems. The cumulative effects of these stresses will be far more serious than those caused by changing climate alone". Although the

overall balance of impacts is arguable, it can be said that anthropogenic pressures are certainly non-negligible.

1.2.4 Lake dynamics in Iceland: Need for further research

While international research is increasing in arctic and subarctic environments (Vincent et al., 2008b), and in particular in Canada where a majority of the lakes are located (Oswald and Rouse, 2004), physical limnological research is presently not well-developed in Iceland. It is, for example, occasionally thought that Lake Lagarfljót (located in North East Iceland) is a river and that the internal flow is simple and the water-column is fully mixed when the lake is ice-free.

In Iceland, several authorities are monitoring lakes; these comprise the National Energy Authority (Orkustofnun), the National Power Company of Iceland (Landsvirkjun), the Icelandic Meteorological Office (Veðurstofa Íslands) and the Marine and Freshwater Research Institute, formerly Institute of Freshwater Fisheries Researches (Veiðimálastofnun). However most reports are available in Icelandic. Academic researches are, also, led in Icelandic lakes, in particular in the field of ecology and paleolimnology. Lake Þingvellir and Lake Mývatn are the two most famous lakes in Iceland and they have been the object of numerous ecological (Lindegaard and Jónasson, 1979; Jónasson, 1979, 1992; Jónasson et al., 1992; Einarsson et al., 2004; Snorrason et al., 2011), paleolimnological (Einarsson, 1982; Haflidason et al., 1992) and chemical limnology researches (Ólafsson, 1979a; Kristmannsdóttir and Ármannsson, 2004). However, very few studies can be found on the physical dynamics of Icelandic lakes and their main focus is set on the thermal regime (Ólafsson, 1979b; Adalsteinsson et al., 1992).

In 2000, the engineering firm VST, in a project for the National Power Company of Iceland, explored the effect of damming on the temperatures of Lake Lagarfljót using the 2D hydrodynamic and water quality model CE-QUAL-W2 (VST, 2001). This study which is the first attempt in Iceland at modeling hydrodynamic processes assumes lateral homogeneity of the water column and focuses on temperature changes and more specifically surface temperatures. Andradóttir (2008) initiated the investigation of internal dynamics in Icelandic lakes in 2007, emphasizing the need for further studies. She compiled the state of the knowledge about Icelandic lakes in a chapter for the Encyclopedia of lakes and reservoirs (Andradóttir, 2012).

1.3 Lake Lagarfljót project and the purpose of this thesis

In 2007, Dr. Hrund Ólöf Andradóttir initiated a new research program with the main goal to increase scientific knowledge on the physical dynamics of deep Icelandic lakes. Lake Lagarfljót was chosen as one of Iceland's largest and deepest lakes, and because of the strong long-term meteorological and hydrological data that had been collected at the lake due to hydropower interests in the region. The research, funded by the National Power Company of Iceland, would enable better predictions of the impact of hydropower development and global warming on Icelandic lakes (Andradóttir, 2008).

The research aimed to characterize more specifically three different physical processes:

1. Development and drivers for lake density stratification
2. Surface and internal waves in weakly stratified lakes
3. Fate of river inflows and deep water renewal

The initial approach was to conduct detailed field data collection of temperature, water velocity and atmospheric energy balance of the lake. However, as the field monitoring progressed, it became clear that the internal dynamics were fully three dimensional (Andradóttir, 2010). In September 2009, a collaboration was formed with Prof. Francisco Rueda at the University of Granada on modeling the physical processes in Lake Lagarfljót with the help of the hydrodynamic Si3D model. Dr. Francisco Rueda set up the model for data from 2009. The goal of the research shifted to verify that the Si3D model could simulate observed thermal dynamics in the lake, and then, use the model to better explain the complex features that field observations could not explain.

In spring 2010, the research started as a doctoral research project. The initial objective was broad and defined as the investigation of the internal dynamics of Lake Lagarfljót, a large deep weakly stratified Icelandic lake, during the ice-free season in order to improve our comprehension of the dynamics in place in the lake, but more generally to improve the understanding of the hydrodynamics of large subarctic water bodies. For that purpose, and because the task is so vast and requires extensive datasets, two approaches were combined.

Firstly, field campaigns for data collection were organized during the two summers of 2010 and 2011, the last instruments being retrieved from the field during summer 2012. Data was also gathered from the different agencies and companies involved in the monitoring of the lake and its catchment. The first task was to acquire a better understanding of the internal motions based on physical data.

Secondly, the results of numerical models were assessed in the perspective of supporting and complementing the knowledge acquired on this water body. Two different models were used and adapted to the system. The simple two dimensional Münnich model (Münnich, 1996; Vidal Hurtado et al., 2007) was modified in order to use it for basin with complex bathymetry. The more complex three dimensional hydrodynamic model Si3D, originally an estuarine model (Smith, 2006) adapted to lakes by Rueda (2001), was also modified in June 2012 during a visit to Dr. Francisco Rueda at the Water Institute of the University of Granada to include the suspended sediments in the equation of state.

1.4 Outline of the thesis

In this thesis, the different chapters are organized in a quasi-chronological manner. In the first chapter, the thermal characteristics of Lake Lagarfljót during the ice-free season are described in depth, supported by in-lake field data collected in 2010 and 2011 and in connection with the meteorological environment. In the second chapter, the lake was analyzed in the previous section as an enclosed basin but in-site measurements

provide evidence of the influence of the inflow in the lake's thermal characteristics. The hydrological characteristics of the watershed are therefore introduced more thoroughly, presenting the diversity of inflows and their specificity. In the third chapter, using the simple 2D numerical approach, we characterize the internal wave regime better and assess the role of the wind. Is the wind forcing or feeding these internal waves? In the fourth chapter, we analyze the response of Lake Lagarfljót to external forcing based on the results of 3D hydrodynamic modeling work. The meteorological and hydrological inputs will be considered to assess the influence of the wind and the inflow on the internal motions of the lake. In the fifth chapter, the fate of the river inflow is characterized, supported by the modeling results and field measurements. Finally, the thesis closes with a synthesis of the most significant findings.

2 Thermal stratification and internal dynamics in Lake Lagarfljót

The thermal process of stratification, combined with kinetic mixing, are the key factors controlling the circulation of heat, oxygen and nutrients between the surface and deep waters. Stratification during the warm season is controlled in most of the cases by the thermal gradient that results in a big part from the heat transfer from the atmosphere at the water surface (Wetzel, 1983; Boehrer and Schultze, 2008). Salinity (Pickard and Emery, 1990) and suspended sediments (Sheng and Villaret, 1989; Winterwerp, 2001) can sometimes also contribute to lakes' stratification. Under stratified conditions, internal waves are initiated by the action of the wind at the surface of the lake (Imberger and Hamblin, 1982; Wiegand and Carmack, 1986; Boegman, 2009). They play a large role in the vertical (Denman and Gargett, 1983) and horizontal (Wain et al., 2013) transport of nutrients and dissolved substances. Bottom current associated with these motions are responsible for the resuspension of particles, organic and inorganic (Gloor et al., 1994).

These hydrodynamic behaviors have been well investigated for temperate lakes, but lakes in the subarctic and polar regions have received much less attention to date, even though the specificity of the climate in these regions (only two seasons) suggests the uniqueness of these water bodies. Discontinuous field measurements interrupted by the cold season and a focus on small lakes have both led to theoretical classifications that do not describe the entire diversity of these lakes.

Arctic and subarctic lakes have been considered to be water bodies with simple hydrodynamic behaviors, isothermal (Carson and Hussey, 1960), fully mixed most of the year and only weakly stratified during the summer (Yoshimura, 1936; Touchart, 2005). Yoshimura (1936) classified subpolar lakes as those whose temperatures stay below 4°C half of the year, with a weak summer stratification. Lewis Jr (1983) reconsidered the Hutchinson-Löffler classification (Hutchinson and Löffler, 1956) which divides the lakes into six categories : amictic, cold monomictic, dimictic, warm monomictic, oligomictic and polymictic and introduces the meromixis / holomixis dichotomy. He kept the original criteria - ice-cover, mixing and direct stratification- and added the effect of depth and fetch on mixing behavior at any latitude and altitude. Hence he divided lakes with winter ice-cover and whose temperatures rise above 4 °C during the summer into three categories: "Dimictic if they stratify for the whole season, discontinuous cold polymictic if they stratify for days or weeks but not the whole season, and continuous cold polymictic if they do not stratify or stratify only for hours at a time". More recent studies (Vincent et al., 2008a; Oswald and Rouse, 2004) emphasize the limnological diversity of lakes in arctic regions, present as much in the summer temperatures and mixing regimes (from isothermal to dimictic) as the chemical

and biological characteristics of the lake. The lack of research in polar lakes has been stressed as early as 1954 by Rawson (1954), and more recently by Touchart (2005).

Lakes respond rapidly to environmental and climate changes, hence can be important markers of global changes (Adrian et al., 2009; Williamson et al., 2009). The necessity of working more specifically towards a better understanding of the lakes in the arctic and subarctic areas was emphasized in Rouse et al. (1997) which pointed out the lack of studies on these environments and insisted on the greater vulnerability of the freshwater systems in these latitudes in a context of global warming (Smith et al., 2005; Riordan et al., 2006).

The focus of this chapter is to describe the internal dynamics of lake Lagarfljót, a deep weakly stratified subarctic lake, based on the data collected during summer 2010 and 2011. Internal motions will be considered in the light of the local forcing, air temperatures that controls the stratification and winds that onset the wave motions.

2.1 Site description

2.1.1 Lake Lagarfljót

Lake Lagarfljót is located in the North East of Iceland (65°N 11' N, 14°36' W) at about 20 m above sea level. The lake has an elongated surface of 53 km^2 and is 27 km long with a maximum width of 2.5 km (Figure 2.1). The lake is a fjord lake resulting from the past erosion activity of glacier Vatnajökull. It is composed of two basins: a 20 km long deep basin located at its southern part, with maximum depth of 112 m and a 7 km long shallow basin (max. depth 45 m) located in the northern part, separated from the first basin by a sill. At it deepest location, bedrock can be found about 200 meters under sea level, about 100 m of sediments are laying over it.

The lake is primarily fed in its south end by the glacial river Jökulsá í Fljótsdal which originates from the largest Icelandic glacier Vatnajökull. The glacial river, historically 57 m^3/s (IMO, 2010b), is very turbid and, as a result, the lake has a whitish - mustardy color (Tómasson, 2001) and a high suspended sediment content (max recorded at 170 mg/L , Aðalsteinsson (2010)). The freshwater river Grimsá is the second largest tributary (24 m^3/s) (IMO, 2010b), entering the lake in the shallower northern basin (Figure 2.1). The outflow of the lake, estimated historically to be 107 m^3/s (Tómasson, 2001), occurs at the northern end by the town of Egilsstaðir.

Since November 2007, a hydropower damming project diverted a nearby glacial river into Jökulsá í Fljótsdal about 12 km before it enters the lake. This additional flow is estimated to be in average of 110 m^3/s, almost doubling the historical flow rate. The lake residence time was estimated to be approximately one year before the diversion, and about half a year afterward (Tómasson, 2001).

The lake is weakly stratified during the summer season and strong winds episodes exert stresses on its surface, hence shear instabilities are strong and following the classification of Boegman (2009), the lake has a type D regime, where upwelling creates a longitudinal temperature gradient in the basin and results in horizontal mixing.

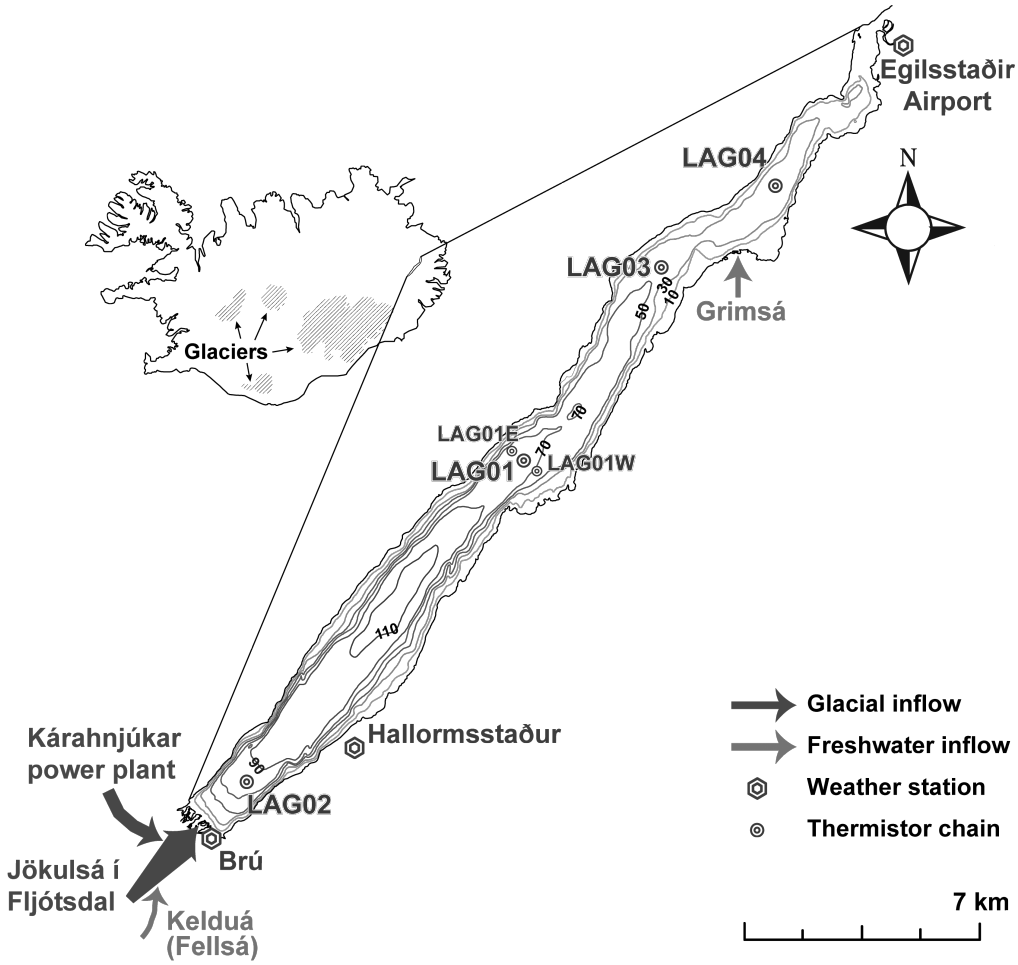

Figure 2.1. Bathymetry map of Lake Lagarfljót with location of thermistor chains (circles) and weather stations (hexagons)

2.1.2 Regional climate

Meteorological data are recorded by two weather stations operated by the Icelandic Meteorological Office IMO (2010a) located near the lake, Hallormsstaður, on the southern part of the lake and Egilsstaðir Airport in its northern end (Figure 2.1). These stations record 10 minute averages for the wind speed and direction and 1 minute averages for the relative humidity, precipitation, air temperature and air pressure (Egilsstaðir Airport only). A solar radiation meter (Licor) was added to Hallormsstaður in August 2008. The cloud cover is assessed daily at Svínafell (28 km north of Egilsstaðir).

Air temperatures Monthly median air temperatures (Figure 2.2A) at Egilsstaðir Airport stay below 0°C between December and March and exceed 10°C only during the months of July and August. 10 minute extremes range from -20°C to 25°C.

Temperatures at the more inland Hallormsstaður forest are about 0.5°C above those recorded at Egilsstaðir Airport. While temperatures are almost constant throughout the day in winter, there is a clear diurnal signal during the summer season with a maximum temperature reached at 1 to 3 PM and a minimum at 3 to 4 AM.

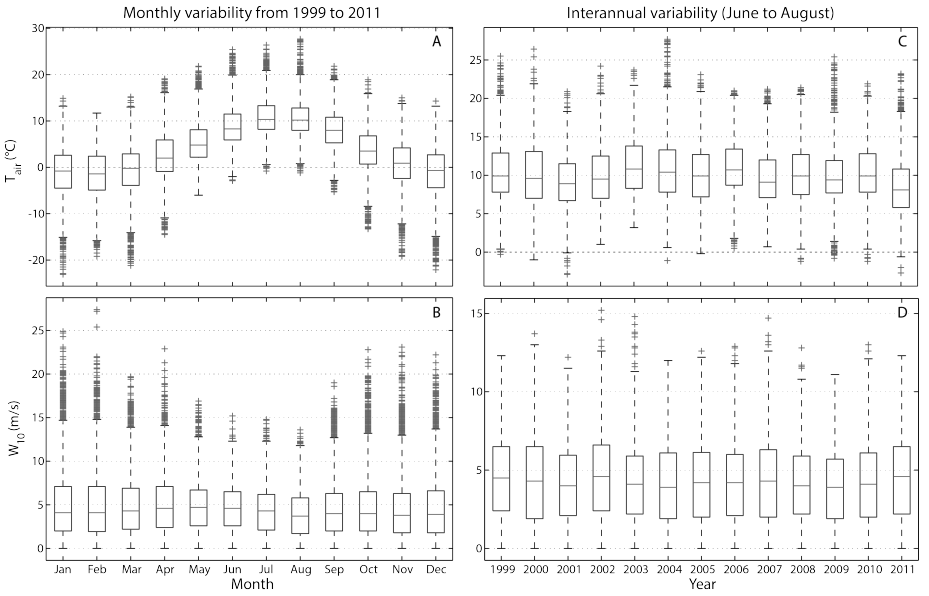

Figure 2.2. Left panel) Monthly distribution from 1999 to 2011 and Right panel)interannual variability for the summer season of the air temperature (A-C) and wind speed (B-D) at Egilsstaðir airport

Figure 2.2C shows the interannual variability of air temperature and wind speeds during the three summer months. Warmest air temperatures (median 10.8°C) were recorded in 2003 and the coldest (median 8.1°C) in 2011. It is notable that air temperature in 2011 rarely exceeded 11 °C.

Wind The main wind directions are aligned with the orientation of the lake basin (S-SSW and N-NNE) (Figure 2.3). The monthly median wind speeds are generally

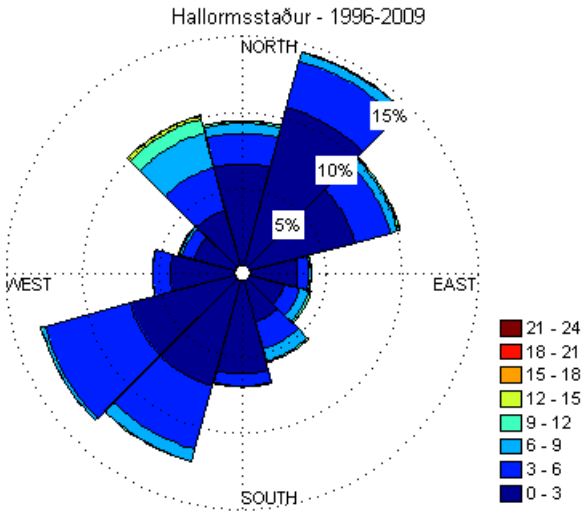

Figure 2.3. Wind rose of the average winds at Hallormsstaður for years 1996 to 2011

around 4.2 $\pm$ 0.3 m/s at Egilsstaðir Airport (Figure 2.2B).

The summer months experience less extreme wind events which rarely exceed 13 m/s, in winter wind speeds can exceed episodically 25m/s. While diurnal variations of wind speed occur in summer, they are not relevant when accounting for directionality.

Figure 2.2D shows the interannual variability of wind speeds during the three summer months. Less interannual variabilities are present in wind speeds (median 4.2 $\pm$ 0.2 m/s) than in air temperature, however the years 2011 and 2002 were windier that the others.

Precipitation Between 1999 and 2011, the average annual accumulated precipitation is 510 mm. Most of the precipitation falls after the summer with a peak reached during the month of October (Figure 2.4). Spring and summer months are the driest with 28% of the precipitation occurring between March and July. However, it can be expected that most of the precipitation that fell during the cold winter time accumulates as snow and fills up the rivers during the melting season.

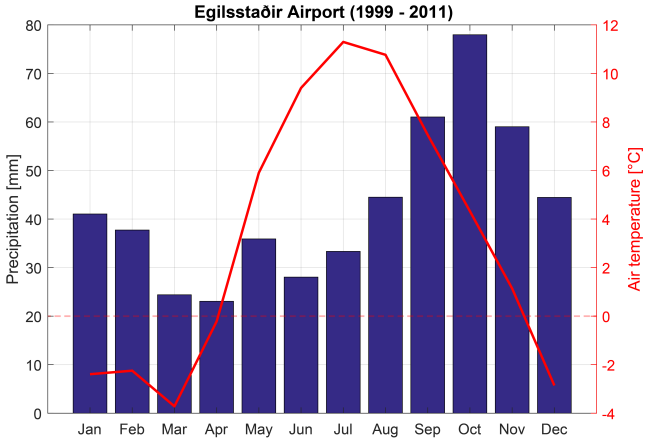

Figure 2.4. Monthly accumulated precipitation at Egilsstaðir airport for the period of 1999 to 2011. Monthly temperature means are plotted in red and the 0°C line in dashed red. Source : IMO.

Short wave radiation The short wave radiations have very strong annual pattern due to the location of the lake in the high latitudes. During the measurement period (2009 to 2011), daily short wave radiation did not exceed 98.4 and 266 W/m^2/d in December and January respectively while the minimum daily measurements exceeded 750 W/m^2/d for the three months of April, May and June (Figure 2.5).

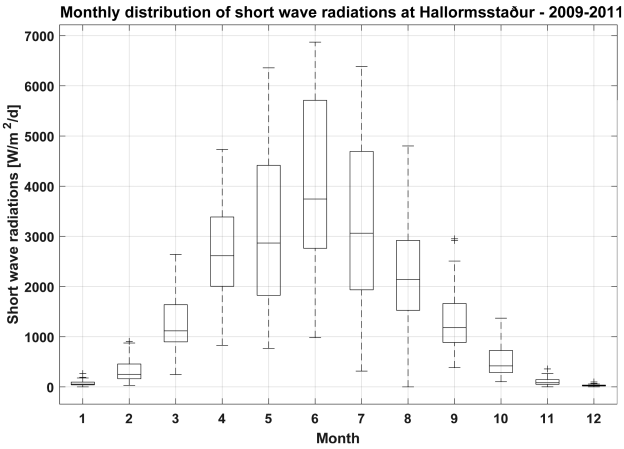

Figure 2.5. Monthly distribution of daily short wave radiations at Hallormsstaðir. Source : University of Iceland.

The hourly distribution of shortwave radiation during the months of December and June shows that shortwave radiations are measured during 6 hours of the day (midday) and are extremely low in December (Figure 2.6a) while, in contrast, solar radiations

are measured most of the day (from 4.00 to 22.00) during the month of the June (Figure 2.6b) but the hourly radiations do not exceed 700 W/m2 even at the peak of the day during the measurement period.

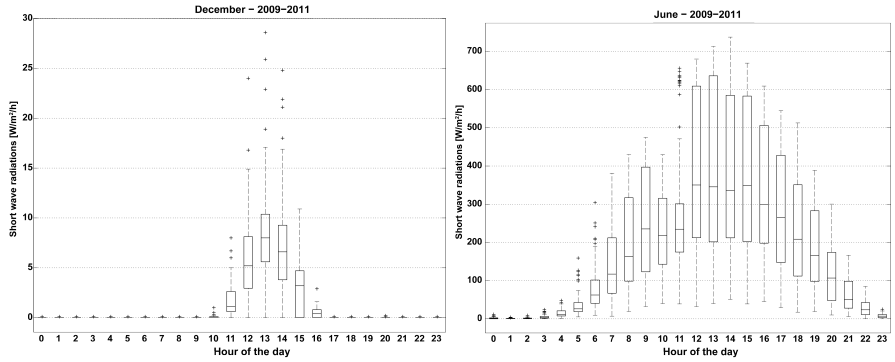

Figure 2.6. Distribution of hourly shortwave radiations measured at Hallormsstaðir for the month of December (left) and the month of June (right). Source: University of Iceland.

Figure 2.7 presents the hourly shortwave radiation for the 3 years of measurements smoothed over a week. The summer months show a strong disparity between years and summer 2011 received less shortwave radiation than the two previous years, and in particular than 2010.

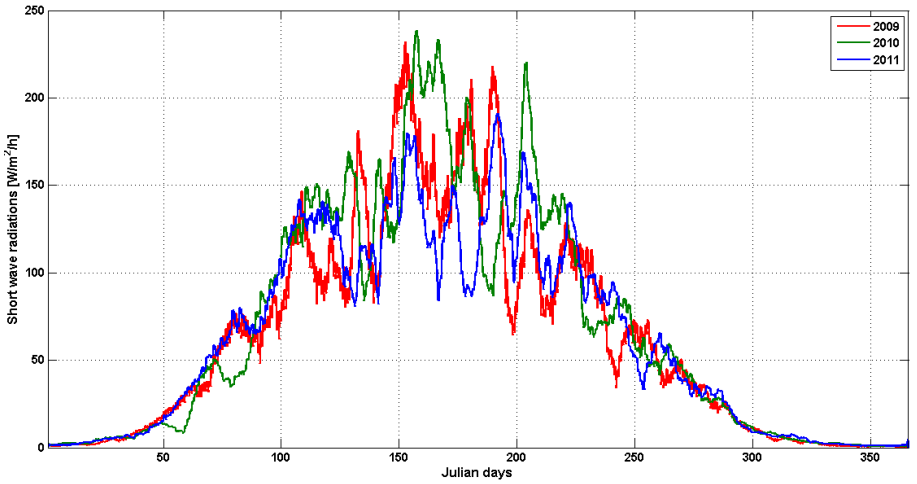

Figure 2.7. Interannual variability of short wave radiations measured at Hallormsstaðir. Comparison between year 2009, 2010 and 2011. The hourly short wave radiation were smoothed over 7 days. Source : University of Iceland.

Moreover strong oscillation of the shortwave radiation signal can be observed during the summer season, with periods ranging from 10 to 30 days.

2.2 Material and methods

2.2.1 Field measurements

Measurements in the frame of this doctoral research started in 2010 and were intensified in 2011. Some sparse measurements had been performed before by the University of Iceland and the National Power Company of Iceland but its spatial resolution was deemed insufficient and the choice of location unsuitable for this study.

Continuous temperature measurements In 2010, chains were deployed the 8^{th} of June (5^{th} of July for LAG01W and LAG01E) and retrieved the 14^{th} of December. In 2011, three chains were deployed the 26^{th} of May (5^{th} of July) and retrieved the 12^{th} of December for the summer deployment. The winter chain was set in the water on the 22^{nd} of January 2011 and finally retrieved the 6^{th} of July 2011 after multiple unsuccessful attempts in May and earlier in July.

Three thermistor chains were deployed along the thalweg of the lake in summer 2010 : in a quasi-central position LAG01 at 78 m depth, at the southern end of the basin LAG02 at 78.5 m and at the northern end of the main basin LAG03 at 46 m depth, close to the sill separating the two basins (Figure 2.1). Two additional chains were added in beginning of August on each side of LAG01: LAG01W at 75 m depth, North West of LAG01 and LAG01E South East of LAG01 at 72 m depth.

Table 2.1. Summary of the thermistor chain setups for 2010 and 2011.

Station	Deployment		Thermistors	
	Period	Depth [m]	No	Elevation from bottom [m]
LAG02	2010	78.5	8	0.3, 18, 28, 38, 48, 58, 68, surface
LAG01	2010	78	7	18, 28, 38, 48, 58, 68, surface
LAG03	2010	46	4	10, 20, 30, surface
	2011	45	6	0.3, 5, 15, 25, 35, surface
LAG01W	2010	75	3	20, 30, 50
LAG01E	2010	72	2	30, 50
LAG04	2011	42	5	0.3, 10, 20, 30, surface
HAF	2011 (winter)	67	7	0.3, 10, 20, 30, 40, 50, 60
	2011 (summer)	70	8	0.3, 10, 20, 30, 40,50,60, surface

In winter 2011, it was decided to measure the temperatures in one location to get an image of what is happening in the lake when ice starts sheltering the lake in parts. To prevent damage and loss of the thermistor chain by the ice cover, no buoy was placed at the surface and the top buoy was designed to be located at 5m below the surface with the first thermistor. However, as the high sediment content of the waters does not allow for visual support for the retrieval of the instruments, it was therefore decided not to deploy the meters in the deepest location in case divers would need to be hired to retrieve the line. The line was deployed at 67m (originally intended 65m) depth close to the deepest point of the lake close to the mouth of the river Hafursá, on the East side of the lake. The top meter was therefore about 7 m under the surface. During deployment, GPS points were taken and a set of lines connected to the chain ran at the bottom of the

lake almost to the shore, in the hope it would ease the retrieval, but in May 2011, the first retrieval attempts were unfruitful. The thermistor chain was finally recovered in July on the third day of attempts, thanks to a fish finder which detected the top buoy. The chain was some 30 m away from the GPS location suggesting that the boat had significantly drifted during the deployment process. Unfortunately, at the reading of the meters, it was discovered that most RBR thermistors had not recorded data due to some update of the driver software prior to the deployment.

During summer 2011, the setup was modified in order to investigate the oscillations in the secondary basin. LAG03 was preserved at the same location at 45m depth. Two thermistor chains, LAG04 and HAF, were also set at new locations in the lake. LAG04 was placed in the secondary basin at 42 m depth, in a sufficient distance from the affluent Grímsá to limit its influence while the third line was placed on the 7^{th} of July at HAF (70 m depth),the same location selected for the winter line.

In general, all chains were equipped with Starmon mini underwater temperature recorders ($\pm$ 0.05 °C accuracy) at 10 m intervals throughout the water column. LAG01 and HAF thermistor chains were an exception: apart from the surface and bottom logger, temperature loggers were RBR loggers($\pm$ 0.002 °C accuracy). Table 2.1 recapitulates the thermistor chain setups for the deployments in 2010 and in 2011.

Vertical profiling Vertical profiles of water temperatures (resolution 0.01°C and accuracy $\pm$ 0.15°C) were carried out with a multi-parameter sonde (YSI 6600). In summer 2010, profiles were recorded over 2 days, the 9^{th} of July and the 9^{th} of August, at 7 locations along the thalweg of the lake. With the exception of the 2 most downstream locations, 3 profiles were taken across the width of the lake at the remaining five locations, totaling 17 profiles. In summer 2011, profiles were recorded over 4 days in July (the 10^{th} and 12^{th}) and in August (the 10^{th} and 11^{th}). Additional locations along the thalweg were added to the previous profiling plan (total of 31 profiles) to improve the resolution, especially around the sill area. Each longitudinal transect (27 km) was completed within 12 hours, which was found to be short compared to the main internal wave periods (order of days). Hence, the measurements represent as best as physically possible a snapshot of the spatial thermal regime in the lake. For practical reasons, the measurements were performed on relatively calm days, sometimes right after strong wind events (Figure 2.8).

Current measurements Bottom and surface currents were both investigated along side the water temperature measurements, but due to the high suspended sediment content it provided us with limited information. A more detailed description of the methods employed is available in Appendix B. The results will be discussed very briefly in the main text.

2.2.2 Data analysis

In order to increase our insights on the complex processes occurring in the lake, it is useful to apply numerical methods to the raw field data.

Surface heat fluxes The net surface heat flux ϕ was estimated as the sum of five heat flux terms and computed as follow:

$$\phi = (1-R)S + \phi_1 + \phi_2 + \phi_S + \phi_L$$

with S the incoming solar radiation measured at Hallormsstaður, R the reflection coefficient is estimated from the relationship between the albedo and solar altitude angle (Bras, 1990, p.38), and the four estimated heat flux terms , ϕ_1 the incoming long wave radiation, the back-radiation ϕ_2, the latent heat flux ϕ_L and the sensible heat flux ϕ_S. These latest are estimated from the weather measurements (temperature, atmospheric pressure, wind, relative humidity and cloud cover) using established empirical relationships (Fischer et al., 1979; Bras, 1990).

Field data analyses Most analyses were performed with Matlab. Periodicities in timeseries of temperature, bottom currents, and meteorology were analyzed with the power spectral density (PSD). The PSD gives a measure of the power intensity of a signal in the frequency domain; in practice, it characterizes the amplitude of a signal at a given frequency. Bottom currents were analyzed with rotary spectrum using the ff_spec_rot function on current velocity component to compute the clockwise and counter-clockwise spectra. Coherence and phase spectrum were computed using the magnitude-squared coherence function and by computing the angle of the cross power spectral density. The associated total signal power is computed using the AVGPOWER function, higher power is associated with larger signal amplitude. To filter data, the smooth function is used which applies a moving average of the timeseries over a given window.

The Brunt-Väisälä frequency, or buoyancy frequency, N (s^{-1}) quantifies the stability of the water column and is computed as follow $N = \sqrt{\frac{-g}{\rho}\frac{\delta\rho}{\delta z}}$ where ρ is the density, g the gravity, and z the depth (positive upward).

Coriolis Coriolis forces result from the rotation of the Earth. As the Earth rotates, it is imposing a rotational movements to the large-scale motions of the atmosphere and the oceans. Two types of waves are distinguished : vorticity waves and gravity waves. The effect increases with the latitude (Wüest and Lorke, 2003; Wetzel, 1983). In smaller water bodies such as lakes, the dimensions of the basin set a limit to the type of waves observed: the smaller the water body, the less the effect the rotation of the Earth will have on the motions present in the system.

The stratification of the water column also influences how much internal waves are affected. Two types of gravity waves are observed : Kelvin waves and Poincaré waves. Poincaré waves are anticyclonic waves with superinertial frequencies.Kelvin waves are cyclonic waves and are associated with subinertial frequencies (Antenucci and Imberger, 2001; Rueda et al., 2003). The inertial period is estimated as $T_i = 2\pi/f$ with f the inertial frequency or Coriolis parameter.

Two parameters allows us to evaluate the influence of the Earth's rotation on waves motions. The Rossby radius of deformation $R = c/f$ with c the phase speed of the wave defines the length scale at which the Earth's rotation effectively influences the internal dynamics of the lake. The criterion for the absence of rotational effect (Patterson et al., 1984; Vidal Hurtado et al., 2007), also called Burger number (Hutter, 2012), is computed

as $S = R/L$ with L a length characterizing the basin length or width. Several methods are used to estimate the phase speed c. The first one used here is a function of L, the length of the basin and T, the internal wave period, $c = 2L/T$ as described in Vidal et al. (2005). The second method is described in Antenucci (2009). There c is defined as a function of the basin mean depth H, the buoyancy frequency N and the number of vertical mode m such as $c_m = \frac{H}{m\pi}N$. When $R < L$ or $S < 1$, the Coriolis effect is significant. When $S >= 2$, it can be considered that the effect of the Earth's rotation are insignificant. Another approach to investigate the presence of rotational effects is to apply a rotary spectral analysis on the water currents (here the bottom currents).

2.3 Results

2.3.1 Stratification

Ice-free season Figure 2.8 presents the wind speed along the lake , the net surface heat fluxes and the lake temperatures recorded at LAG03 (Figure 2.1), the station furthest from the glacial river inflow, thus least influenced by the river inflow, from day of year (DOY) 160 (9^{th} of June) to DOY 270 (27^{th} of September) in 2010 (left panel) and 2011 (right panel).

Summer 2010 was representative of typical weather conditions (Figure 2.2). Figure 2.8A shows average wind velocities along the lake axis: positive when the wind comes from the South-South West, negative when coming from the North-North East. There is a clear oscillatory pattern with wind speeds changing directions every 4.2 days. The speed range was in general 6 m/s, both years.

Figure 2.8B presents the net surface heat fluxes over Lake Lagarfljót, positive fluxes implies a warming up of the water surface of the lake. Early summer 2010 (DOY 160-220), the daily net heat fluxes (bold line) are positive and above 100 W/m^2. High daily variations (max 600 W/m^2, thin line) are observed. The heat fluxes become null or negative by DOY 225 (13^{th} of August), reflecting the start of cooling.

The water temperatures measured at different depths on figure 2.8C) show that the lake was isothermal early June (DOY 160). After that, the temperatures increased to a maximum of 10°C at the surface and a thermal gradient started developing. The lake stratification reached a maximum of 4.92°C temperature difference (surface to 36 m depth) on DOY 213 (1^{st} of August). The lake starts mixing again on DOY 260 (17^{th} of September), corresponding to high south westerly winds followed by negative net heat fluxes (Figure 2.8B). The 2010 stratification period lasted for about 100 days, only interrupted by a partial mixing event on DOY 230 that can be associated to a strong wind event and quasi-null surface net heat fluxes.

Summer 2011 was characterized by lower air temperatures and higher wind speeds (Figure 2.2). Wind velocities (Figure 2.8D) appeared to have a stronger synoptic response than in 2010. The net surface heat fluxes (Figure 2.8E) were lower, particularly at the start of the summer season. This resulted both in a 10 days delay of the onset of stratification (Figure 2.8F), and lower thermal gradient in the water column, only reaching a 4.26°C temperature difference between surface and bottom (45 m) on the DOY 211 (30^{th} of July) 2011.

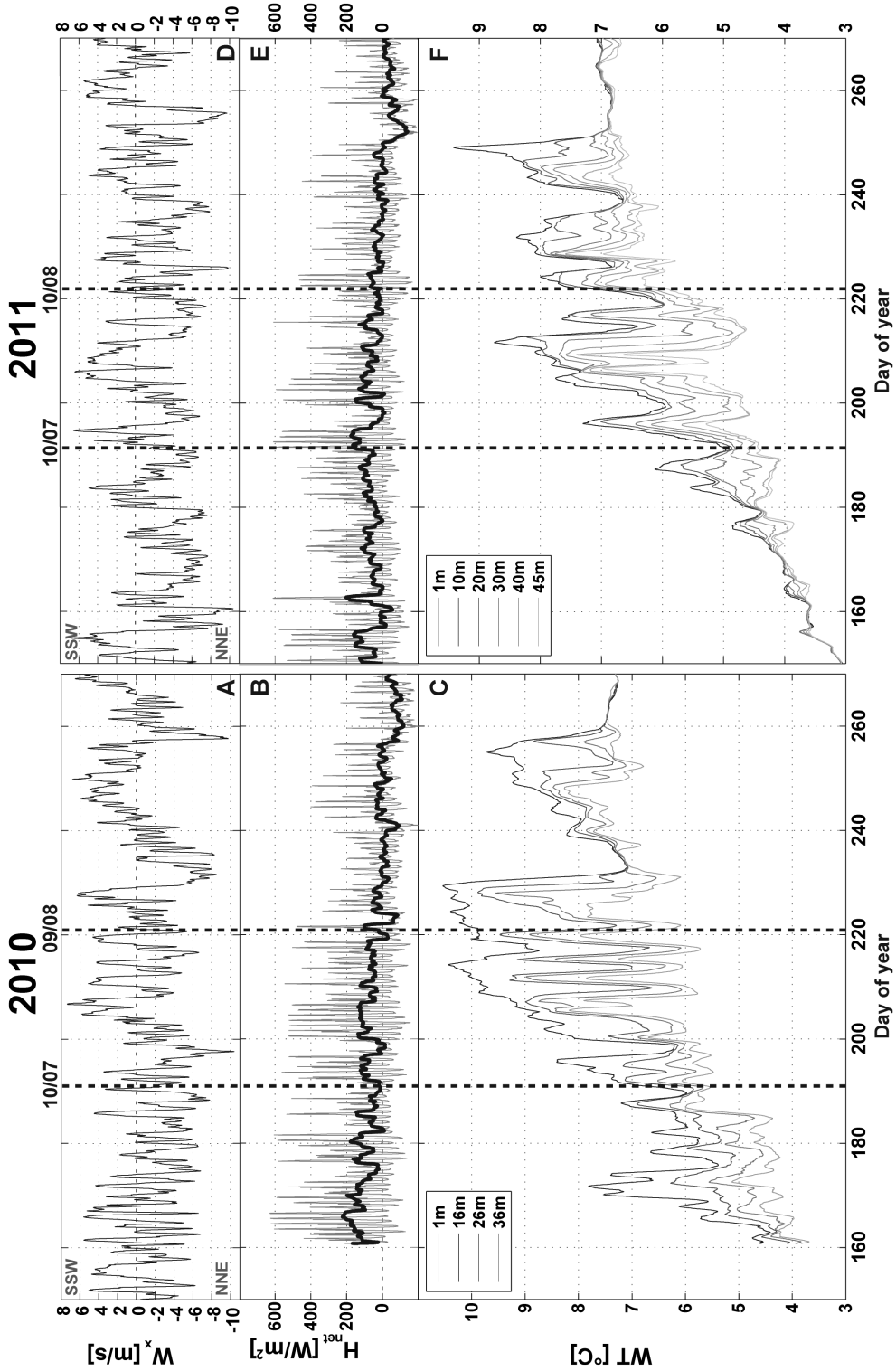

Figure 2.8. Wind velocity, net heat fluxes and water temperatures for summer 2010 (A, B and C respectively) and 2011 (D, E, F) at the northern station LAG03. The measurements are smoothed over 24h.

At around DOY 240, partial mixing occurred, associated to a strong wind event with daily net surface heat fluxes close to zero. The water column mixed almost fully by DOY 252 during a strong wind and negative net surface heat fluxes episode. Overall the summer stratification period lasted only 80 days, to wit, 20 days less than the previous summer.

Fall overturn and winter cooling When the column cools down, it slowly gets closer to the temperature of maximum density (estimated to be close to 3.98°C). Then the warmer waters sinks and colder water rises, resulting in turnover. If the column cools further, an inverse stratification will appear with colder waters on top of warmer bottom waters.

Looking more in details at the measurements during the winter season, it is clear that the lake does not experience a clean mixing episode leading to turnover and inverse stratification once the temperatures have dropped under 4°C. As observed in Figure 2.9, the water column at LAG03 appears to be mostly quasi-isothermal from day 260 with a short 7 days period of weak stratification ($\approx$ 0.5°C) until day 318 when the water column experiences turnover and inverse stratification develops when the temperatures in the water column are close to 4°C.

Measurements at LAG02 and LAG01 are performed from surface to bottom in the water column and show that the bottom temperatures behave very differently from the upper layers far into the winter season. At LAG01,the 60 upper meters mix at around day 260 but weakly stratifies 5 days later in the deeper layers until day 293; the water column becomes then quasi-isothermal around day 305 and turnover occurs day 325. At day 294, the bottom temperatures suddenly exceed the temperatures measured in the rest of the water column by a couple of tenth of degrees. At LAG02, a very similar behavior is observed. The bottom temperatures are presenting very singular diurnal oscillating signal with temperatures up to 1°C colder. Turnover and inverse stratification really occur once the temperatures throughout the column have dropped below 4°C.

When the thermistors are retrieved in mid-December 2010, temperatures measured are well below 4°C, with colder temperatures measured at LAG03 ($\prec$2.5°C) and warmer at LAG02 (between 3.5 and 2°C).

In 2011, measurements at HAF shows again that mixing in the 10 deeper meters does not occur in the early part of winter and if the 50 upper meters of the water column appears to be quasi-isothermal, sudden drops of temperature in the 50 lowest meter results in short-lived weak stratification (see day 290 and day 316 to 325). Complete turnover happens only when the water column has reached temperatures below 3.5°C.

At LAG03 and LAG04, the water column is quasi-isothermal from surface to bottom before day 260. A short episode of weak stratification is observed at LAG03 over 7 days period starting at day 265. At LAG04, the thermal signal of the bottom of the water column behaves also quite singularly and sudden drops by up to 0.5°C are observed (see day 281 and 294). Turnover is complete at day 302, when water temperatures fall under 5.5°C. Between days 323 and 325 however, the bottom 25 m starts re-stratifying temporarily. Inverse stratification starts developing when the temperatures within the water column drops under 3°C.

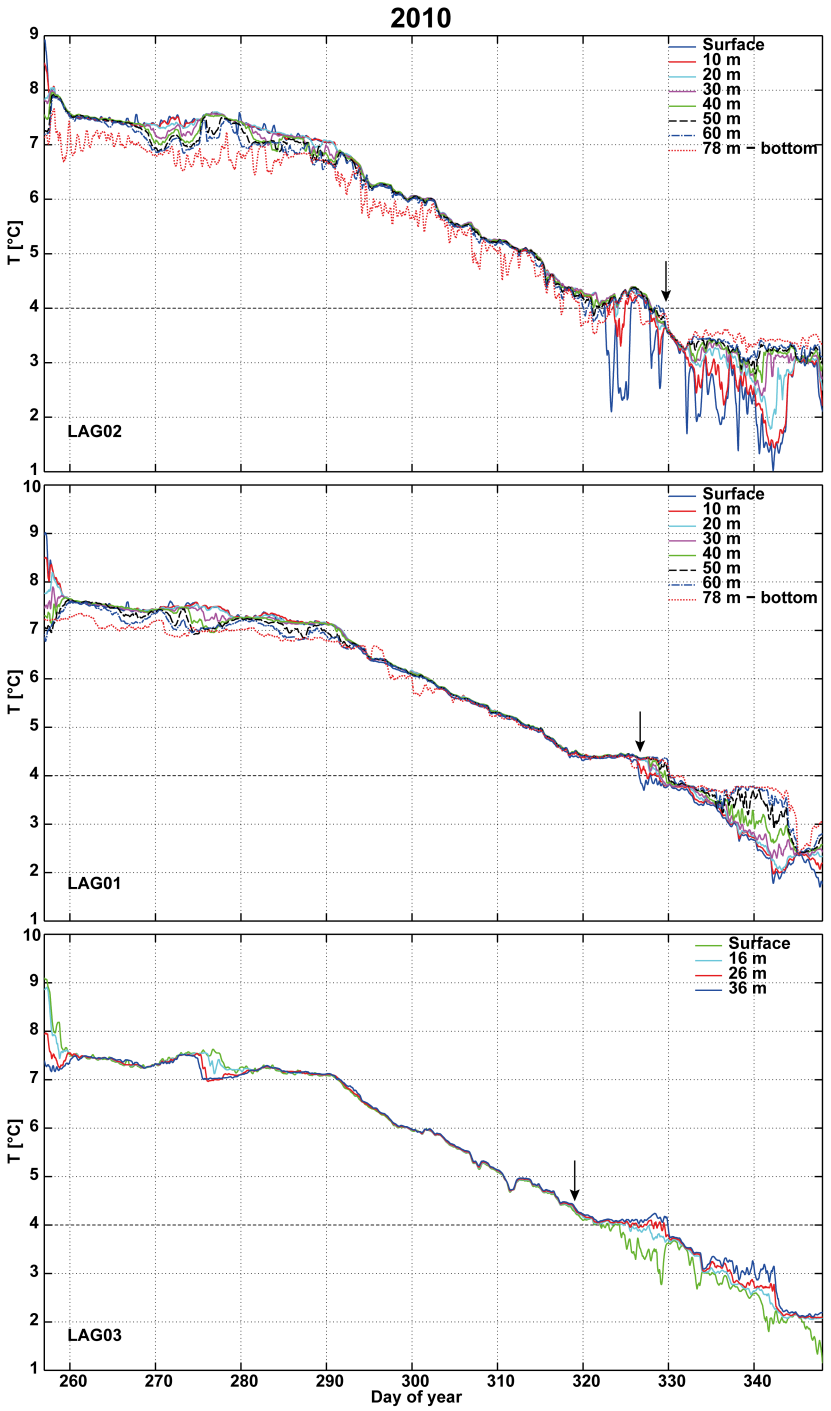

Figure 2.9. Fall overturn and winter cooling captured at LAG02, LAG01 and LAG03 during winter 2010. The temperature measurements are smoothed over a 6 h period. Black arrows indicate the identified date of complete turnover in the water column, the spirals emphasize short stratification event occurring after turnover started in the water column.

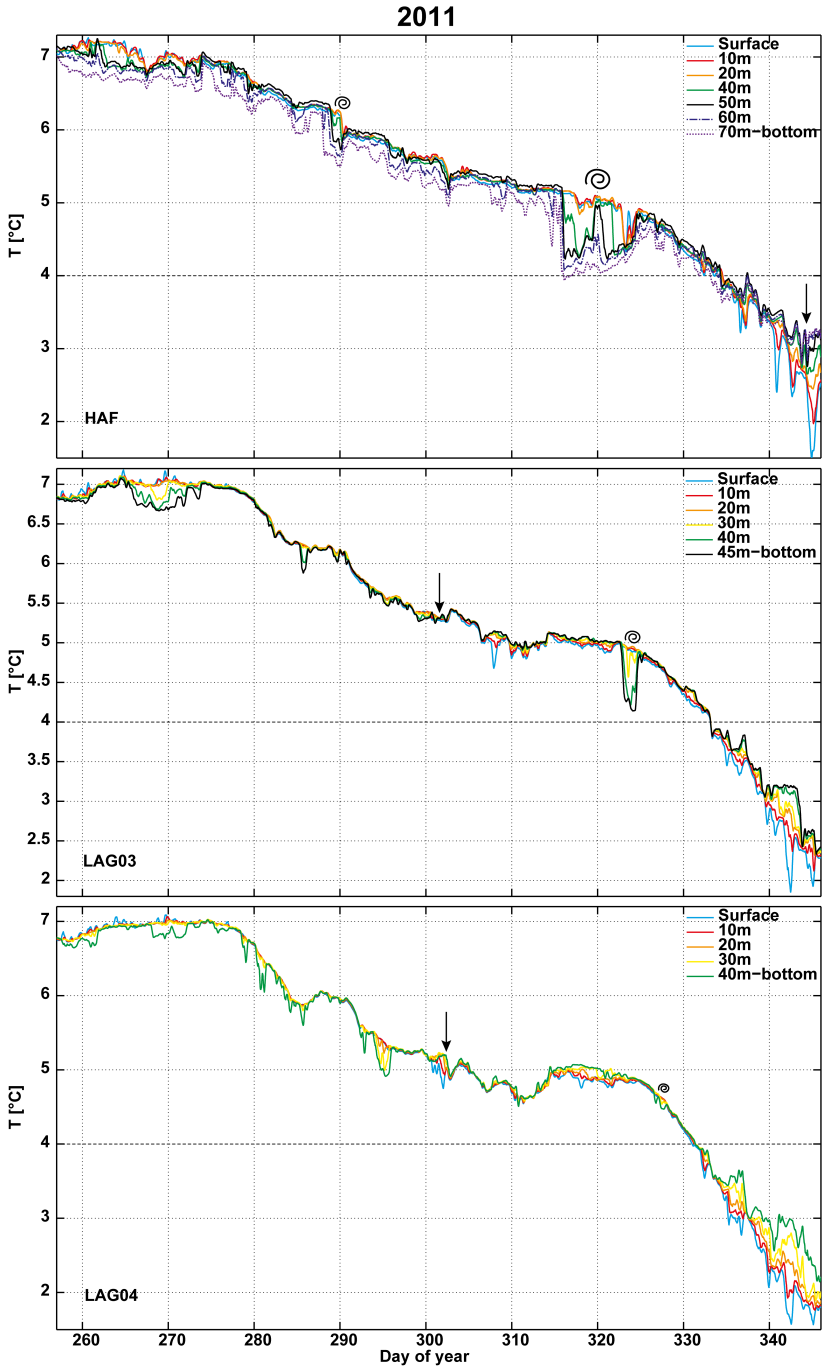

Figure 2.10. Fall overturn and winter cooling captured at HAF, LAG03 and LAG04 during winter 2011. The temperature measurements are smoothed over a 6 h period. Black arrows indicate the identified date of complete turnover in the water column, the spirals emphasize short stratification event occurring after turnover started in the water column.

In late January 2011, when the thermistors are deployed for the winter measurements, the temperatures at the bottom of water column at HAF are close to 0.5°C. The temperatures then drop further to reach a minimum on day 81 (end of March) and shortly after the temperature increases at a steady rate of 0.04°C day^{-1} until it passes the 4°C threshold on day 181 (30^{th} of June).

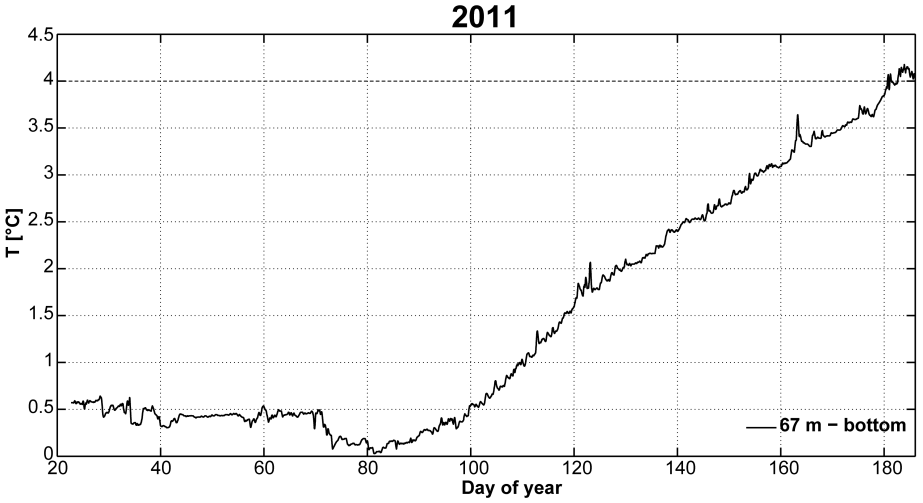

Figure 2.11. Bottom temperatures at HAF early 2011. The temperature measurements are smoothed over a 6 h period.

2.3.2 Internal waves

Temporal variability Internal motions are clearly visible from the water temperature oscillations at shallow station LAG03 on figure 2.8C and F.

Figure 2.12 presents the spectral analyses of the wind aligned along the lake axis, the surface heat fluxes and the water temperatures at 26 and 30m depth in 2010 and 2011 respectively. During 2010, the primary periods of wind oscillation were 6.8, 20 and 4.7 days. The net surface heat fluxes however had a strong diurnal signal with secondary oscillation periods of 10 and 3.6 days. The dominant internal wave oscillations is 4 days corresponding to both wind and net heat fluxes, secondary oscillations matches the wind synoptic (20 days) and weekly oscillations. The diurnal oscillation signal is negligible.

In contrast, the primary oscillation period of the wind is 12 and 20 days in 2011. Secondary oscillations were 6.8, 5.5 and 4.1 days. As a result, the synoptic (20 days) oscillation is prevailing in the basin followed by weekly and 4.7 days oscillations. The spectral analyses suggest that internal waves are forced by the wind.

The spectral analyses (Figure 2.12) shows some interannual variability in the wave oscillation periods that can be associated to variability of the external stimuli such as the wind and the surface net fluxes. Looking at the stratification period at LAG01 in better details for the year of 2010 (Table 2.2), it appears that the oscillation period gets larger

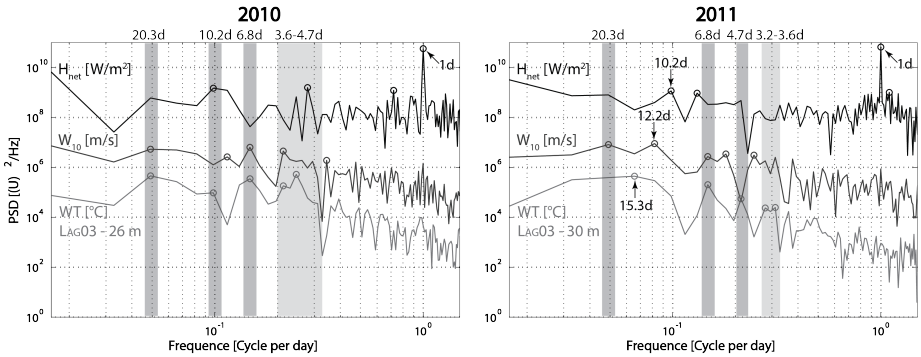

Figure 2.12. Power spectral density (PSD) for wind velocities along the lake axis, net heat fluxes and water temperatures measured at LAG03 (at 26 m depth in 2010 and 30m in 2011) for the months of July and August in 2010 and 2011. Periods superior two months are smoothed out from the water temperature time series.

in August and the average power associated with these oscillations increases from July to August at all depths except at 11.5 and more particularly 21.3 m where the power decreases by half and the oscillation periods shorten. The thermistors located at 50 and 60 m depth show that the average power associated to these oscillations triples at these depth.

Table 2.2. Five main oscillation periods (T) resulting from the spectral analysis of the thermistor data at station LAG01 and their associated average power (AVPWR) for the months of July and August 2010

	July 2010		August 2010	
Depth [m]	T [days]	AVPWR [°C^2/Hz]	T [days]	AVPWR [°C^2/Hz]
1.5	4.7, 1.8, 2.8, 1.0, 1.4	0.25	14.2, 4.7, 1.3, 1.8, 0.7	0.4
11.5	7.1, 2.8, 2.0, 1.1, 1.3	0.21	14.2, 4.7, 2.8, 1.0, 0.7	0.19
21.3	2.8, 14.2, 2.0, 1.2, 1.6	0.13	4.7, 1.0, 1.6, 2.4, 1.3	0.06
31.1	1.8, 2.8, 7.1, 1.0, 1.3	0.07	7.1, 2.4, 1.6, 1.0, 1.3	0.1
40.6	1.8, 14.2, 2.8, 1.4, 0.7	0.04	7.1, 2.8, 1.6, 1.0, 0.7	0.11
50.4	4.7, 14.2, 2.4, 1.4, 1.8	0.04	14.2, 4.7, 2.8, 1.8, 1.0	0.12
60.3	4.7, 14.2, 2.4, 1.6, 0.5	0.04	14.2, 4.7, 2.8, 1.8, 1.2	0.17
78	4.7, 2.8, 1.6, 0.8, 1.2	0.02	7.1, 1.4, 2.4, 1.8, 1.1	0.05

Figure 2.13A presents the strength of the stratification measured as the Brunt-Väisälä frequency N (s^{-1}) at the central 80 m deep station LAG01 during the summer stratification period 2010. It shows that the water column was continuously weakly stratified ($N^2 \approx 10^{-5}$ s^{-2}) until DOY 195. After that a thermocline started appearing at about 10-12 m depth, reflected by the local increase in the N^2 value. This thermocline region widened and became stronger, reaching values of $N^2 \approx 7\times10^{-5}$ s^{-2}, which is still considered weak stratification. Three different layers can be distinguished: a 8 m

narrow epilimnion at the surface, a 22 m thick metalimnion and a deep hypolimnion from 30 m depth to the bottom. Considering again the results from table 2.2, the average power can be related to temperature changes at the discussed depth and frequency and therefore can be related internal wave amplitude in the basin. However, the stronger the stratification, the smaller the wave amplitude associated with temperature changes. Hence,a decrease of the average power associated to a strengthening of the thermal stratification between 8 and 30 m depth defined as the metalimnion suggests a even further decrease of the internal wave amplitude. A large increase of average power is observed where the stratification is the weakest (50-60 m depth), which can be related to both a relative increase of the stratification as well as an increase of the internal wave amplitudes.

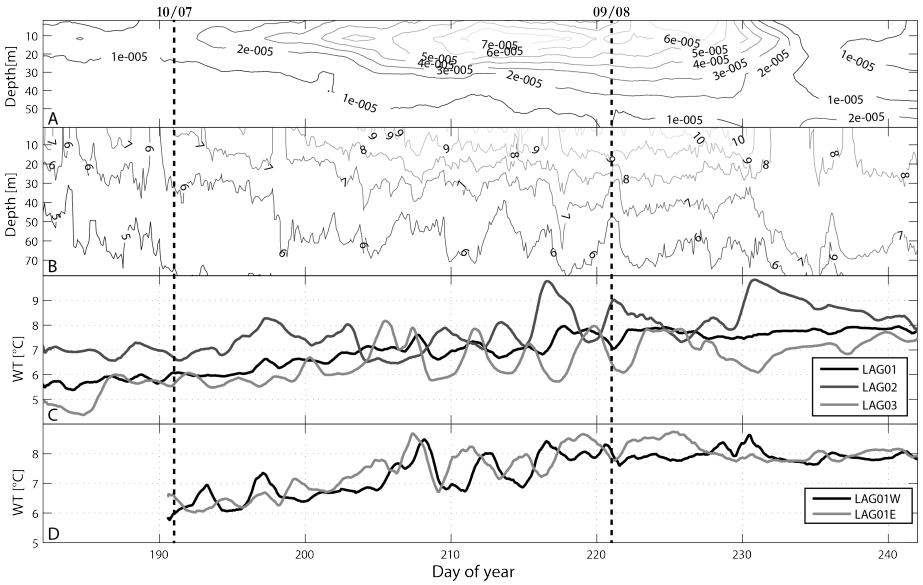

Figure 2.13. Temperature measurements in Lake Lagarfljót during the stratification period, summer 2010. A) Water column stability (N^2 in s^{-2}) smoothed over 7 days. B) Isotherms at LAG01. C) Temperatures recorded along lake thalweg at respectively 21m (LAG01, LAG02) and 26 m depth (LAG03), smoothed over 1 day. D) Temperatures recorded across width of lake at LAG01 at respectively at 21-22 m depth, smoothed over 1 day. The dotted lines indicate the dates of multi-parameter surveys represented in Figure 2.15.

Representing the measurements from the thermistors in an isothermal plot (Figure 2.13B) allows a better visualization of the oscillation periods and amplitudes of the internal waves. Weakly stratified waters are associated with larger oscillations, in terms of amplitude as well as period. This is apparent by considering the larger oscillations before DOY 200 and after DOY 230 when the lake was weakly stratified. During the peak stratification period where the oscillations in the 6°C isotherm at 60 m depth were 20 to 30 m peak-to-peak.In comparison, the amplitudes of the 8°C isotherm at 20m

depth were 6 to 10 m peak-to-peak.

From around DOY 200, second (possibly third) vertical mode waves clearly started to appear (see isotherms 6 and 7°C that are at times in quasi antiphase), suggesting high oscillation modes at least in the vertical direction (MÜnnich et al., 1992; Gómez-Giraldo et al., 2006).

Spatial variability The plot of synchronous water temperature recorded at about 20 m depth at the three stations along the basin (Figure 2.13C) shows that the oscillations have slightly different periods and are out of phase with one another. The oscillations recorded at the two ends of the lake (LAG02 and LAG03, Figure 2.1) were almost exactly in anti-phase with one another. The temperature oscillations at LAG01 have the smallest amplitude and the temperature measurements are consistently between those of LAG02 and LAG03. This suggests that LAG01 is located close to a node whereas LAG02 and LAG03 are anti-nodes. The existence of a seasonal horizontal gradient is evidenced over the summer period by water temperatures at 20 m depth greater at LAG02 by about 0.7 and 1.2°C than at LAG01 and LAG03 respectively. This is discussed in greater details below.

Figure 2.13D) shows the water temperature measured across the basin at LAG01W, LAG01 and LAG01E at about 30 m depth. The temperature oscillations at these three locations were out-of-phase, revealing lateral variability or tilting of the isotherms. Temperatures at LAG01W and LAG01E were almost in anti-phase, indicative of transverse oscillations.

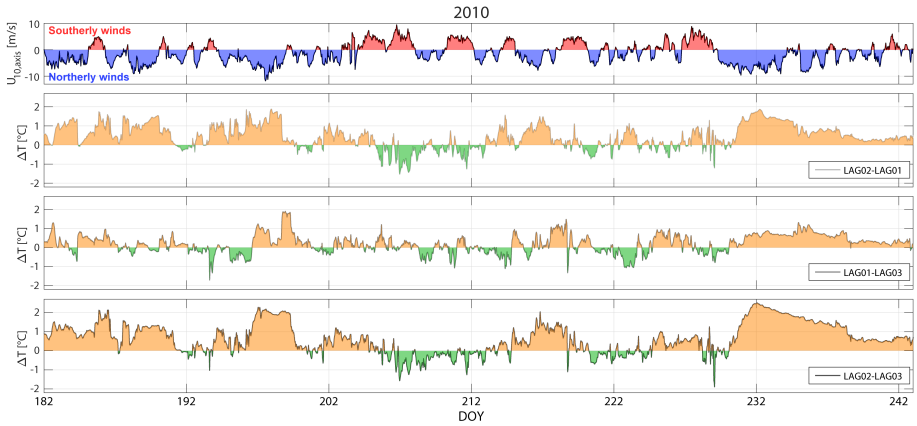

Figure 2.14. Wind velocity (A) and surface water temperature gradients (B, C, D) along the lake axis. Water temperature gradients are smoothed over an hour to be with results comparable to the wind.

A seasonal horizontal gradient is observed at 20 m depth along the talweg, this gradient is also observed in the surface temperatures. Figure 2.14 shows the horizontal water surface temperature gradients between the three stations located along the thalweg in the main basin and the wind forcing along the lake axis. Color coding is used to ease the reading of the plot, with blue color associated with wind from the North and

red wind from the South and similarly, orange and green associated with temperature gradients positive and negative towards the south, respectively.

Mean surface temperatures are 0.4 and 0.6°C colder at LAG01 and LAG03 than LAG02 over the summer period (day of year 182 to 243). Several forcing factors can come as an explanation of this seasonal horizontal water temperature gradient: the differential heating with air temperatures being recorded to be in average 0.5°C larger at Hallormstaður than at Egilsstaðir Airport, the wind forcing that can promote horizontal gradients through downwelling-upwelling and the river inflow entering the lake at the southern end (discussed in section 3).

The gradients between stations LAG02-LAG01 and LAG02-LAG03 are most similar and present a lag with the wind along the axis of 16 and 11 hours respectively, however the gradient LAG01-LAG03 show a very different oscillation pattern and the time lag found with the wind is 51 hours. This indicates that the wind events from the North are resulting in downwelling in the southern end of the basin. However, the wind could be forcing more than a simple basin-scale seiche, and higher horizontal modes are suggested by surface temperature measurements between DOY 194 and 200: while a positive gradient is present simultaneously between LAG01 and LAG02 and LAG03 and LAG02, the temperature gradient between LAG01 and LAG03 is negative part of the time, with colder temperatures being measured at more central station LAG01.

Higher vertical and horizontal modes The long term deployments discussed in the previous figures (Figure 2.13) hinted the presence of higher modes oscillations in the basin. The sonde vertical profiles provide a better spatial resolution to observe and identify the modes. Figure 2.15 displays isotherms along the thalweg of lake Lagarfljót in July and August on two different summers: cold 2011 (left panel) and warm 2010 (right panel). The wind directions on measurement days were mostly from the North (see details in Figure 2.15). The location of the profiles, identified by crosses, were doubled in 2011.

July 2011 (Figure 2.15A and E) has the scenario with the weakest stratification ($\Delta T \sim$ 2°C and N^2=0 to 2.5x10^{-5}). Three vertical layers can be defined (see black isolines). The top layer is a 5 to 10 m thick surface layer with temperatures of 6-6.5 °C. The central metalimnion starts wide, reaching down to 70 m depth, and compresses to 20 m towards the northern end of the lake. Once it reaches the sill, the isotherms expand again twice and compress once in between. This suggests a V2H3 internal wave. The bottom layer is characterized by uniform temperatures around 4.2°C. The increase in temperatures near the bottom represents the river signal entering the lake, which, at this time of the year, plunges towards the bottom.

In July 2010 (Figure 2.15A and C), the stratification was slightly stronger ($\Delta T \sim$2.6°C and N^2=0.2 to 1.4 x 10^{-5})). Three different water layers were also observed. The surface layer was deeper than in 2011 and tilted towards the southern end (x=0). Again, the metalimnion expands and compresses at least 2 to 3 times. This supports the 2011 findings of a V2H3 oscillation mode or higher.

For both measurement periods occurring in July was the wind blowing from the North; in both case, water temperature measurements suggest the presence of upwelling (rising of deeper colder water to the surface) at the northern end of the southern basin and downwelling (accumulation and sinking of the warmer surface water) at the southern

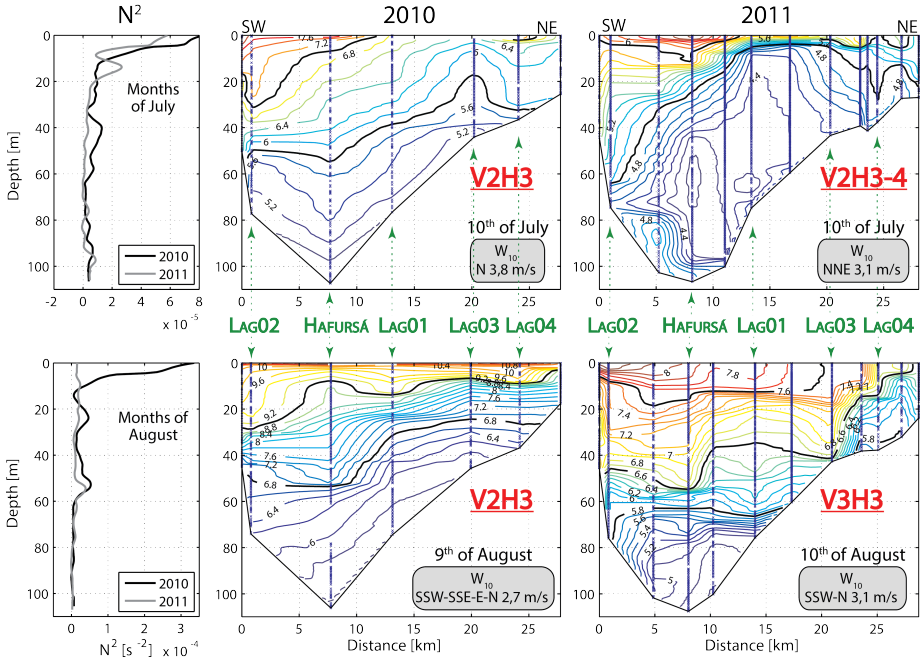

Figure 2.15. N^2 at Hafursá in A) July and B) August 2010 and 2011 and C) to F) associated longitudinal cross-sections (SW end at location 0 to NE end at location 12) of the temperatures in Lagarfljót recorded by the sonde in 2010 (left panel) and 2011 (right panel). The blue crosses represent the location of the actual measurements, in black, some isotherms are emphasized and in green some known locations the lake are indicated by green arrows.

end of the basin.

In August 2011 (Figure 2.15 B and F), the stratification was stronger ($\Delta T \sim 4°C$ and N^2=0.5 to 3.5x10^{-5}). Four layers are outlined in the figure. The surface layer, with temperature from 7.5 to 8.3 degrees, is thickest in the center reaching a maximum 20 m depth. The second layer is on average 30 m thick and upwells in the north end. The layer does not compress and expand as strongly as observed in July 2010 and 2011. The third layer, located at 50 to 70 m depth in the northern end (x=0 m), however compresses and expands significantly at least twice. The area around the sill generates a discontinuity in the internal wave pattern, leading to what looks like a 20 m high hydraulic jump. The presence of four layers may indicate a third vertical mode, the horizontal modes are at least 3 (similar to July).

In August 2010 (Figure 2.15 B and D), the vertical thermal gradient in lake Lagarfljót has reached 7°C and N^2 is of the order of 0.5 to 5 x 10^{-5}. Three distinct water layers are present and the epilimnion has deepened and is clearly visible along the whole basin.

Plotting all the sonde measurements performed the same day allows the definition

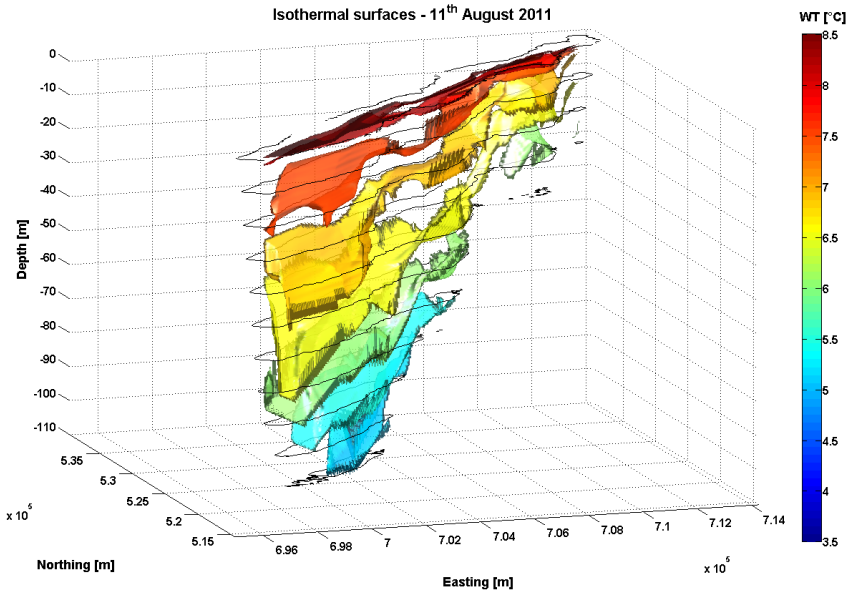

Figure 2.16. Isothermal surfaces interpolated from the sonde profiles measurements performed on the 11th of August 2011. The isothermal surfaces are defined for every 0.5°C, from 8.5°C for the upper surface. The black lines delineate the lake bottom.

of isothermal layers in the basin of lake Lagarfljót (Figure 2.16). This plot shows that the layers are tilted laterally in the basin. This supports the findings from the current components analyses (Figure B.9), that the waves do not simply travel up and down the longitudinal axis of the lake.

2.3.3 Coriolis effects on Lake Lagarfljót

Looking at the sequence of oscillation from DOY 210 to 220 on Figure 2.13 C and D, an anti-clockwise rotation of the tilting emerges, suggesting Kelvin waves (Hutter et al., 2011).

The Burger number is computed according to the method used in Vidal et al. (2005) (see 2.2.2). Considering two basin lengths of 27 km (whole lake) and 20 km (southern basin) and width of 2.5 km at latitude 65.18°N, internal waves with a period superior to 1.3 to 1.8 days will be significantly affected by the Coriolis forces(Figure 2.17).

The inertial period is found to be about 13h, which suggests that the presence of Poincaré waves in the basin is unlikely because rotational effects are so small for waves periods below 16.8 h to 1 day. However, Kelvin waves can be expected.

Figure 2.18 shows a rotary spectra of the bottom currents in August 2010 and August 2011. Kelvin waves can be denoted by the presence of increased energy of the counter-clockwise component. The energy in the clockwise and counter-clockwise directions are similar, suggesting that there is no preferential rotating direction. This

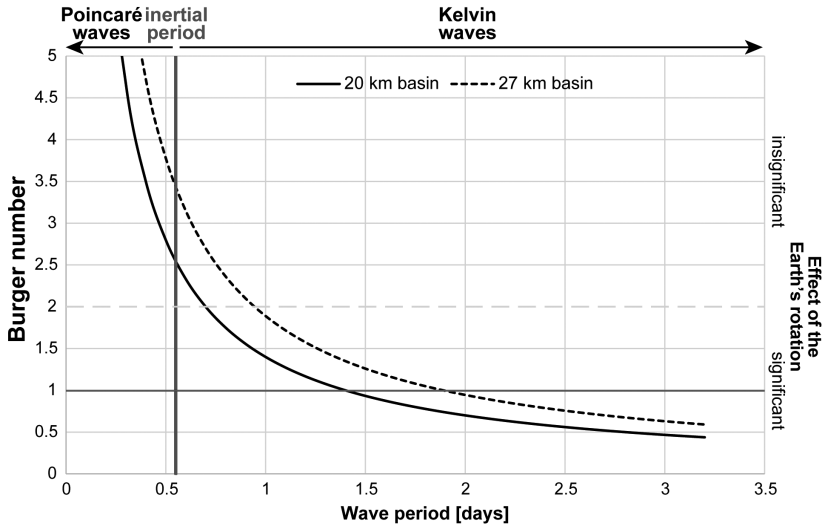

Figure 2.17. Burger number as a function of the internal wave period in Lake Lagarfljót, computed for the whole lake (27 km) and the southern basin (20 km). The inertial period delimits the periods at which the two gravity (Poincaré and Kelvin) waves are important. The gray dash line defines the value 2 of the Burger number over which rotational effects can be considered negligible.

analysis does not allow us to discriminate the type of gravity waves present in the basin nor their associated period.Surface currents tracked on day 222 (August 10^{th} 2011) in the southern basin suggest a counterclockwise rotation in the top layers (Figure C.11), but these measurements are too limited in time to be deemed sufficient to demonstrate the presence of Kelvin waves.

Correlation of the water temperatures measured at 30 m depth around the lake shows high correlation associated with a phase lag between stations suggesting a counterclockwise rotation of the wave for oscillation periods of 4.4 days. This counterclockwise rotational motion of waves at sub-inertial frequencies is consistent with a Kelvin wave.

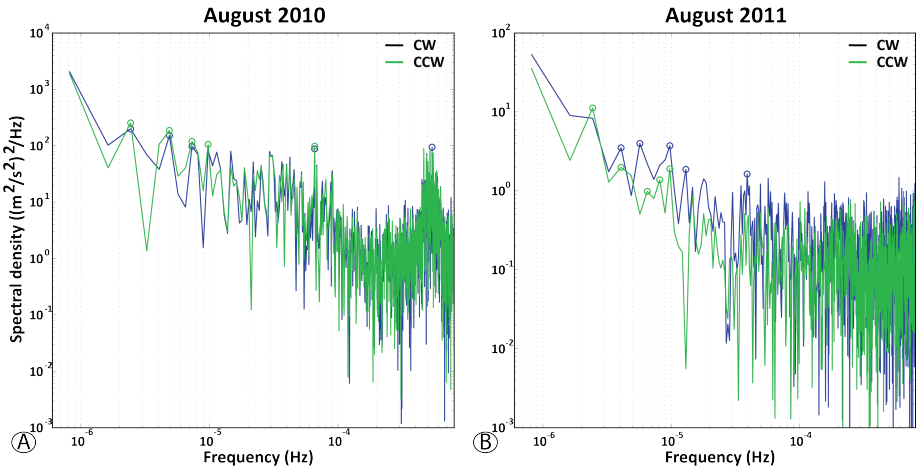

Figure 2.18. Rotary spectral analysis of bottom currents at LAG03 W in August 2010 (A) and LAG04 in August 2011 (B). It can be expected that clockwise motions are associated with Poincaré waves while counter clockwise motions are associated with Kelvin waves.

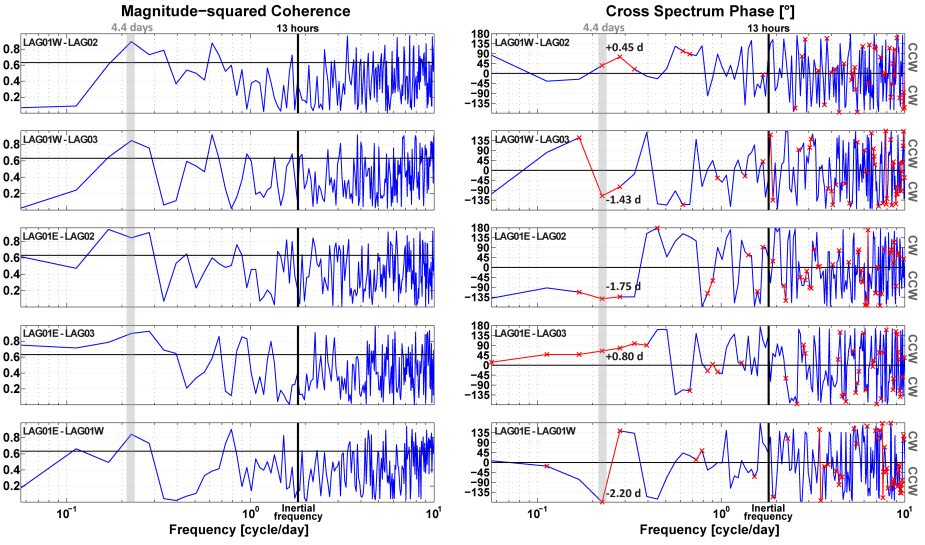

Figure 2.19. Coherence and phase of temperatures measured at 30 m depth at stations around the lake during summer 2010 (days 191 to 262). The seasonal trend is smoothed out to remove oscillations with period greater than 21 days.

2.4 Summary

Field data from 2010 and 2011 show that summer stratification lasts roughly 100 days and reaches a maximum at the end of July-early August. Null to negative heat fluxes

and strong NNE wind events trigger mixing in the water column.

Measurements during the winter season shows that mixing is not complete throughout the water column until late in the winter and bottom temperatures close to the river inflow and in the deepest section behave singularly until the water column experience complete overturn and inverse stratification builds up. Bottom temperatures drop to almost 0°C.

Vertical profiling throughout the lake shows that the wave regime is complex, and higher vertical and horizontal modes are observed during both summers. Large tilt of the isotherms are observed in the basin : internal waves with peak-to-peak amplitudes in the order of 30 m are recorded at station LAG01 and large upwelling occurring in the northern end of the southern basin are associated to wind forcing from the North.

The main periods of oscillation of the internal waves are very close to the periods of the wind velocity along the lake axis suggesting that the wind is a strong forcing agent of these internal motions. It is, though, difficult to define if there is resonance between the wind forcing and the internal waves or if these waves are strictly forced motions.

Isotherms tilted laterally across the width of the lake, both during continuous recordings at LAG01W and LAG01E as well as during discrete temperature profiling of the lake. This suggests that the internal waves are affected by Earth rotation. The Burger number for Lake Lagarfljót indicates that internal waves with periods longer than 1.8 days are significantly affected by the rotation of the Earth and therefore likely to be Kelvin waves; Poincaré waves on the other hand, with period below the inertial period (13 h), are therefore not expected to be preponderant in the basin according to that first estimate. A three dimensional view of the isotherms support the notion of Kelvin waves. The rotational spectra of bottom currents were not conclusive, showing not prominent direction of rotation but the cross-spectrum analysis shows a strong coherence at 4.4 days oscillation period associated with phase lags congruous with a kelvin wave.

The residence time in Lake Lagarfljót is estimated to be now half a year which is fairly short for a lake of that size. It is therefore expected that the river inflow influence on the internal motions of the lake is non negligible. In addition, the largest tributary is a glacial river feeding the lake at its southern end and has the particularity to have a high suspended sediment content.

3 Hydrological characteristics of Lake Lagarfljót

Lake Lagarfljót is often mistaken for a large river due to its elongated shape. Strictly speaking, Lagarfljót is the name for the lake and the outflowing river, "fljót" being a large river flowing towards the sea or possibly a lake. Lögurinn is the name sometimes used to identify the lacustrine section of Lagarfljót.

In Chapter 2, in-lake measurements are analyzed as if Lake Lagarfljót was an enclosed basin. Some of its tributaries are mentioned briefly but not considered in the analysis. However, part of the originality of the lake can be attributed to the diversity of streams and rivers within its catchment. Many of features in the measurements cannot be explained solely with the meteorological forcings. It is therefore crucial to take a better look at the nature of this catchment to understand the possible impacts the different inflows may have on the internal motions present in the lake.

In a first section, we will describe the catchment, focusing on the main tributaries of the lake; in a second section, we will consider more closely the suspended sediments present in these inflows and finally, in a third section, measurements and observations will analyzed to obtain evidence of the river signal within the lake.

3.1 Watershed characteristics

Lake Lagarfljót drains a 3616 km^2 large watershed, about a third of it encompasses part of the largest and most voluminous Icelandic glacier Vatnajökull and more than half of the catchment (2342 km^2) enters the lake by it southern end (Figure 3.1). In all, nearly twenty streams and rivers enter the lake along its course.

The river inflow is primarily glacial waters feeding the lake at its southern end. Freshwater tributaries run down the surrounding mountains into the lake all along its path, the largest of them being Grímsá river. The flow rate and temperatures of the largest rivers are monitored by the Icelandic Meteorological Office and Landsvirkjun. Monitoring of smaller freshwater streams is often discontinuous over the years for flow rates and/or water temperatures, sometimes nonexistent.

Figure 3.1. Delimitation and surface area of the different parts of the watershed of Lake Lagarfljót. Source : Landsvirkjun.

3.1.1 Southern glacial and freshwater inflows

Figure 3.2 shows measurements of three types of rivers that enter the lake in its southern end: natural rivers, spring (Fellsá and Kelduá) and glacial (Jökulsá í Fljótsdal) and a dammed (glacial) river, Jökulsá í Dal (Kárahnjúkar). There are significant differences between the regime of these rivers, in terms of flow rates and temperatures.

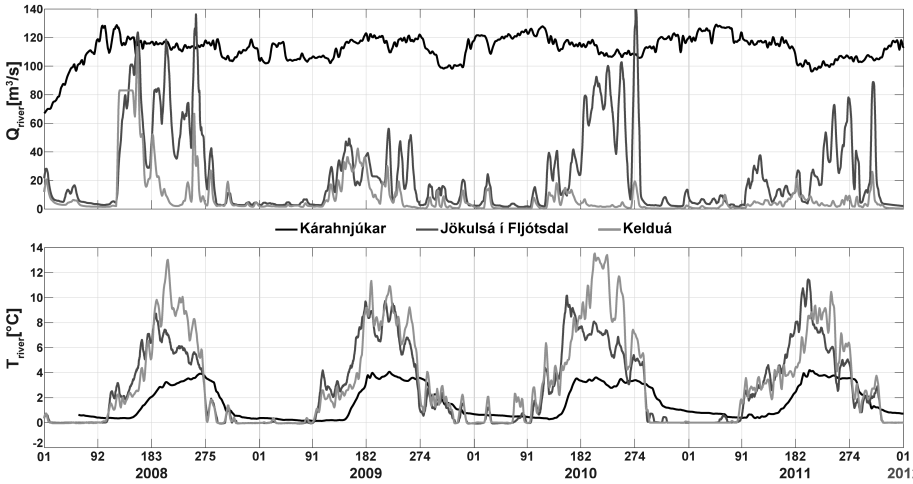

Figure 3.2. Water discharges (up) and temperatures (down) of some Lake Lagarfljót tributaries for years 2008 to 2011.

The natural spring rivers experience two flow rate peaks: the first peak occurs at the end of June beginning of July (spring thaw), the second one at the end of the summer (September-October), it can be connected to the autumnal increase of precipitation.

The natural glacial river presents these two peaks but, in addition, shows a third peak during the summer due to the melting of the ice cap. While the water temperature in these rivers are similar between the two common peaks, it drops significantly in the glacial river during the ice melting period.

The dammed glacial river has a completely different behavior, it presents a high quasi-constant flow rate (at around 110 m^3/s) and much lower temperatures (with a range of fluctuations of 4°C); the temperatures increase later in the summer season but remain lower than the temperatures measured in the natural rivers for the fall period and early winter.

3.1.2 Freshwater rivers - Grímsá

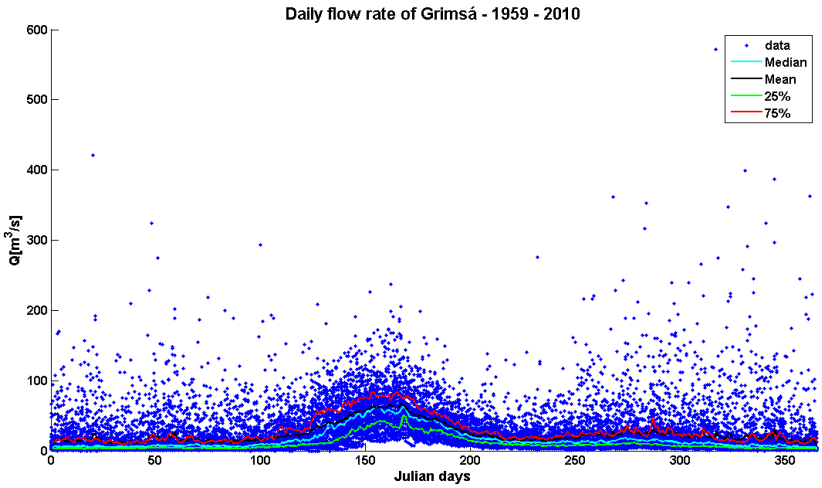

Figure 3.3. Flow rates recorded at Grímsá river between 1959 and 2010.

Grímsá river flows in Lake Lagarfljót in the shallower southern basin with an annual mean discharge of 24,2 m^3/s (Figure 3.3). The maximum mean flow rate is observed mid-June (66,8 m^3/s on DOY 167) and the minimum end of December (8,4 m^3/s on DOY 365).

Figure 3.4 compares the water temperatures measured in Grimsá river and the air temperatures recorded at Egilsstaðir airport. In summer 2011, the river temperatures were colder than in summer 2012. The measurements also show that the river was at freezing point (or frozen) for about three months during the winter. Water and air temperatures are closely correlated.

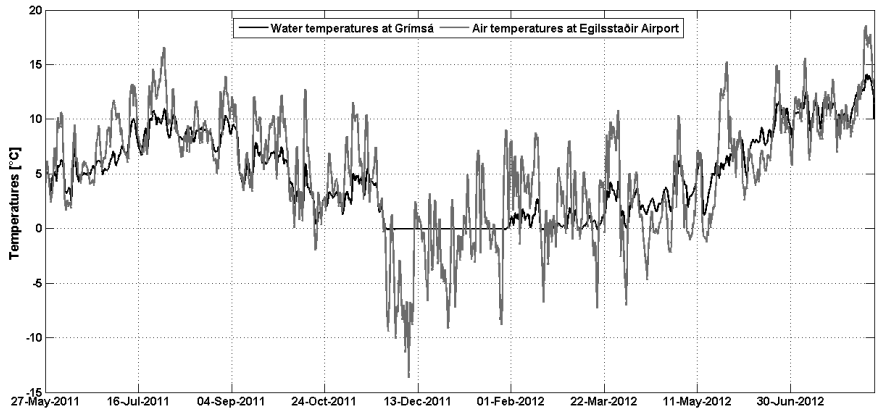

Figure 3.4. Water temperature measured in Grímsá river and associated air temperature measured at the nearest weather station (Egilsstaðir Airport).

These water temperature measurements are rather limited in time, however Orkusalan, which is managing Grimsá hydroelectric power plant, has unprocessed water temperature measurements for the river. Figure 3.5 shows that a simple linear regression gives a very good correlation (R^2=0.9921) between the measurements of Orkusalan and those of the University of Iceland. This suggests that the data of Orkusalan can be used to extrapolate water temperatures in Grímsá for a longer period of time.

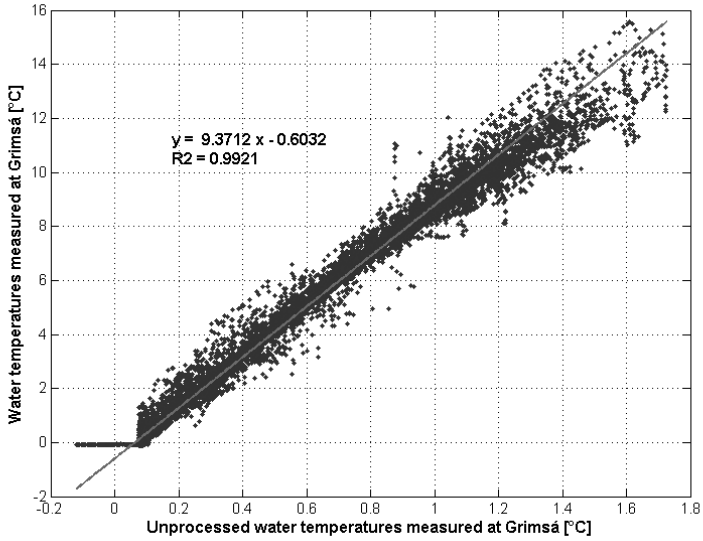

Figure 3.5. Correlation between the measurements performed in Grimsá in 2011 and 2012 by the University of Iceland and some unprocessed measurements in Grimsá performed by Orkusalan.

The water temperatures for Grimsá measured by Orkusalan present some temporal gaps. The correlation with two other rivers (the freshwater river, Kelduá and the glacial river, Jökulsá í Fljótsdal) monitored during the same period of time is tested (Figure 3.6). Good correlations are found with the two rivers, the best fit being associated to Kelduá (R^2=0.9780).

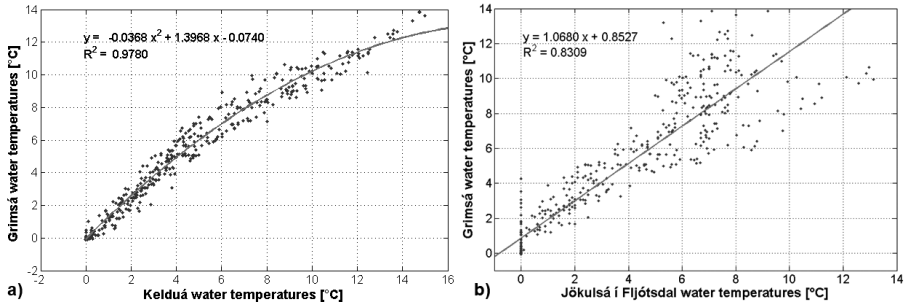

Figure 3.6. Correlation between the measurements performed in Grímsá in 2011 and 2012 by the University of Iceland and water measurements performed by Landsvirkjun a) in Kelduá and b) in Jökulsá í Fljótsdal.

The gaps can, therefore, be filled with extrapolated obtained from Kelduá's relationship (Figure 3.7).

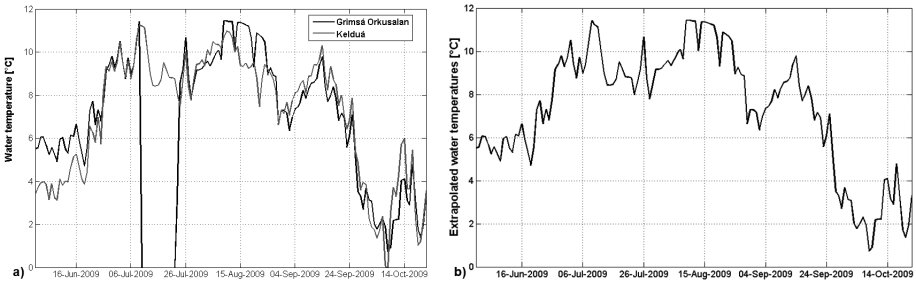

Figure 3.7. Extrapolation of water temperatures in Grímsá based on a) the correction of measurements performed by Orkusalan (blue line) and the relationship found with Kelduá (green line); b) the correction of measurements performed by Orkusalan bridged using the results from the relationship with Kelduá.

3.1.3 Other tributaries to Lagarfljót

Lake Lagarfljót has a multitude of other tributaries (Figure D.15), mostly freshwater (spring and run-off) that enters the lake all along its course (Figure 3.8).

Figure 3.8. Aerial picture of Lake Lagarfljót taken in June 2010. On the right hand-side, freshwaters coming from small tributaries and entering the lake are clearly visible due to their dark blueish color contrasting with the gray color of the lake.

To estimate the specificities of the streams measurements were performed in the largest and most accessible streams, in total 12 streams and rivers were investigated (Figure 3.9). A multi-parameter sonde (Ysi 6600) was used to collect water temperatures. In addition, a simple flow rate estimation technique (using a float, a stop watch and some rough estimate of the volume of water present in the portion of channel navigated by the float) was employed to evaluate the significance of each streams relatively to others.

Table 3.1. Water temperatures and flow rates of some of the tributaries of Lake Lagarfljót - July 2011.

Name	WT [°C]	Q [m^3/s]
Höfðaá	11.33	0.28
Unalækur	9.65	0.30
Urriðalækur	10.47	0.26
Kaldá	6.88	0.57
Grimsá	7.24	37*
Hafursá	7.27	0.97
River 7	8.32	0.02
Þorleifará	13.05	0.72
Ormarsstaðaá	12.08	1.95
Stream 10	10.97	0.42
Hrafnsgerðisá	15.44	NaN
River 12	10.18	0.19

* daily mean for Grímsá for that day (daily median 31 m^3/s)

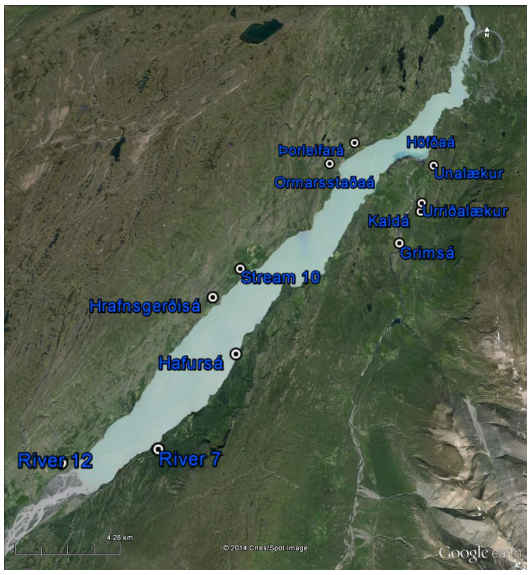

Figure 3.9. Map of tributaries investigated around Lake Lagarfljót. In blue, the name of rivers when known, the white and black dot indicates the exact location of measurements performed.

Urriðalækur and Kaldá are two tributaries of Grimsá, they enter that larger river just before it flows into the lake. Table 3.1 present a summary of the main results. There is no evident relationship between the flow rates associated with the streams and the water temperatures. The largest flow rate measured was 1.95 m^3/s for Ormarsstaðá. These measurements reveal that these minor tributaries have an unsignificant discharge when compared to Grimsá and Jökulsá rivers.

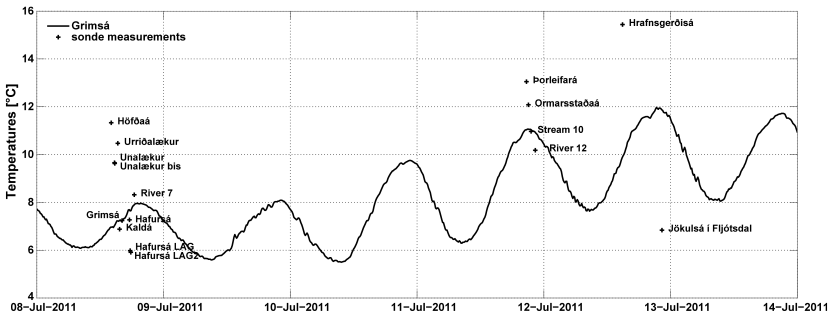

Figure 3.10. Water temperature measurements at Grímsá (Star Oddi temperature meter) and at other (minor) affluents (multi-parameter sonde) of Lake Lagarfljót. In addition, two measurements were performed directly in the lake, at the mouth of Hafursá.

Figure 3.10 shows that water temperatures in these freshwater tributaries vary by 5°C. Hafursá and Stream 10 have the water temperature closest to the one measured

in Grimsá river. Jökulsá í Fljótsdal is by far the coldest tributary, being about 5°C less than Grimsá river.

3.2 Suspended sediments in the greater catchment

3.2.1 Density of the particulates

The sediments are originating from the Vatnajökull glacier and are very fine till. Limited information are available about till density in Iceland. The average value of the density of suspended sediments in Icelandic river is found to be around 2.8 g/cm^3, the average value for Jökulsá í Fljótsdal is slightly lower and closer to 2.7 g/cm^3 (Pálsson and Vilmundardóttir, 1983, 2003). According to Striberger et al. (2011), most of the sediments or rock flour brought by Jökulsá í Fljótsdal stays in suspension in the water in the summer and deposit during the winter time when the river discharge is low and the lake is protected from the wind action by an ice cover. Sediments brought by Grimsá river are coarser and hence deposit soon after they entered the lake, they do not contribute to the density of the water column.

3.2.2 Grain sizes and settling velocity

Sediments in suspension have a settling velocity dependent on the grain size, it is therefore important to identify the type of grain size present in lake Lagarfljót. The glacial rivers Jökulsá í Fljótsdal and Jökulsá á Dal (Hálslón) are the main contributors in the sediment inflow in the lake.

Table 3.2. Grains size distribution in Jökulsá í Fljótsdal and associated settling velocity.

Grain size and distribution in Jökulsá í Fljótsdal (Harðardóttir and Þorláksdóttir, 2004)				
< 0.002 mm Fine clay	0.002-0.02 mm Clay to fine silt	0.02 -0.06 mm Medium to coarse silt	0.06 -0.2 mm Very fine to fine sand	>0.2 mm > fine sand
18-27%	34-46%	21-29%	10-14%	<4%
Associated settling velocities (quartz, 20°C – spheres, (Gibbs et al., 1971)) Wentworth grain size chart				
<0.00036 cm/s	0.00036-0.023 cm/s	0.023 – 0.329 cm/s	0.329-3 cm/s	>3 cm/s

More than 50% of the grains are smaller than 0.02 mm to which the maximum associated settling velocity is 0.023 cm/s (Table 3.2).

According to the report from Pálsson and Vilmundardóttir (2003), Jökulsá í Fljótsdal has the finest sediment content of all the rivers sampled. Sediments with a grain size superior 0.02 mm represent less than 30% of the sediment content.

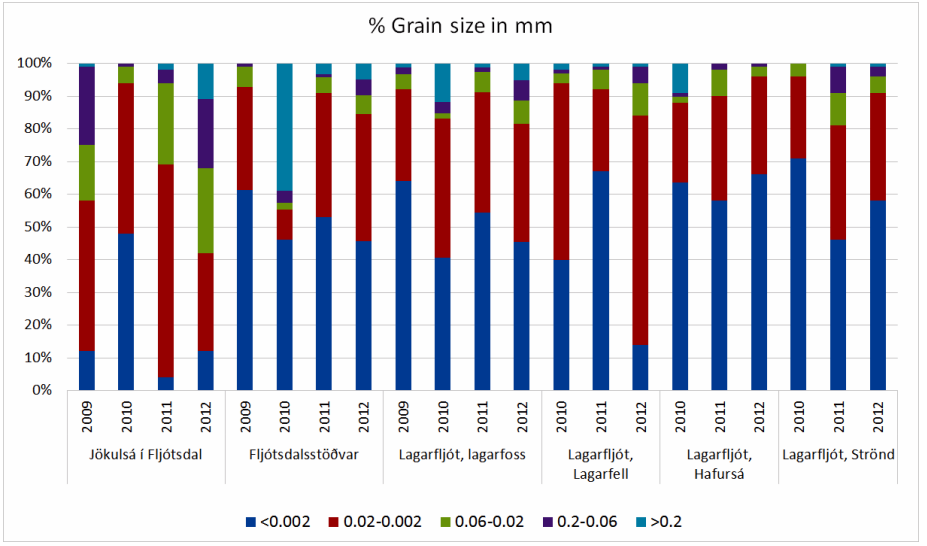

Figure 3.11. Minimum percentage of fine suspended sediments observed in Jökulsá í Fljótsdal and Lake Lagarfljót over years 2009 to 2010 (Þorláksdóttir et al., 2014).

Figure 3.11 shows the lowest percentages of fine sediments in suspension found during the different sampling sessions performed in 2009 to 2012 (several sampling per year). The lowest percentage of sediments smaller or equal to 0.02 mm (diameter) occurs in 2012 in Jökulsá í Fljótsdal. Then they represent only 42% of the sediments in suspension. In lake Lagarfljót, these fine sediments represent at least 80% of the sediments in suspension. This high ratio is not too surprising as the samples are taken at the surface of the lake.

Settling velocity Knowing the size distribution of suspended sediments in the inflowing allows us to estimate the settling velocity of the sediments once in the lake. The mean size of the grains is calculated according to the methods described by (Kamphuis, 2000, p. 285):

$$M_\phi = \frac{\phi_{16} + \phi_{50} + \phi_{84}}{3} = \frac{12+6+4}{3} = 7.3$$

with $\phi = -log2(D)$ and D the grain diameter. This corresponds to a mean grain size of approximately 0.006346 mm. The settling velocity ω_f can be then computed (Hemond and Fechner-Levy, 2000, p. 95)

$$\omega_f = \frac{(2/9).g.(\rho_s/\rho_f - 1).r^2}{\eta_f}$$

with

- ω_f the settling velocity in cm/s
- g the acceleration due to gravity = 981 cm/s^2

- ρ_s the density of the spherical particle = 2.7 g/cm^3
- ρ_f the density of the fluid = 1g/cm^3
- r the radius of the particle in cm
- η_f the kinematic viscosity of the fluid = 0.0147 cm^2/s (at 6°C)

Therefore, $\omega_f = 0.0025 cm/s$: in other words, in completely still water, sediments in the lake would take approximately 111 hours or 4.6 days to travel 10 m down.

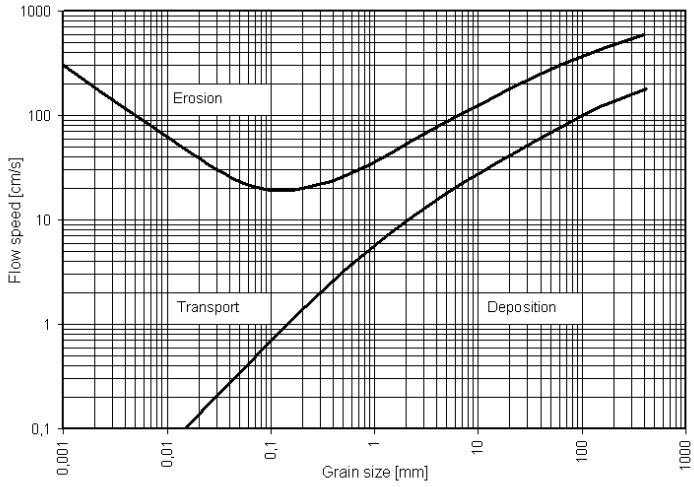

Figure 3.12. Hjulström curve. Source: wikipedia

In 2010 and 2011, mean bottom currents were exceeding 1.5 cm/s (Figure C.1), which suggests that particles with grain size smaller than 0.2 mm are not depositing (Figure 3.12): it is then possible to infer that most particles stay in suspension in the lake.

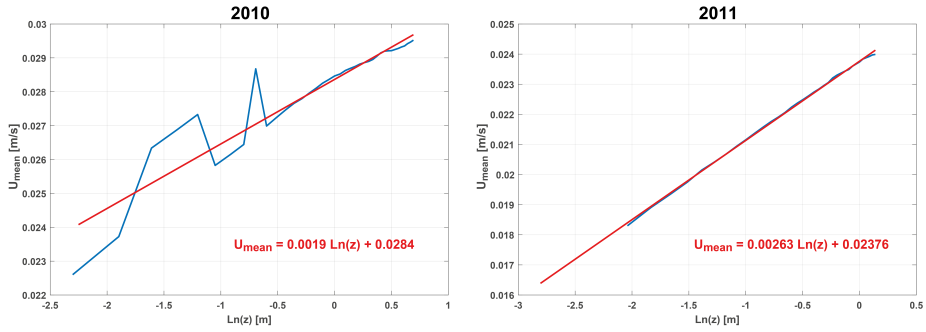

Figure 3.13. ADCP measurements performed at the bottom of Lake Lagarfljót at LAG03 in July 2010 and at LAG04 in August 2011.

The Rouse number $\beta = \frac{\omega_s}{\kappa u*_b}$ is used as a first approximation about the fate of suspended sediment in the lake. The time-averaged speeds within the bottom 1-2 meters boundary layer follow a characteristic log relationship (Figure 3.13). Building on the theory of a log-linear velocity profile near a fixed boundary, the near bed shear velocity, $u*_b$, was determined as the slope between U(z) and Ln(z), and is defined to be 0.19 cm/s in July 2010 to 0.263 cm/s in August 2011. The von Karman's constant, κ is 0.41. The Rouse number is estimated to be between 0.03 and 0.02 which suggests that the suspended sediment is transported as wash load.

3.2.3 Riverine sediment load relationships to discharge

Suspended sediments have a non-negligible contribution in the density computation and the river intrusions can introduce significant variations throughout the water column. Suspended sediment concentration C_{SS} are not monitored continuously in any of the tributaries of lake Lagarfljót, it is therefore necessary to estimate the suspended sediment content based on one of the available variables. Walling and Webb (1986) and Gislason et al. (2006, 2009) show that there is a good dependence between the river water concentrations and the river discharge, the variations follow a power law such as : $C = aQ^b$ where C is the concentration, Q the river discharge and a and b some constants describing the power dependence. Nevertheless, these relationships need to be considered with caution as Clifford et al. (1995) and Lawler et al. (1992) emphasize, as inter-annual, seasonal and even diurnal variations result in some considerable non-stationarity of the relationship.

For Jökulsá í Fjóltsdal (Hóll), a first relationship was found to be as follow:

$$log(SIM) = 1.99 logQ - 2.24$$

with SIM the total suspended inorganic particulate matter fluxes in Kg/s and Q the river discharge in m^3/s. The R^2 associated to that linear regression was 0.849.

This relationship was defined for data gathered between 1998 and 2003 (Gislason et al., 2009). However new data were acquired between 2004 and 2012 (Þorláksdóttir et al., 2014) leading to a slightly different relationship (Figure 3.14).

The coefficient of determination R^2 is quite high (0.9642) implying a strong correlation between the data. For the period between 2004 and 2012, the following relationship SIMF = 0.0223 $Q^{1.8732}$ should be assumed.

The second glacial river, Jökulsá á Dal, was diverted in 2008 towards Lake Lagarfljót when the Kárahnjúkar damming project started being effective. Measurements were performed ahead of the damming project and the following relationship between the sediment fluxes qs and the river discharge Q was established with an excellent correlation coefficient of 0.95 (Pálsson et al., 2000):

$$q_s = 0.000103 Q^{2.60}$$

with q_s in kg/s and Q m^3/s .

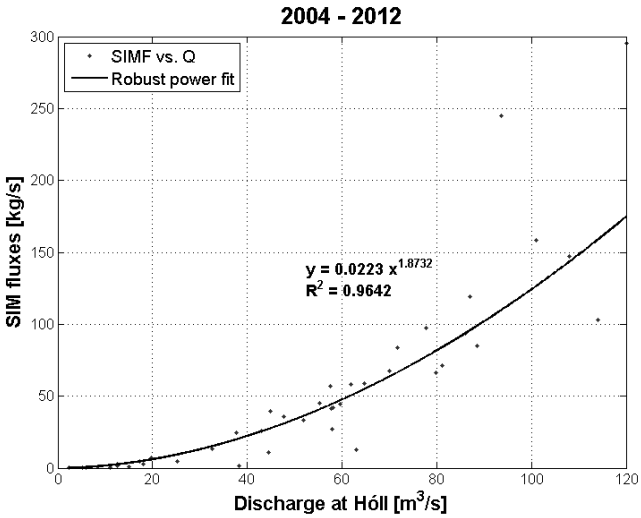

Figure 3.14. Robust (bisquare) power fit of the relationship between SIM fluxes (SIMF) against the discharge (Q) of Jökulsá í Fljótsdal (Hóll).

However, after the damming the water resides in a reservoir, Hálslón, before being diverted towards the turbines and Jökulsá í Fjóltsdal. Looking at sediment concentration measurements performed from 2008 in connection with the discharge of the diverted river show that there is little to no correlation between the two variables. It is therefore more relevant to look at statistical values such as the mean, the median and the standard deviation.

Grímsá is the largest freshwater tributary of Lake Lagarfljót. According to Gislason et al. (2009), the following relationship log(SIM)=1.32 log Q- 2.60 governs the sediment fluxes from that river in the lake, the linear regression however is of slightly lower quality with R^2=0.757.

In order to obtain the suspended sediment concentration from these equations, the following formula is applied $F = C \times Q$ with F the sediment fluxes in kg/s, C the suspended sediment concentration in kg/m^3 and Q the river discharge or flow rate in m^3/s.

3.2.4 Effects on water density

Sediments suspended in the water column affect the density of the water. The equation of state can be defined as :

$$\rho_W = \rho_T + \Delta\rho_{TDS} + \Delta\rho_{SS}$$

with ρ_W, the water density (kg/m^3), ρ_T the water density resulting from the temperature variations, $\Delta\rho_{TDS}$ the density increment due to total dissolved solids (kg/m^3) and $\Delta\rho_{SS}$ the density increment due to suspended solids (kg/m^3) (Ford and Johnson, 1983). The

contribution of the suspended sediment is estimated as :

$$\Delta\rho_{SS} = C_{SS}(1 - \frac{1}{SG}) \times 10^{-3}$$

with C_{SS} the suspended solids concentration (g/m^3) and SG the specific gravity of the suspended solids.

Hence, the contribution of the suspended solids in Lake Lagarfljót can be estimated to be

$$\Delta\rho_{SS,Lag} = (1 - \frac{1000\left(\frac{kg}{m^3}\right)}{2700\left(\frac{kg}{m^3}\right)})C_{SS}\ \left(\frac{kg}{m^3}\right) = 0.6296\ C_{SS}(kg/m^3).$$

3.2.5 Relationship between turbidity and sediment concentration

A very simple way to investigate the turbidity level throughout the water column is through the use of a turbidity sensor or nephelometer which gives a measure of the light scattering caused by suspended sediments. Turbidity, to have an environmental relevance, should, however, be calibrated against suspended sediment concentration or other measurements of the visual clarity (Davies-Colley and Smith, 2001).

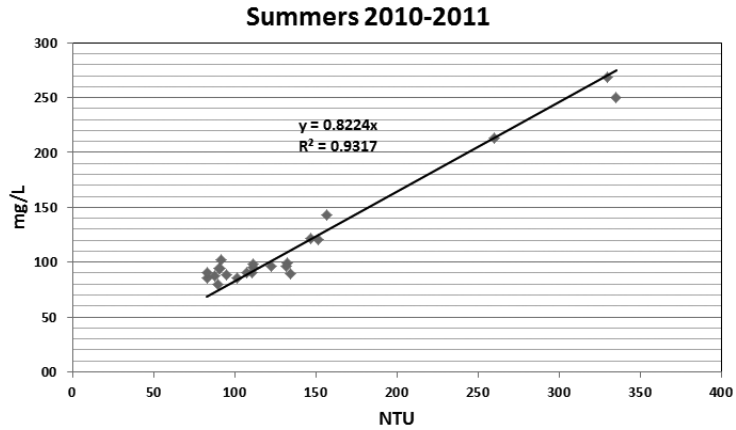

Figure 3.15. Linear regression between the turbidity (NTU) measured by the multi-parameter sonde and the total suspended sediment (mg/L) estimated from the sample analyses.

In summer 2010 and 2011, samples from the surface water of the lake and the main tributary were collected for total suspended sediment (TSS) analyses. The use of a Niskin bottle in 2011 (Figure D.13) allowed a complementary sampling of the water at 30 m depth in the lake. Nine samples were collected in 2010, 19 in 2011 (Figure D.14). They were analyzed with 20μ filters. The TSS measurements were correlated with optical turbidity measurements conducted with the multi-parameter sonde in order to establish the relationship between optical properties (in NTU) and suspended solids content (mg/L). TSS analyses are not as precise as SSC measures (Gray et al., 2000),

however the grain size distribution observed in Jökulsá í Fljótsdal (Table 3.2) suggests that the subsampling procedures should not affect significantly the results.

From TSS analysis of the water samples collected, a good linear relationship (1 mg/L = 0.8224 NTU with $R^2 = 0.9317$) between turbidity and suspended sediments was found (Figure 3.15).

As seen in Chapter 2, in-lake temperatures in Lagarfljót are close to the temperature of maximum density (3.98°C, see Figure 3.16) throughout the year, with maximum surface temperature around 10-11°C. The closer to the temperature of maximum density and the less the density gradient associated to temperature changes, thus a one degree change around 5°C results in a 16 g change of the density while around 7 and 9°C it will result in respectively 46 and 74.3 g change of the water density. Hence, the significance of changes in ionic strength or suspended sediment concentration of waters is greater near the temperature of maximum density.

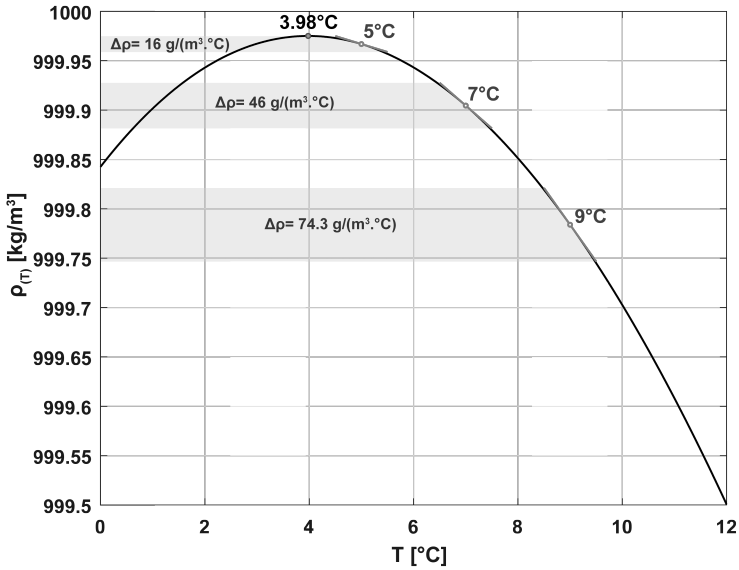

Figure 3.16. Temperature-dependent density of water. The maximum density is estimated to be 999.975 kg/m^3 for degassed Standard Ocean Water (Boehrer et al., 2010). Tangents to the curve show the rapid change of density gradient as the temperature rises above the temperature of maximum density (in red).

Maximum thermal gradients were observed to be close to 5 to 6°C in 2010 and about 4°C in 2011, so a change of 3°C from 5 to 8°C in the water column can a reasonable estimation of the gradient in the water column and would produce a change by 116 g/m^3 of the water density. Comparatively, a change of turbidity by 75 NTU would produce a change by 61,7 g/m^3 of the water density. In these condition, suspended sediments contribute approximately half as much to the water column stability as the temperature.

The contribution of suspended sediments to density will be particularly significant at the start of the stratification when the water column is quasi-isothermal and close to the temperature of maximum density.

3.3 River inflow signal in Lake Lagarfljót

Inflows intrude water bodies at the level of neutral buoyancy, where the density of the water body is the same as the density of inflowing river (Alavian et al., 1992; De Cesare et al., 2006; Laborde et al., 2010). In most cases, the density depends on temperature, but salinity gradients and differences in suspended sediment content can be significant enough to affect the intrusion point.

Thermistor and sonde measurements performed in 2010 and 2011 in Lake Lagarfljót present incongruities that can not be explained by the observed meteorological forcings, such as the temporary building up of stratification during the winter cooling period or inverse thermal stratification within the water column during the summer stratification.

3.3.1 Temporal variability of the intrusion depth using temperature as a tracer

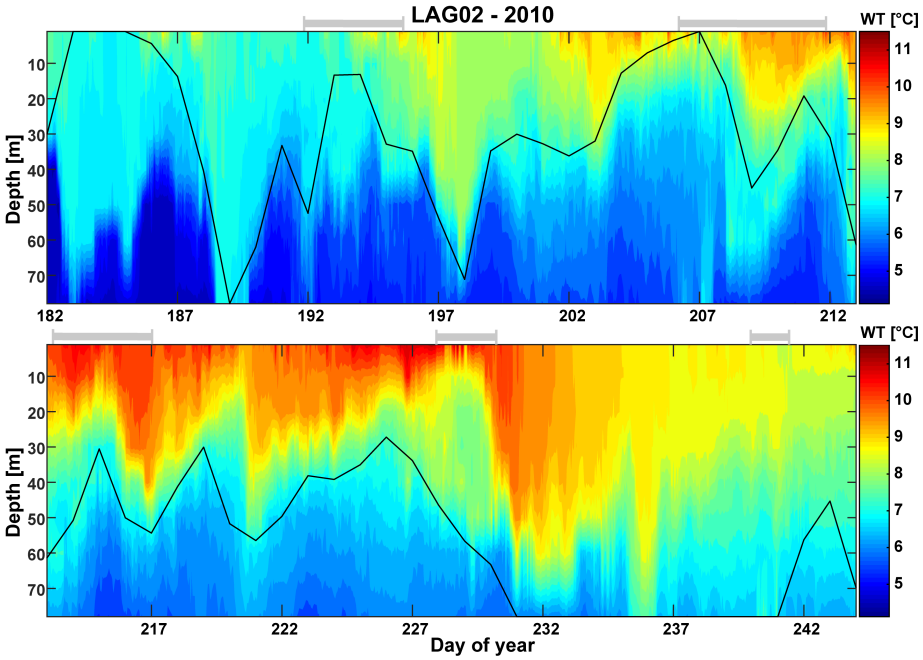

Figure 3.17. Theoretical depth of intrusion of Jökulsá í Fljótsdal (black line) at station LAG02 if the water temperature is the sole parameter considered. The color bar indicates water temperature measured at LAG02. The gray bars on top the plots outline period of time when inverse stratification is recorded by the thermistor and is particularly evident.

Station LAG02 is the station closest to the mouth of the glacial river Jökulsá í Fljótsdal. Using the water temperature measurements in the river, the depth of intrusion of the river is estimated. It is assumed that temperatures are the sole contributor to the

density of water, suspended sediments are neglected and that the river inflow reaches a level of neutral buoyancy when it reaches the water in the lake water column with the same temperatures.

This first approximation (Figure 3.17) shows that the river inflow intrusion would vary from overflow and interflow (July) in the early stratification season to underflow in the late stratification season (end of August). However, as emphasized in the figure by the gray bars on top of the plots, local thermal gradient inversions appear in the water column by episodes signifying that density can not derived from temperatures solely and suspended sediments should be included in the equation of state.

3.3.2 River inflow and stratification

Further evidences of the importance of the river signal on Lake Lagarfljót are available in Figures 2.9 and 2.11 where short-lived weak stratification episodes are observed both in 2010 and in 2011.

In 2010, the isobaths spread below 20 m depth between day 265 to 292 at LAG02 and LAG01, and more briefly between 275 and 282 at LAG03 which corresponds to a large discharge event at the southern inflow peaking on day 276 to a daily average flow of 139 m^3/s (Figure 3.2). In 2011, two large discharge events are observed after day 260, the first one starting on day 256 and peaking on day 272, the second one, larger, reaching a peak about 42 later on day 314. These events are associated to sudden, weak, stratification episodes at HAF and LAG03 in the main southern basin. This phenomenon is not clearly observed in the measurements performed at LAG04 located in the shallower northern basin.

3.3.3 Evidences of interflow (summer 2010 and August 2011)

The transects performed with the multi-parameter sonde during summer 2010 and 2011 can be used to increase our understanding of the glacial inflow behavior in the lake. The turbidity level in the glacial river Jökulsá í Fljótsdal is significantly higher than in the lake itself. Turbidity values in the river are found to be around 260 NTU in August 2010 and 330 NTU in July 2010 and 2011. Turbidity values measured in the lake are significantly lower which suggests that part of the sediments deposits early on when entering the lake or/and the river inflow mixes in part with the lake waters. A clear gradient is observed demarcating the river plume.

On Figure 3.18 (up), a horizontal (and vertical) gradient of turbidity levels can be observed in July. Highest turbidity levels (170 NTU) are seen at the bottom of southern end of the lake, however a high turbidity pulse at 20 to 50 m depth suggests that at least part of the river inflow intrudes at these depths.

In August 2010 (Figure 3.18 down), the river is seen plunging to 40 m depth where it starts intruding the lake as an interflow. The river plume then expands vertically and seems to divide into two branches, a first one at about 20 m depth and a second one with higher turbidity levels at about 50 m depth. However, even though a horizontal gradient is present in the basin, the lowest turbidity level (140 NTU) is found at about 20 km from the southern end of the basin (Station LAG03) while high turbidity levels (>170 NTU) are found further North, in the shallower basin.

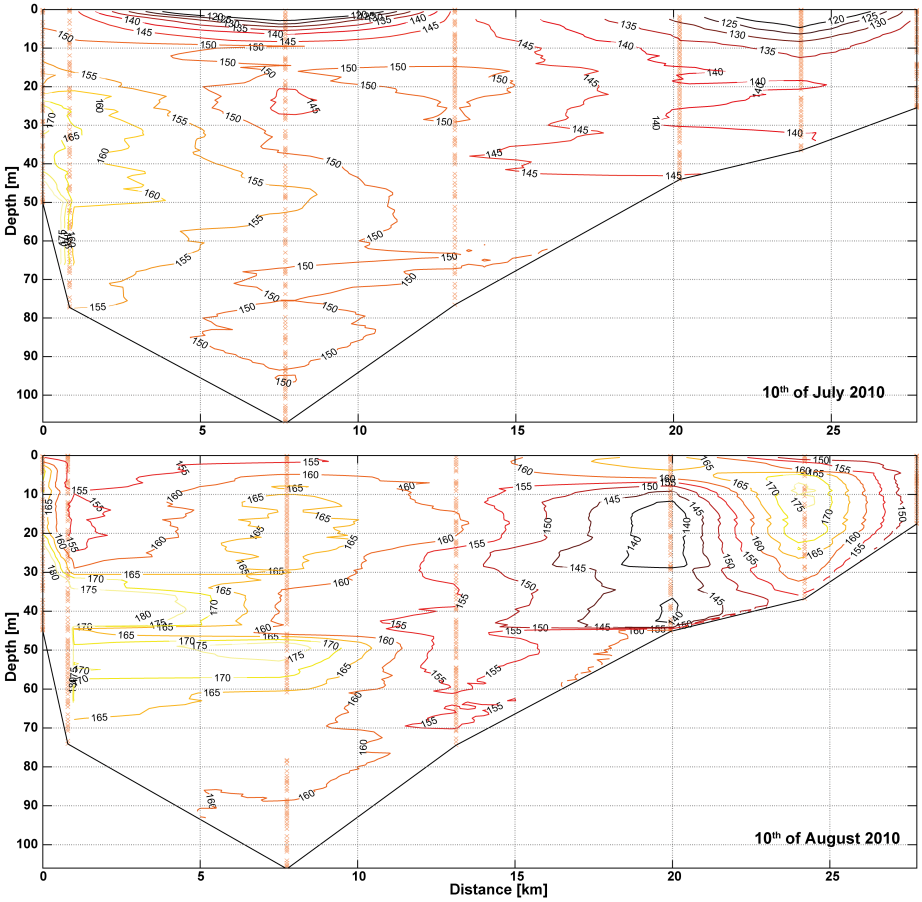

Figure 3.18. Longitudinal cross-sections (SW end at location 0 to NE end at location 12) of the turbidity in Lagarfljót recorded by the sonde on the 10th of July (up) and 9th of August (down) 2010. The blue crosses represent the actual location of the measurements.

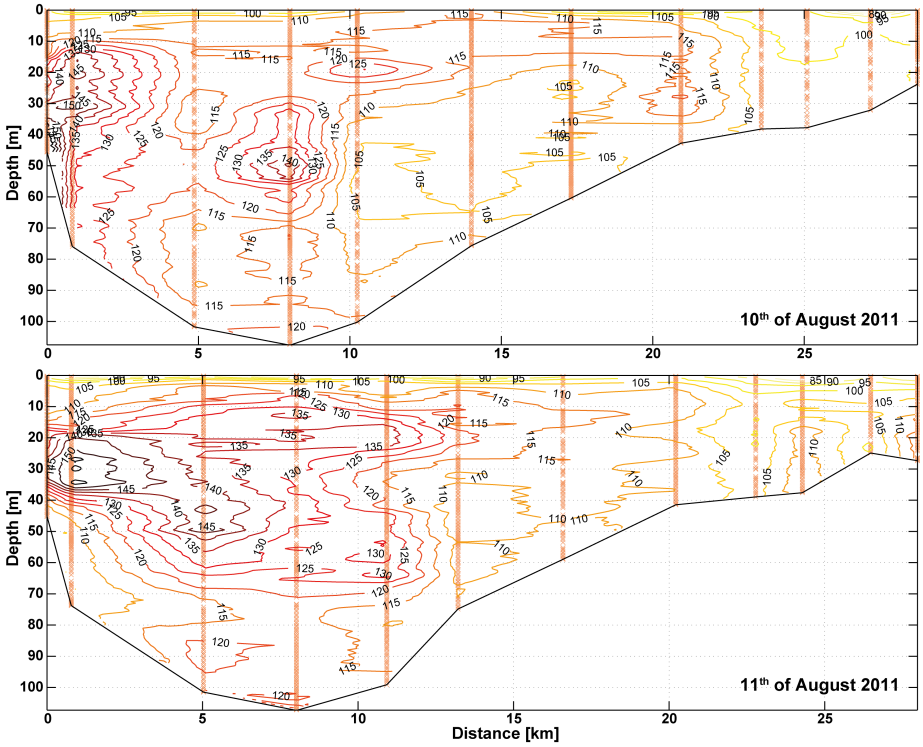

Figure 3.19. Longitudinal cross-sections (SW end to NE end) of the turbidity in Lagarfljót recorded by the sonde on the 10th (up) and 11th (down) of August 2011. The brown crosses represent the location of the actual measurements.

In August 2011, Figure 3.19 indicates that the glacial river inflow intrudes the lake between 20 and 40 m depth. It travels through the water column up to 12 km in the lake on the 11th of August 2011.

The lateral cross-sections (Figure 3.20) bring additional insights and show that the river inflow (higher turbidity level and temperatures) is still deflected as an underflow towards the shallower East bank of the the lake while spreading as an interflow towards the center of the lake at between 20 to 40 m depth (station LAG02).

At Hafursá, the river signal is still stronger on the East side but a high turbidity level is observed at around 20-30 m depth throughout the transect (Figure 3.20). At LAG20-18-19, the highest turbidity levels are detected in the center of the cross-section at 20 m, associated with a spreading of the isotherms and at 50-60 m depth. Further away from the river mouth, a slightly higher turbidity level is detected on the eastern side of the lake and ass to slightly spread isotherms, however the signal of the river is weaker.

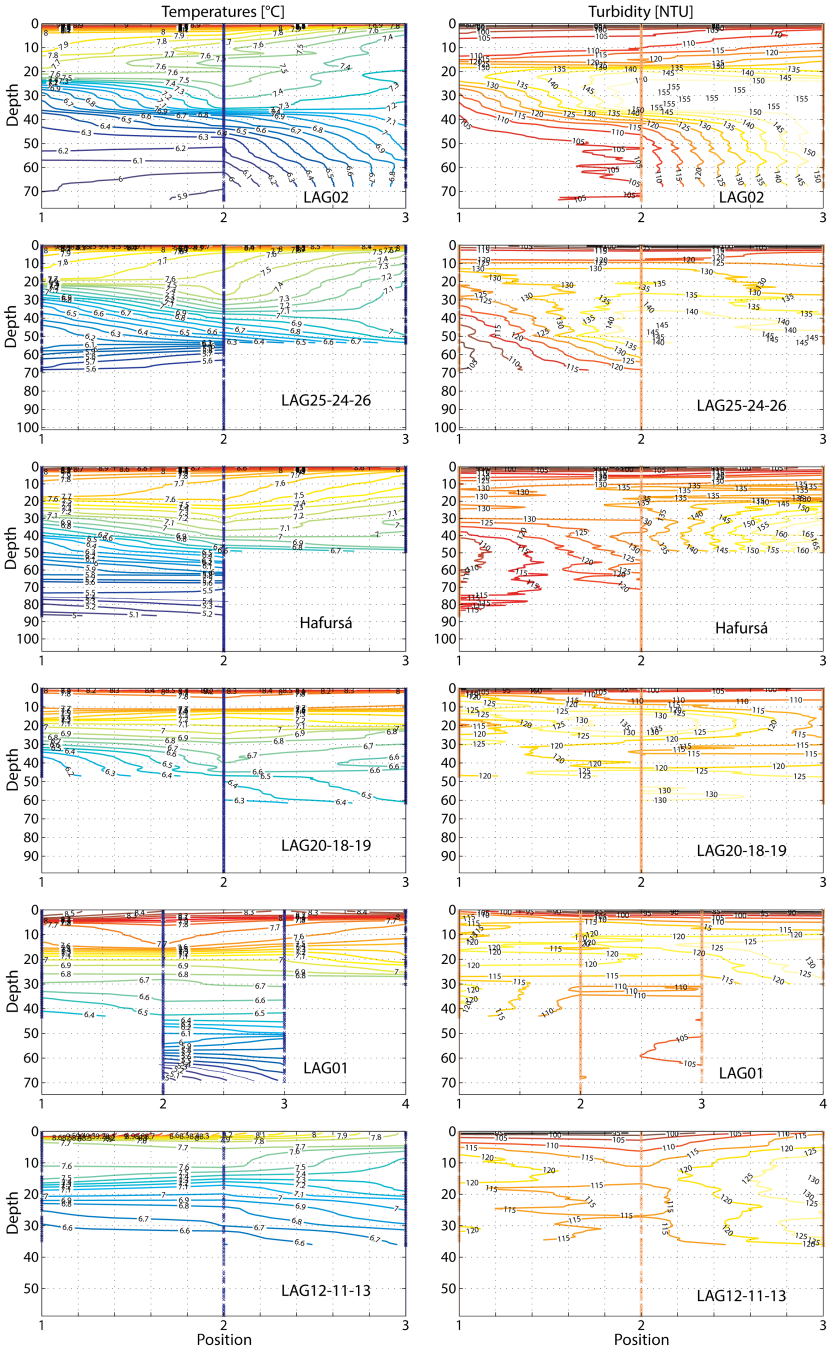

Figure 3.20. Cross-sections along lake Lagarfljót. Measuremements performed on the 11^{t}h of August 2011 are interpolated between the stations (isotherms on the right hand side plots and turbidity isolines on the left hand side), from 1 on the west bank to 2 in the center of the lake and 3 on the East bank, station 4 at LAG01 corresponds to measurements in the dead zone.

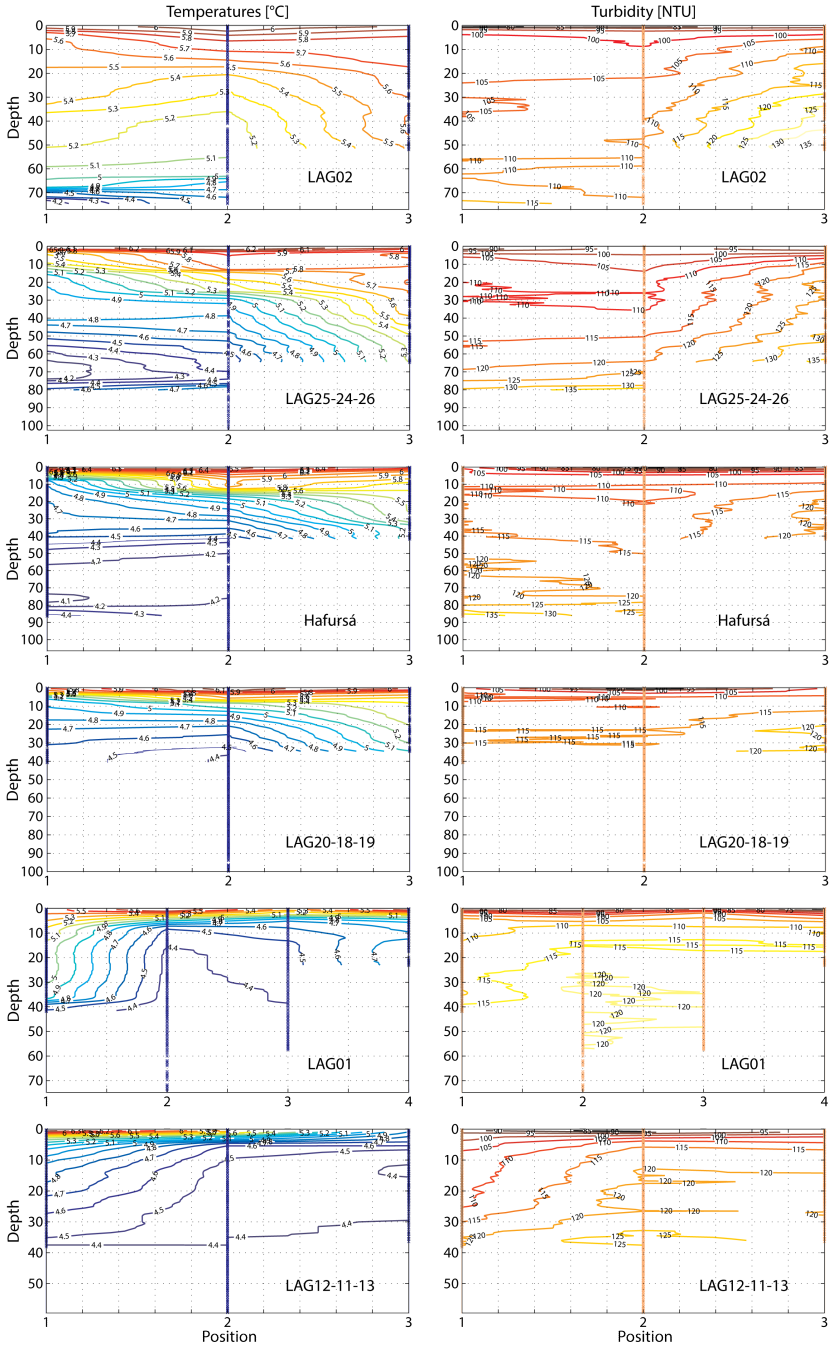

Figure 3.21. Cross-sections along lake Lagarfljót. Measuremements performed on the 10th of July 2011 are interpolated between the stations (isotherms on the right hand side plots and turbidity isolines on the left hand side), from 1 on the west bank to 2 in the center of the lake and 3 on the East bank, station 4 at LAG01 corresponds to measurements in the dead zone.

3.3.4 Coriolis force as a driver for maintaining the river on higher grounds

Lateral cross-sections (Figure 3.21), showing the temperature and turbidity isolines, indicate that the river inflow gets deflected to the East when entering the lake, suggesting a significant influence of the Earth rotation on this underflow. The inflow signal appears also at the bottom of the lake in the center and on the West side of the lake from station LAG25-24-26 and is characterized by a thermal inversion (with temperatures exceeding 5°C at the bottom) and a higher turbidity (up to 170 NTU), as observed on Figures 3.22 and 2.15.

From stations LAG12-11-13 (Figure 3.21), higher turbidity levels are observed on the East side of the lake, however they are associated to colder waters unlike in the previous cross-sections, suggesting that this stronger signal is more likely associated to a tilt of the layers rather than the intrusion of the river inflow.

3.3.5 Evidences of underflow (July 2011)

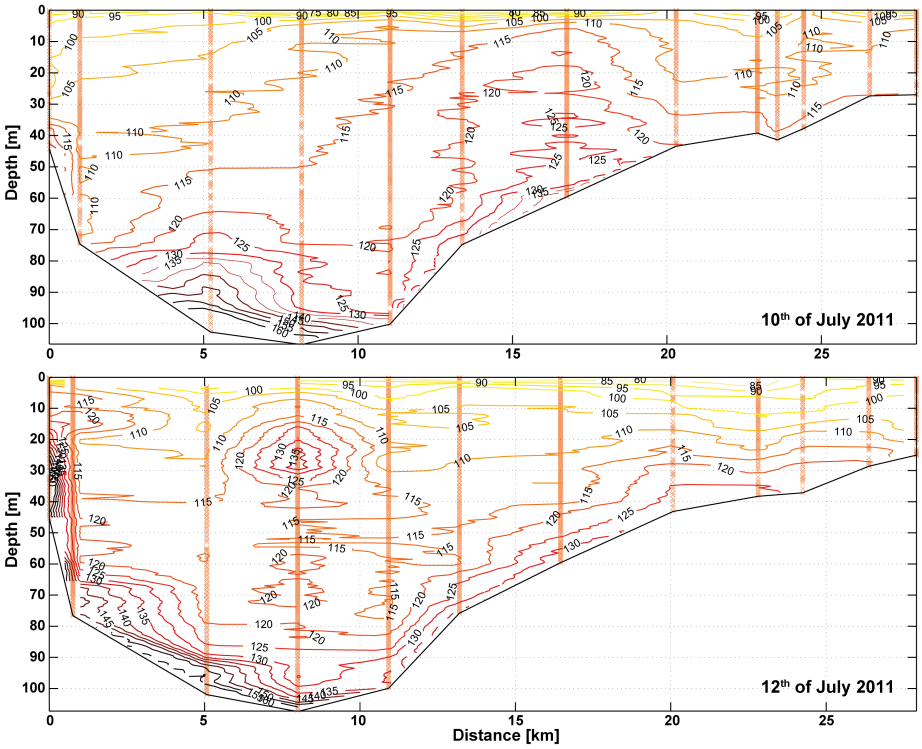

Figure 3.22. Longitudinal cross-sections (SW end at location 0 to NE end at location 12) of the turbidity in Lagarfljót recorded by the sonde on the 10th (up) and 12th (down) of July 2011. The brown crosses represent the location of the actual measurements.

Considering Figure 3.22, it appears that the inflowing river sinks to the bottom of the lake in July 2011 leading to the inverse thermal stratification (Figure 2.15). These

figures show that the river inflow result in a density current that seems to propagate up to LAG01 following the bottom of the lake. These figures suggest also the presence of an hydraulic jump at the bottom of the slope at about 5 km from the glacial river mouth.

The 12^{th} of July, a high turbidity signal is observed at Hafursá at about 20-30 m depth which corresponds to the intrusion depth of the river as detected at the most southern location in the lake.

3.4 Summary

Rivers in the greater catchment of Lake Lagarfljót are diverse in size and type. The main inflow is located in the southern end of the lake and is composed of a partly unregulated glacial inflow Jökulsá í Fljótsdal which presents a mix of nival and glacial regime, the heavily regulated glacial discharge from the dammed river Jökulsá í Dal (Kárahnjúkar) and freshwater streams such as Kelduá that present a nival regime. The freshwater river Grímsá is a tributary entering the lake in its northern basin.

The glacial rivers are heavily loaded with suspended sediments, Jökulsá í Fljótsdal carries along very fine glacial till. It is estimated that most of the suspended sediment will be transported in the lake and stay in suspension, hence contributing in the density gradient between the river inflow and the lake waters.

Field measurements and observations reveal the presence of the southern inflow signal throughout the southern deep basin, with a greater influence the closer to the mouth. The river intrusion depth in the lake varies over the summer season, the river plume brings warmer water in deeper layers of the lake. During the cooling period of fall, episodes of weak thermal re-stratification measured by the thermistor chains placed in the lake can be connected to large discharge events occurring in the southern inflow. In addition, the deflection of the river towards the eastern banks of the lake observed in the sonde profiles is an evidence of the effect of Coriolis in the lake. These findings show that to understand fully the hydrodynamics of lake Lagarfljót, it is important to take consideration of the main tributaries of the catchment.

4 Natural internal waves in Lake Lagarfljót

Wind sets off seiches and internal waves in water bodies, the rate of oscillation of these latest however depends on the stratification of the column, the basin bathymetry and/or the wind forcing periodicity (Farmer, 1978; Antenucci and Imberger, 2003; Vidal and Casamitjana, 2008; Valerio et al., 2012). Resonance occurs when the wind period approaches the period of the free mode of oscillation of the internal waves and the phase between both is zero. This will result in amplified internal waves as the wind brings additional energy in the system.

In Chapter 2, it was shown that the main internal wave oscillation periods are very close to the main periods of oscillation of the wind velocities along the lake basin. However, from field data alone, it is difficult to define to what extent the internal waves are strictly forced oscillations or if there is a phenomenon of resonance between the wave motions and the external wind forcing. The use of a simple 2D model adapted from the Münnich model (Münnich, 1996; Vidal et al., 2005; Vidal Hurtado et al., 2007) helps us understand the effect of bathymetry on the wave regime and define the action of the wind. In this chapter, this simple model is described and tested for Lake Lagarfljót, the free mode of oscillations are investigated for summers 2010 and 2011 and compared to the observations and finally, the relation between wind forcing and natural modes in the basin is studied for summer 2010.

4.1 Methods

Most energy is expected to be in the H1 mode, however resonant forcing and basin shape can affect the energy distribution between modes (Boegman, 2009). It is therefore interesting to evaluate the effect of the bathymetry on the internal wave regime in order to assess the role of the wind in the forcing of these waves.

4.1.1 Model description

The 2D Münnich model (Münnich, 1996) as used and described by Vidal (Vidal et al., 2005, 2007; Vidal Hurtado et al., 2007) was adapted to the two-basins bathymetry of lake Lagarfljót to estimate the natural basin scale oscillations while accounting for the basin shape.

Neglecting the rotational effects, the 2D (x and z) governing equation for a stream function ψ of free, infinitesimal internal gravity waves in a hydrostatic Boussinesq fluid is $\frac{\partial^4 \psi}{\partial t^2 \partial z^2} + N^2 \frac{\partial^4 \psi}{\partial x^2} = 0$.

The main input into the model is the Brunt-Väisälä frequency $N = N(z)$ which

varies with depth z. Assuming the absence of waves at the surface (rigid lid) and inflows/outflows, the boundary conditions can be expressed as $\psi = 0$.

The velocity components u and v can be computed from the stream function : $u = -\frac{\partial \psi}{\partial z}$ and $v = \frac{\partial \psi}{\partial x}$

For sinusoidal seiches with angular frequency ω, the spatial structure of the stream function becomes $\psi = \phi(x,z)sin(\omega t)$, which yields the following eigenvalue problem: $\frac{\partial^2 \phi}{\partial x^2} - \frac{\omega^2}{N^2}\frac{\partial^2 \phi}{\partial z^2} = 0$.

Discretizing the longitudinal cross-section of the lake basin, the matrix formulation of the problem takes a generalized eigenvalue form: $\mathbf{A}\phi = \lambda \mathbf{B}\phi$ where $\mathbf{A}$ is a matrix determined by the discretization on the x-axis, $\mathbf{B}$ a matrix determined by the buoyancy frequency and the discretization on the z axis, $\lambda = \omega^2$ and ϕ the eigenvalues and eigenvectors of the generalized eigenvalue problem. The eigenmodes obtained were sorted by overall shear connected to the flow field (Münnich, 1996; Vidal et al., 2005). The shear is estimated based on the amount of shifts in the direction of the streamlines.

The model has been used in previous studies with parabolic basins (Münnich, 1996) and simple basin with an irregularly sloping bottom (Vidal et al., 2005). For this project, it was adapted in order to adjust to more complex basin shapes, allowing for the presence of sub-basins/sills.

4.1.2 Sensitivity analysis

Experimentations with the model show that the spatial resolution (Δx and Δz) affect the ranking and in particular of the vertical modes, however it does not affect the associated period. As Δx decreases or Δz increases, the ranking of H1V1 gets lower and inversely, as Δx increases or Δz decreases, the rank of higher vertical modes increases.

Tests in rectangular basins show that simple V1 modes ranks highest, H1V1 is the first mode observed in all rectangular basins, including the composite basin, except when the N^2 profile for July 2010 is used. Comparing results produced by three different types of basins and with a constant N^2=10^{-4}, we find that H1V1 is not ranking first in non-rectangular basin and is less clearly defined; in addition, higher modes (both horizontal and vertical) are more prominent. Several stability profiles have also been tested in the basins, showing that as the stability increases the period of oscillation of free internal waves shortens. Further tests with rectangular basins suggest that the prominence of vertical mode increases with the ratio between the depth and the length of the basin.

The model was adapted for Lake Lagarfljót bathymetry using Δx= 300 m and Δz=5 m for the 28 km long and 112 m deep basin to optimize the computational efficiency. N^2 was determined using the sonde profiles measured at the deepest location Hafursá during early and late summer 2010 (9^{th} of July and 9^{th} of August). Due to the significance of the suspended sediments on the water density in the lake, it was included in the computation of N^2.

4.2 Results

4.2.1 Free modes of oscillations

The circulation regime in the lake was simulated with a 2D analytical model for two different periods of a typical stratification year (2010) and cold 2011. First, for weakly stratified July and second during more stratified August. The periods and circulation modes associated with the main free modes of oscillation, ranked according to the overall shear connected to the flow field (Münnich, 1996; Vidal et al., 2005), are presented in Table 4.1. In 2010, the free oscillations have periods ranging between 0.7 and 7 days. The first ranked oscillation is 6.5 days in July and 7 days in August. In 2011, the periods are longer and of the order of 10 days for July and August.

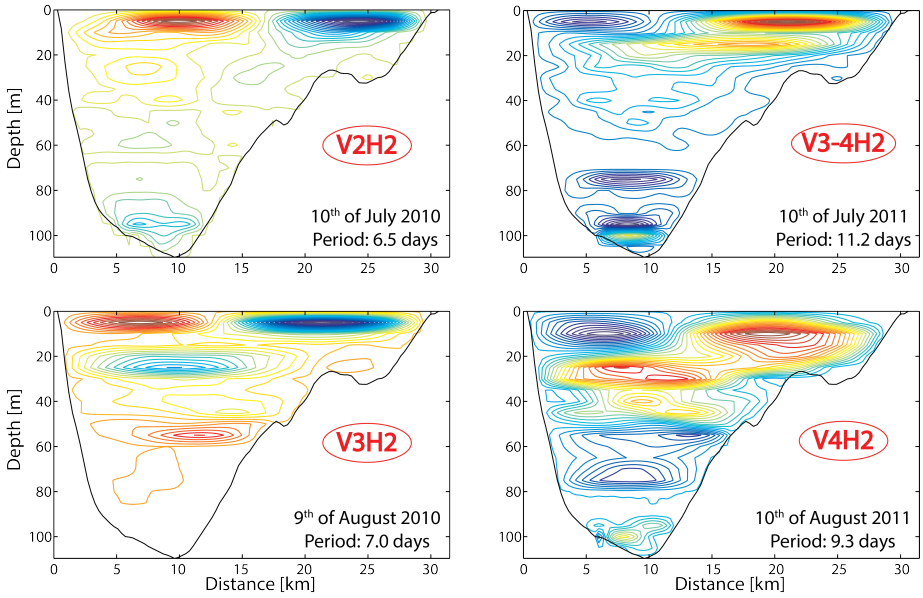

Figure 4.1. Contour plot of the stream function for the main natural circulation mode in the basin for July (a) and August (b) 2010 and July (c) and August (d) 2011.

The corresponding velocity field of the main modes are represented as contour plots of the stream function on Figure 4.1. Closed circles represent circulation cells, positive means anti-clockwise, negative clockwise. In July 2010, two main horizontal cells and 3 vertical cells are observed, suggesting that the circulation associated with the 6.5 days period is V3H2. In August 2011, however, 4 vertical cells appear, suggesting a V4H2. The increase in vertical modes between July and August is in agreement with the spatial field measurements discussed in Figure 2.15. However, the measurements suggest higher horizontal modes. By considering Table 4.1, the second ranked oscillation is associated with H10 in 2010.

Table 4.1. Ranking of the free modes of oscillation of the internal waves in Lagarfljót for summer 2010 as found by the adapted Münnich model.

	10^{th} of July 2010		9^{th} of August 2010		10^{th} of July 2011		10^{th} of August 2011	
#	T [days]	Modes	T [days]	Modes	T [days]	Modes	T [days]	Modes
1	6,5	V2H2	7,0	V3H2	11,2	V3-4H2	9,3	V4H2
2	0,8	V2H10^{+}	0,7	V3H10^{+}	8,7	V4H3	3,9	V3-4H3
3	7,2	V3H2	2,8	V5H4	3,7	V3H4	10,6	V5H2
4	0,9	V2H10^{+}	4,3	V3H3	5,5	V2H2	15,7	V5H1
5	3,7	V3H4	1,0	V5H10^{+}	5,7	V2H3	14,5	V4H1
6	4,6	V2H3	0,4	V4H10^{+}	0,9	V2H10+	0,5	V2H10+

4.2.2 Wind forcing and resonance

The 2D analytical model only predicts the free oscillations. In natural environments, external forcing might affect the behaviour of the water body, resonance can occur when the natural frequency of the system coincides to the frequency of the forcing (Norton and Karczub, 2003; Sakai and Redekopp, 2010). To understand forced oscillation, a spectral analysis of wind along the main axis of the lake was performed for each profile measurement dates (Table 4.2). The main period of oscillation for the wind is 7 days in 2010 which matches the main free oscillation simulated for August but slightly longer than that in July. This period is appearing strongly in the measurements around 20 m depth in August and deeper in the water column (40-60m) in July. Second strongest wind has 4.2 days period which according to the analytical model would force a V2H3 basin circulation in July and a V3H3 in August.

Table 4.2. Four main periods found in the spectral analysis of the longitudinal component of the wind measured at Egilsstaðir in 2010 and 2011. The 2 weeks periods centered on the vertical profiling dates were considered with periods larger than 21 days smoothed out.

		T [days]			
2010	10^{th} of July	7.1	4.2	1.6	2.0
	9^{th} of August	7.1	4.4	2.1	2.6
2011	10^{th} of July	10.0	3.7	2.8	5.2
	10^{th} of August	6.8	4.1	19.0	3.0

This period is well represented at the two stations furthest apart (LAG02 and LAG03) in July and August (Table 4.3). The third strongest wind period are between 1.6 to 2.6 days, which harmonize very well with data in LAG01 both July and August (Table 2.2). The thermistor chain data indicate strong oscillations with periods of 5.7 days at all locations, both July and August, these oscillations do not correspond to the main wind forcing time periods nor to free oscillation modes. However, it is between the two main wind oscillation periods. Despite observed diurnal land breeze (appearing also in 2.8), the energy associated with diurnal and sub-diurnal winds is not most prominent. Hence, the wind is less likely to force the H10 free modes predicted by the analytical model.

Table 4.3. Five main oscillation periods (T) resulting from the spectral analysis of the thermistor data at station LAG02 and LAG03 for the months of July and August 2010.

		Main oscillation periods [days]	
Station	Depth	July 2010	August 2010
LAG02	1.5	7.1, 2.0, 1.0, 1.3, 0.9	14.2, 4.7, 2.8, 1.1, 0.6
	11.8	7.1, 3.6, 1.8, 1.0, 1.2	7.1, 2.8, 1.8, 1.0, 0.5
	21.6	7.1, 3.6, 2.0, 1.3, 0.6	7.1, 2.8, 1.6, 1.0, 0.7
	31.4	14.2, 2.4, 1.6, 0.9, 1.0	14.2, 4.7, 2.4, 1.2, 0.9
	41.1	4.7, 14.2, 2.4, 1.6, 1.0	14.2, 4.7, 2.4, 1.0, 0.9
	50.9	4.7, 2.8, 2.0, 1.0, 1.2	14.2, 4.7, 2.4, 0.9, 1.0
	60.8	4.7, 2.8, 1.8, 1.0, 1.2	4.7, 14.2, 1.6, 0.9, 1.3
	78.5	4.7, 14.2, 2.8, 2.0, 1.4	4.7, 2.4, 1.6, 1.3, 0.7
LAG03	1.5	7.1, 1.0, 2.0, 1.2, 2.8	14.2, 1.4, 1.1, 0.8, 0.6
	16	14.2, 4.7, 2.8, 1.2, 0.8	14.2, 4.7, 1.8, 1.1, 0.9
	26	4.7, 14.2, 1.8, 1.4, 0.9	7.1, 2.4, 1.6, 1.1, 1.3
	36	14.2, 4.7, 2.4, 1.4, 0.9	4.7, 14.2, 2.0, 1.2, 1.6

The close match between the main wind period and the natural oscillations in the basin suggests a phenomenon of resonance, partial in July (first and third ranked oscillations) but perfect in August (first ranked oscillation). The increase of stratification of the water column over the summer season is slowly tuning the system into resonance (Boegman, 2009).

The wind seems to be resonating with basin oscillations with periods around 4 days, ranked in sixth position by the eigenvalue model in July 2010, as these oscillations appear to be of high energy in the measurements. These oscillations are associated with horizontal mode 3 and vertical modes 2 in July 2010 and 3 in August 2010. The stratification strength governs the number of vertical modes which increase from 2-3 to 3-5 between July and August 2010.

4.3 Summary

Results from the 2D Münnich model indicate that the natural modes in the basin match closely the periods of the wind, which promotes resonance between the internal waves and the wind. As stratification builds up, the free internal waves periods shorten and higher modes become more prominent, in accord with field measurements (see section2). Sorting of the eigenmodes based on the shear in the streamline needs to be interpreted carefully as it changes slightly with the choice of grid size, however it suggests that in July 2010, the main wind period does not correspond to the most energetic natural modes in the basin, hence forcing secondary natural modes while in August 2010, the wind period is very similar to the ranked 1 mode in the basin, the wind possibly entered in resonance with the natural waves oscillating in the basin, amplifying them.

This simple model supports the concept that the wind is the main driver in this water system but internal wave regime is controlled by the bathymetry and the seasonal

stratification. It is, however, too limited to explain in details the circulation in the basin as it ignores both the Coriolis effect. The use of a 3D hydrodynamic model can bridge the gaps left by simpler models.

5 Three-dimensional modeling of the internal motions of a subarctic lake

The term limnology appeared in the early XX^{th} century with the work of François-Alphonse Forel. The study of inland waters started then to develop as a discipline. Early on, analyses were mostly based on basic field observations and measurements. The tools used to identify the processes in these water bodies improved dramatically during the XX^{th} century. However, due to the cost of equipments, the difficulty and time consumption associated with field deployment and their spatial restriction, field measurements are often still insufficient to describe fully the internal motions of lacustrine environments. In addition, some lakes, such as those in the subarctic regions, are difficult to monitor because of their location in less densely inhabited areas and to the climate associated to these locations.

Models can fill up spatial and temporal gaps and improve the understanding of processes involved in the internal behaviors of lakes. It is estimated that the optimal lake model, in terms of computational efficiency and accuracy, is 0D for small lakes, 1D for medium lakes and 3D for large lakes (Leon et al., 2008). One dimensional models are used to model the temperature of the water column and energy balance in small shallow lakes (Aija-Riitta et al., 2007; Res, 2010) but encounter difficulties when it comes to giving acceptable results for larger lakes or over the entire basin. Two-layer numerical models are used to model internal waves in larger lakes (Lemmin et al., 2005) , sometimes as the first steps towards a 3D model (Naithani et al., 2003). Three dimensional numerical models are computationally heavy but allow the investigation of the dynamics of complex environments, such as large lakes. However, these models have been mostly used and validated for temperate lakes with stratified waters during the summer season.

Two 3D models are mostly represented in physical limnology researches: the Estuary and Lake Computer Model (ELCOM) and the Semi-Implicite 3 Dimensional model (SI3D). ELCOM was written by Dr. Ben R. Hodges (Hodges et al., 2000; Laval et al., 2003) is sometimes aimed at being coupled with other models such as some particle dynamics model (Chung et al., 2009), a water quality module (León et al., 2005) or a climate model (León et al., 2007).

SI3D was firstly developed by Smith for estuarine environments (Smith, 2006) and adapted by Rueda (2001) for lacustrine environments (SI3D-L). This model has incorporated an ecological module (King et al., 2009), in addition to allowing tracers studies (Rueda et al., 2008) and the incorporation of inflows (Rueda and MacIntyre, 2009). It was validated for lake modeling purposes by Rueda and Cowen (2005) and used by Rueda and MacIntyre (2009). The validation of the model for the shallow

polymictic lake of Clear Lake, California, (Rueda and Schladow, 2003) suggests that it would be appropriate for larger weakly stratified lakes.

In this chapter we first verify that the existing 3D hydrodynamic model SI3D-L can adequately simulate the motions in the subarctic weakly-stratified Lake Lagarfljót. The results are extensively analyzed to validate this approach. The model results provide us with a new set of data. The key contributions of this model are then described in a second part. The internal wave regime of the lake during the ice-free season is analyzed further with regard to the main external forcing. The fate of the river (pathways and flushing times) is also described and conceptualized.

5.1 Methods

5.1.1 SI3D-L model

Models are important tools to improve the comprehension of hydrodynamic processes in lakes. It is an open source code model written in Fortran 95, new modules and variables can easily be introduced. IN 2010, a parallel version of this z-coordinate 3D-hydrodynamic, transport and mixing model was developed Acosta et al. (2010).

The model solves the 3D shallow water equations using a semi-implicit, three-level, iterative leapfrog-trapezoidal finite difference scheme on a staggered Cartesian grid. These equations are derived from the Navier-Stokes equations by assuming that the weight of the fluid identically balances the pressure (hydrostatic approximation) (Rueda and Schladow, 2002).

Non-active (i.e. tracers) and active-scalar (influencing water density) transport equations were solved using a two-level semi-implicit scheme, in which only vertical diffusion is discretized implicitly. The advection terms in the scalar transport equation are discretized with flux-limiter methods (Durran, 1999), in which, the corrected fluxes are constructed with the monotone upstream differencing scheme, the Lax-Wendroff second-order method, and the Superbee limiter (Roe, 1984). Turbulent mixing is represented in the 3-D model using diffusion-like terms. A Laplacian operator with constant mixing coefficients (Kh) is used to represent horizontal mixing of momentum and scalars. Vertical eddy coefficients of mixing Kz are calculated using the two-equation model originally proposed by Mellor and Yamada (1974).

In June 2011, in the frame of a collaboration with Dr. Rueda-Valdivia at the University of Granada, the suspended sediment variable (along with the salinity variable) was added into the source code of the model for the computation of the water density.

Pre-processing Matlab routines help us build the input files to the model. To run the model five different input files need to be created. A file divides the space on the horizontal plane, it defines the bathymetry grid with a matrix of depth values; for these runs Δx and Δy were set to 100m.

A second file divides the space on the vertical plane, layers of different thicknesses are defined. The layer thicknesses (Δz) vary from 0.5 m in the top layers to slightly more than 6 m in the deepest layers.

A third file describes the initial conditions in the water column in terms of tem-

peratures but also in terms of salinity and sediment concentration if needed. Data is provided for each of the layers defined by the layer file, previously described. Hafursá, the deepest location, is used as a representative location for the water temperature at the start of the season. Sonde profiles or thermistor chain measurements are used to define the conditions in the lake at the given starting date.

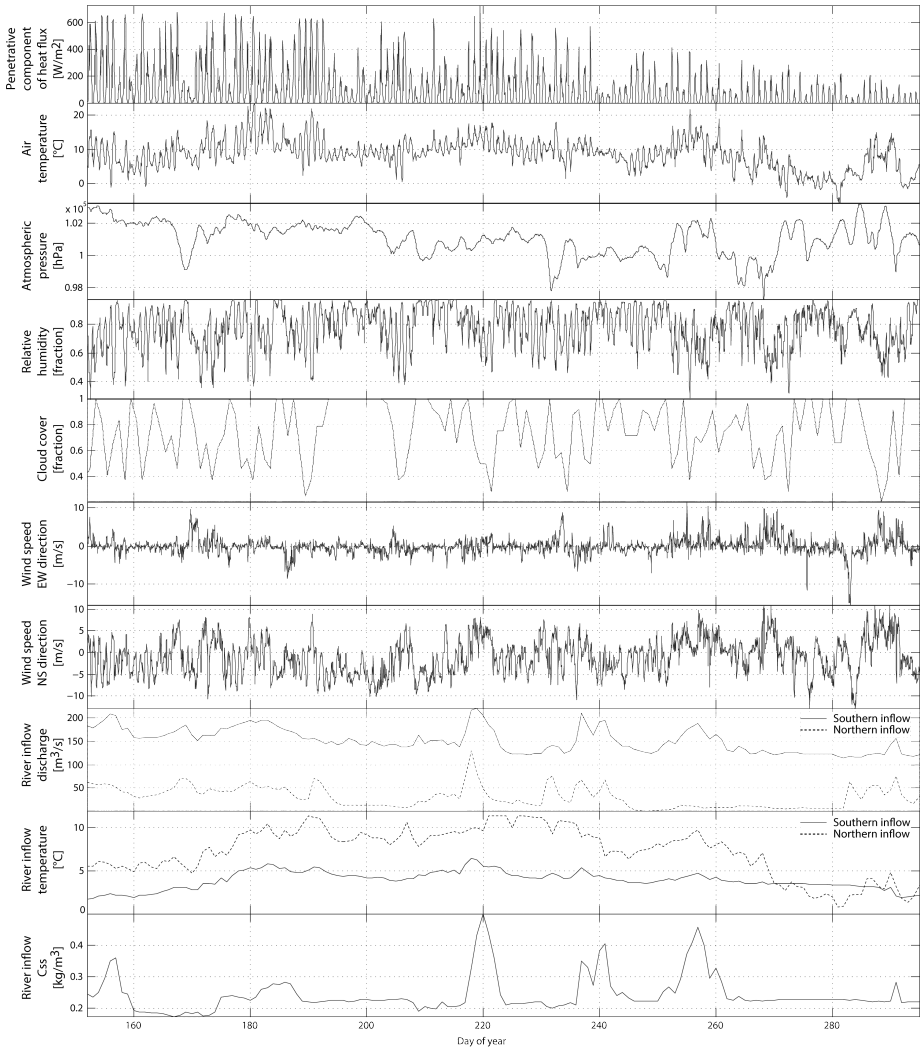

Figure 5.1. Meteorological and hydrological model inputs to the model (IMO, 2010b,a, 2011).

A fourth file contains the surface conditions (Figure 5.1). This file contains time series for the principal weather parameters (IMO, 2010a) as well as the light attenuation coefficient (Martin and McCutcheon, 1998, p. 368) computed as $\eta = 1.1 \times Z_s^{-0.73}$ with Z_s the observed Secchi depth (0.2 m) and the wind drag coefficient defined as 1.5×10^{-3}

(Pond, 1975). The penetrative component of the heat fluxes H_{sw} is computed as $H_{sw} = sw(1-alb)$ with sw the shortwave radiations measured at Hallormsstaður and alb the albedo computed as described by Pivovarov (1973) which takes into consideration the cloud cover (here observations at Svínafell). The basic setups of SI3D-L assumes a homogeneous weather field over the water system which can bring limitation in the case of long water systems or water systems with complex surrounding topography. precipitation are not included in this model.

Finally the last and fifth file is the input file which summarizes the different assumptions and constants of the simulation, such as the Coriolis parameter f, set to 1.32×10^{-4} s^{-1}. Additional files are needed to characterize each of the river inflows and the outflow.

Model setups Different setups were put to the test, from the simplest to the most complex, to test the sensitivity of the model. Three main setups were evaluated.

Firstly the lake was considered to be an enclosed basin with neither inflow nor outflow, the sediment content was considered insignificant and was not included in the water density computation. Under these general conditions, three different runs are performed : a first run considered as the most basic where the wind data from Egilsstaðir Airport are used ; a second run with wind corrections, the wind data from the original run being converted to wind velocity along the lake and corrected to correspond to the wind along the lake as it could be measured at Brú following the relationship $W_{Br} = \frac{W_{Egils.}+0.12}{0.77}$; a third run similar to run 1 but with a longer spin-up time, as the simulation starts on the 1^{st} of May 2009. For that third run the initial condition is the water are inferred from temperature measurements performed punctually in the lake by IMO (2012).

Secondly, the river inflows and the outflow were included; the data of the two glacial rivers Jökulsá í Fljótsdal and Jökulsá í Dal as well as the freshwater river Kelduá were combined and introduced as one inflow at the southern end of the lake. The flow rate of the combined flow is the addition of the two rivers' flow rate; the water temperature is computed as an average of the three rivers' temperatures proportional to their flow rate such as $T_m = \frac{Q_1\times T_1+Q_2\times T_2+Q_3\times T_3}{Q_1+Q_2+Q_3}$ with T_m the water temperature of the combined flow, T_1, T_2 and T_3 the water temperatures and Q_1, Q_2 and Q_3 the flow rates of respectively rivers 1, 2 and 3. It is assumed that the difference in density of the water of the three rivers is negligible as well as the flow of the three rivers is fully mixed as it enters the lake. The second largest inflow Grimsá river was also introduced in the South-East part of the smaller basin (Figure 5.1).

Thirdly, the sediments present in the water column were added in the model (Figure 5.1), uniform throughout the depth in basin at the start (initial conditions), time dependent in the inflow files. The sediment content in the rivers was estimated using the relationships described in Section 3. Particle settling was assumed negligible as 75 to 90% of the glacial sediments had diameters below 0.02 mm (Þorláksdóttir and Harðardóttir, 2013), with settling velocity of 0.24 mm s^{-1}, which is considerably slower than the bed shear velocity of O (1) mm s^{-1} both estimated from measurements , and calculated from simulations at Hafursá assuming a drag coefficient of O (10^{-3}) for mud bottom (Smith, 2006). The Rouse number is therefore expected to be inferior to 0.6 and the sediment to be transported as wash load. The assumption of negligible deposition conforms with Striberger et al. (2011) finding that most of the sediments or

rock flour brought by Jökulsá í Fljótsdal stays in suspension in the water in the summer and deposit during the winter." The influence of salinity on the density was considered negligible due to the low conductivity values found during the field measurements: specific conductivity values measured in the lake were ranging between 36 and 39 μS cm^{-1} during summer 2009.

Table 5.1 presents in more details the different setups tested. The progressive corrections or additions helped us evaluate the sensitivity of the model. Most simulations ran for 143 days starting from the first of June 2009, with a 60 s time step.

Table 5.1. Details of the different model setup tested.

Name	dx,dy [m]	Time step [s]	Sim. period [d]	Inflow	C_{SS}	Specificities
No inflow	100	60	143	No	No	The lake is considered an enclosed basin
Wind Corr	100	60	143	No	No	Wind velocities along the lake axis following the relationship between Egilsstaðir Airport and Brú
Spin up	100	60	174	No	No	The simulation is given longer time to heat up.
Inflow	100	60	143	Yes	No	Inflow at the southern end (Jökulsá í Fljótsdal and Hálslón) and at Grimsá
Turbidity	100	60	143	Yes	Yes	Suspended sediments are added in the equation of state
Turbidity spin	100	60	174	Yes	Yes	Longer simulation period
Turbidity 30s	100	30	143	Yes	Yes	Time steps reduced to 30 s
Turbidity 50m	50	60	143	Yes	Yes	Grid size reduced to 50m in the x and y directions.
No coriolis	100	60	143	Yes	Yes	Coriolis factor f set to 0 s^{-1}

Evaluation of the results for validation The output results are complex, a different set of analyses will help determining the best model setup. As the time series from the model were recorded with a 15 min time step while the observations were recorded every 10 min, the analyses are performed on 1h smoothed and resampled data sets.

Timeseries quality assessment Heat transfer and stratification are two important characteristics that control the hydrodynamics of a water system. To evaluate the agreement between the observed and computed water temperatures in the water column, it is convenient to use several error measures, such as the error norms l_1, l_2 and l_∞ as

well as the Root Mean Square Error (RMSE) (Table 5.2).

Table 5.2. Error measures for the different simulations at LAG02, LAG01 and LAG03.

Error measures	Definition
Least Absolute Deviation	$l_1 = \frac{\sum_{i=1}^{N_{max}} \lvert N_n - O_n \rvert}{\sum_{i=1}^{N_{max}} \lvert O_n \rvert}$
Euclidean norm	$l_1 = \frac{\left[\sum_{i=1}^{N_{max}} (N_n - O_n)^2\right]^{1/2}}{\left[\sum_{i=1}^{N_{max}} (O_n)^2\right]^{1/2}}$
Maximum error	$l_\infty = \frac{max_{\forall n} \lvert N_n - O_n \rvert}{max_{\forall n} \lvert O_n \rvert}$
Root Mean Square Error	$RMSE = \sqrt{\frac{\sum_{i=1}^{N_{max}} (N_n - O_n)^2}{N_{max}}}$

l_1, l_2 and l_∞ are relative error norms while RMSE is an absolute error measure. Unlike l_2, l_1 is resistant to outliers therefore giving a better idea of general trends, while l_∞ focuses on the outliers.

Several indicators can give us a finer understanding of the discrepancies between the observed and computed data. By comparing the least-square linear fit of the datasets to the 1:1 line, we obtain some more detailed pieces of information on heat transfer and on how well the model is able to represent the temperatures introducing a distinction between warmer and colder temperatures.

The modified coefficient of efficiency E_1 (Legates and McCabe, 1999; Krause et al., 2005) is a generally preferred alternative in hydrology-related analyses to the coefficient of determination (R^2) traditionally used in statistics. It is computed according to the following equation:

$$E_1 = 1 - \frac{SS_{res}}{SS_{tot}}$$

with the sum of squares of residuals $SS_{res} = \sum_i |O_i - N_i|$ and the total sum of squares $SS_{tot} = \sum_i |O_i - \bar{O}|$, O being the observed data and N the numerical results. E_1 is a relative error measure of the goodness-of-fit of the modeled data to the observed data. The use of absolute rather than square limits the effect of the outliers on the coefficient. The coefficient values vary from 1.00 to -infinity. The closest to 1 the better the model predicts the observations, for E=0 the mean value of the observed data is as good of a prediction as the model results, for E<0 the mean value would be a better prediction.

The model results were also compared to the observations to assess whether it predicts the seasonal changes in stratification, and the internal wave dynamics. The length of the stratification period and the stratification strength, parametrized in terms of the top-bottom temperature difference, were calculated from model observations

and simulations and compared. Different values are used to estimate the onset of stratification (Foley et al., 2012; Stefan et al., 1996), 0.5°C or 1°C depending the type of lake studied. As Lake Lagarfljót is weakly stratified, the stratification period is estimated to start when the difference exceeds 0.5°C and end when it becomes inferior to 0.5°C.

The power spectral densities (PSD) of temperature simulations at determined depths were also computed using the periodogram function of Matlab, and compared to those calculated from the field measurements at the three sampling stations LAG01, LAG02 and LAG03, to evaluate the ability of the model in representing the internal wave dynamics. Finally, the total suspended sediment (TSS) distribution in the water column was also investigated and compared to field measurements.

5.1.2 Further analyses using the model results

Lake number LN The lake number LN is a dimensionless parameter that is effectively describing the balance between the force of gravity associated with density stratification providing stability in the water column and the destabilizing forces (here the wind). Low lake numbers suggest a weak stability of the water column considering the external forcings, here the potential capability to the wind to onset internal waves or even mixing (Stevens and Imberger, 1996). The lake number is computed as follow :

$$LN = \frac{M_{BC}}{\tau A z_v}$$

with M_{BC} the baroclinic moment, A the surface area of the water body over which τ the surface stress acts and z_v the distance from the water surface to the centre of volume.

Wavelet power spectrum The 1D wavelet transform algorithms proposed by Torrence and Compo (1998) were applied, using the Morlet mother wavelet function on integrated potential energy (IPE), calculated as in Rueda et al. (2003) from the temperature simulations at station LAG01 and the North South wind component. The IPE provides information on the frequency content of the internal wave field and the relative distribution of potential energy among frequencies. This analysis simplifies the comparison of the frequency distribution of two complex signals over the summer stratification period.

Tilt displacement of the thermocline In order to investigate for Coriolis effect on internal waves it is possible to consider the (vertical) tilt displacement of the thermocline along the shores of the lake. The model allows us to extract data in multiple locations along the lake basin (Figure 5.2). Temperatures at 19 stations located along the shore of the southern basin of Lake Lagarfljót are extracted and thermocline depth computed for each of them over the simulation period.

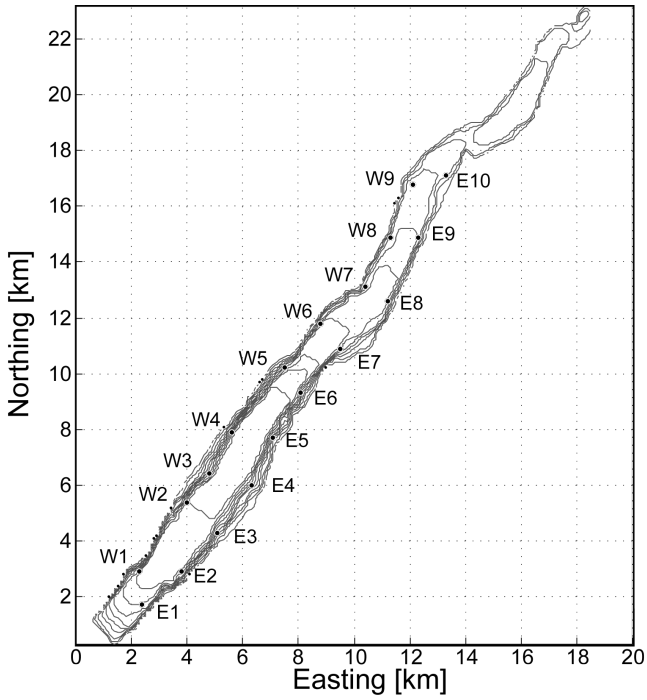

Figure 5.2. Location of the different time series used in the analysis of the rotational effects of the Coriolis forces.

5.2 Results

Figure 5.3 presents the results obtained at station LAG01 for three different setups tested. This shows that the river inflow has a significant influence on the stratification period and the bottom temperatures. The improvement brought by the addition of the suspended sediments in the computation of the water density seems minor and it mostly appears to affect the temperatures at the bottom of the lake.

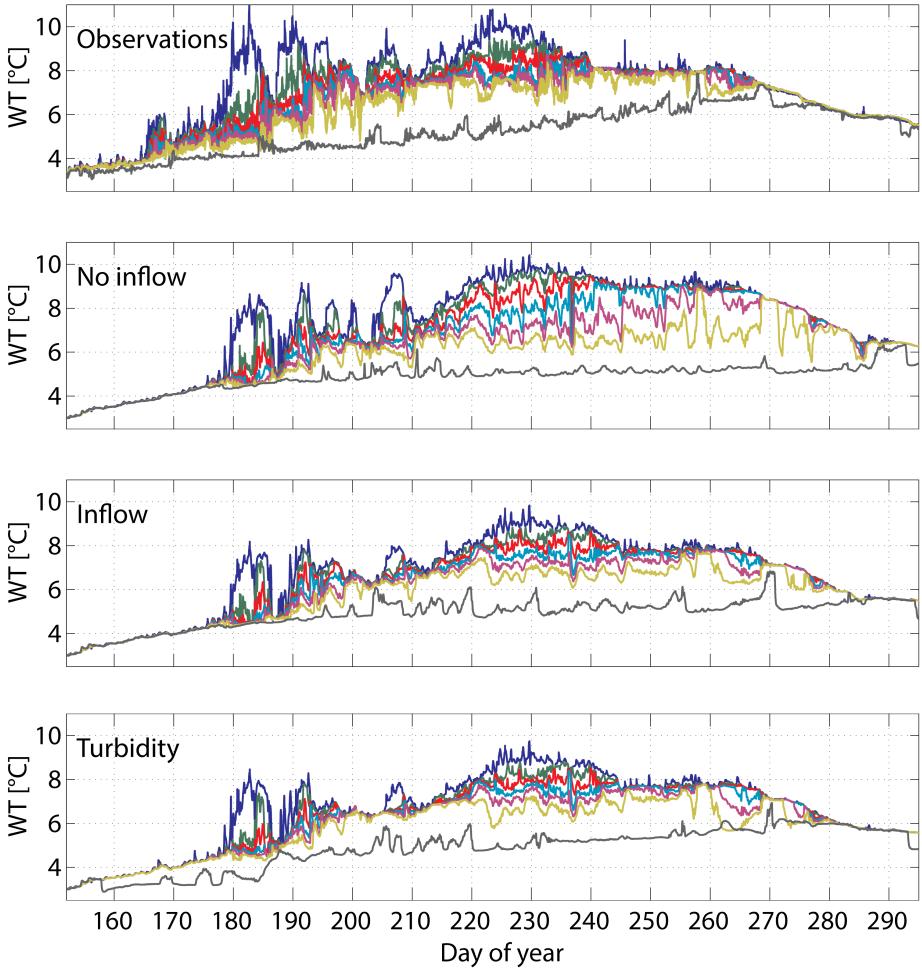

Figure 5.3. Comparison between the temperatures recorded at LAG01 at the surface, 16, 22, 28, 32, 32, 40 m depth and at the bottom (79 m depth) and modeled by SI3D-L.

At station LAG02 (Figure 5.4), the addition of the inflow improves the temperatures at 40 m depth and the definition of the stratification, though underestimating its strength. The sole addition of the inflow without the sediment load results in an unobserved inverse stratification at the start of the season.

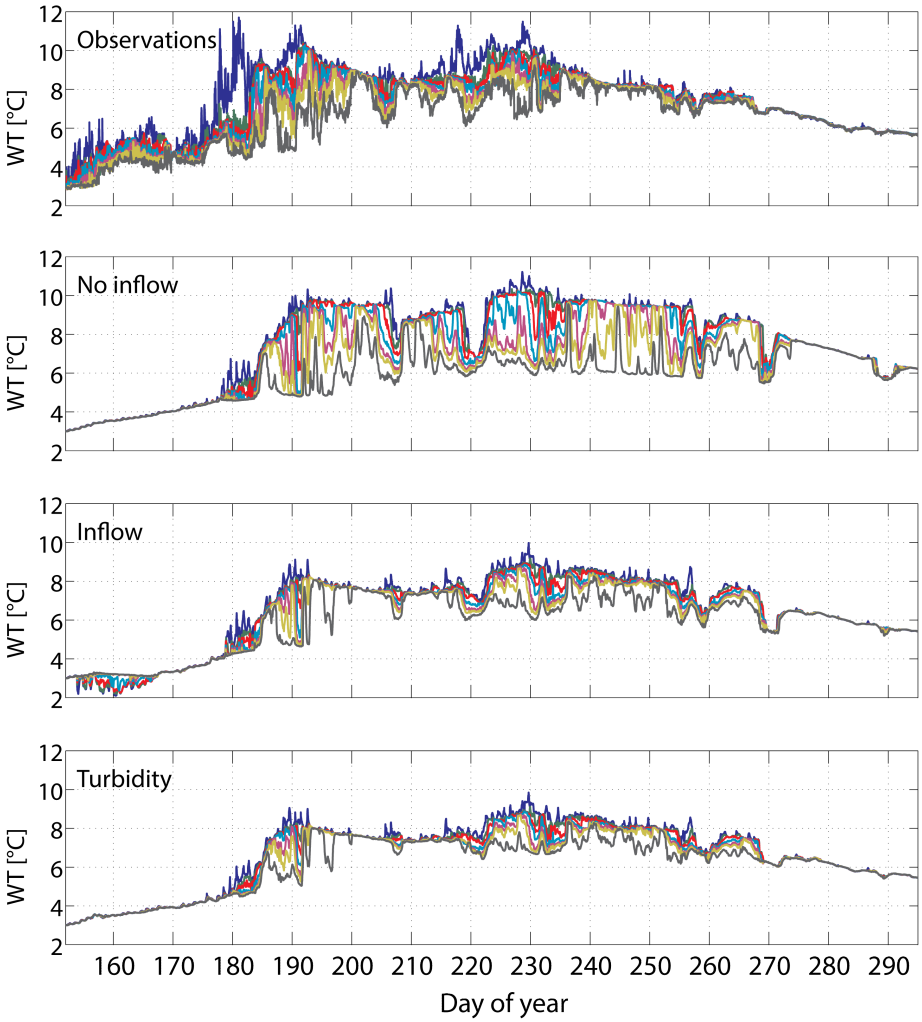

Figure 5.4. Comparison between the temperatures recorded at LAG02 at the surface, 12, 16, 22, 28, 32, 40 m depth and modeled by SI3D-L.

At the northern station LAG03 (Figure 5.5), the addition of the inflow results in a better representation of the start of the mixing season (past DOY 270). The inclusion of the sediment content in the model leads to an earlier (and closer to observed) start of the period of stratification.

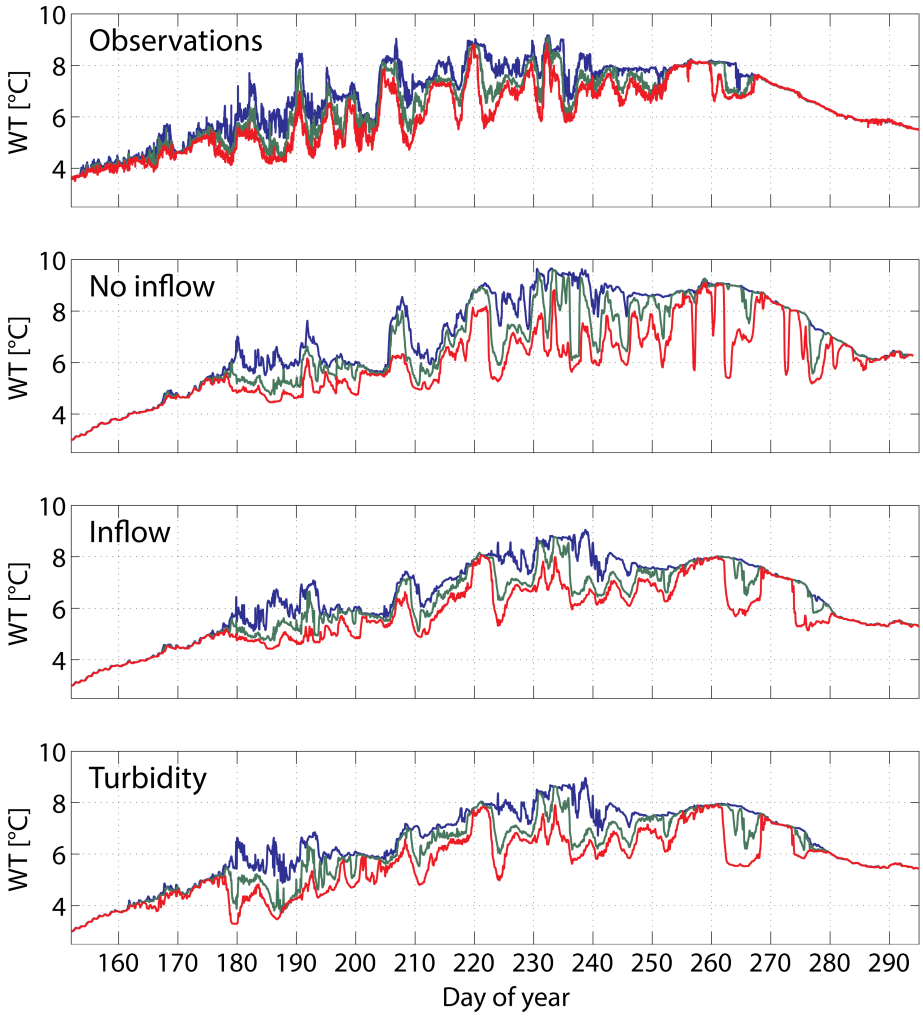

Figure 5.5. Comparison between the temperatures recorded at LAG03 at 16, 26, 36 m depth and modeled by SI3D-L.

Further analyses described above will identify more precisely the quality of the results provided by the different setups.

5.2.1 Validation of the model results

The validation of the model is a crucial step that will give the modeler a better understanding of the weaknesses and strengths of the model. In order to validate the model results, it is customary to use actual measurements and apply different statistical and time series analysis tools. Most of the discussion in this section will focus on the three main model setup results : no inflow, inflow, inflow and turbidity.

Temperatures Most of the measurements available for the lake are in the form of temperature measurements obtained through thermistor chain deployments. Observations and simulations are smoothed with a moving average over an hourly window and resampled hourly for the following analyses.

Table 5.3. Results from the error measure analysis of the temperatures simulated at LAG02, LAG03 and LAG01, from surface (1^st row) to bottom of the lake. In red, the best result between the simulation setups, in blue the worse. In bold, the general results for the stations.

	Depth	No inflow, no turbidity				Inflow, no turbidity				Inflow and turbidity			
	[m]	L1	L2	Linf	RMSE	L1	L2	Linf	RMSE	L1	L2	Linf	RMSE
LAG02	12	0.11	0.13	0.32	1.11	0.12	0.16	0.39	1.17	0.11	0.15	0.38	1.12
	16	0.11	0.12	0.35	1.05	0.1	0.14	0.39	1	0.09	0.13	0.39	0.95
	22	0.11	0.13	0.37	1.07	0.1	0.14	0.38	0.98	0.09	0.13	0.4	0.91
	28	0.11	0.13	0.48	1.08	0.1	0.14	0.49	0.97	0.09	0.12	0.41	0.87
	32	0.11	0.13	0.4	1.04	0.09	0.12	0.46	0.87	0.08	0.11	0.37	0.74
	40	0.12	0.14	0.28	1.02	0.09	0.12	0.34	0.79	0.07	0.09	0.28	0.66
	bottom	0.15	0.18	0.32	1.2	0.1	0.13	0.29	0.86	0.09	0.11	0.27	0.72
	all	**0.12**	**0.14**	**0.47**	**1.08**	**0.1**	**0.14**	**0.47**	**0.95**	**0.09**	**0.12**	**0.39**	**0.87**
LAG01	12	0.11	0.12	0.28	1.02	0.09	0.13	0.37	0.98	0.09	0.13	0.39	0.99
	16	0.1	0.11	0.2	0.92	0.08	0.11	0.28	0.8	0.09	0.12	0.27	0.83
	22	0.1	0.11	0.19	0.86	0.07	0.09	0.22	0.65	0.08	0.1	0.27	0.68
	28	0.1	0.11	0.2	0.82	0.07	0.09	0.24	0.6	0.07	0.09	0.29	0.61
	32	0.1	0.11	0.2	0.77	0.08	0.1	0.22	0.65	0.08	0.09	0.23	0.61
	40	0.11	0.13	0.23	0.83	0.1	0.11	0.25	0.72	0.09	0.11	0.25	0.7
	bottom	0.13	0.17	0.4	0.86	0.12	0.15	0.41	0.8	0.09	0.12	0.35	0.62
	all	**0.11**	**0.12**	**0.28**	**0.87**	**0.08**	**0.11**	**0.37**	**0.75**	**0.08**	**0.11**	**0.39**	**0.73**
LAG03	16	0.11	0.12	0.29	0.94	0.07	0.1	0.29	0.72	0.07	0.1	0.31	0.7
	26	0.11	0.13	0.29	0.97	0.09	0.11	0.3	0.75	0.09	0.12	0.37	0.78
	36	0.11	0.14	0.27	0.88	0.11	0.14	0.29	0.85	0.12	0.15	0.33	0.89
	all	**0.11**	**0.13**	**0.29**	**0.93**	**0.09**	**0.12**	**0.29**	**0.78**	**0.09**	**0.12**	**0.36**	**0.79**

The norm and RMSE analyses (Table 5.3) show that it is difficult to improve the results linearly across the basin and throughout the water column by adding a new parameter. Overall the addition of the inflow results in general improvements at the three stations. The addition of the turbidity results in further improvements at the southern station LAG02 close to the glacial river mouth and in the bottom layers of LAG01 the central station. The maximum error norms l_∞ are minimal for the first setup suggesting that this setup gives smaller extreme outliers even though the results of l_1 indicates that it is not able to represent as well the general trends.

The largest RMSE value, 1.17, is found for the surface temperatures at LAG02 for the setup with the inflow. While the RMSE exceeds 1 at multiple occasion with the no inflow setup, it is exceeding 1 only for surface temperatures at LAG02 for the setup with the added inflow and turbidity.

Goodness of fit The goodness-of-fit coefficients aim at describing how well the observations are represented by the model results. It is detailing the discrepancies between what is expected and what is simulated.

Table 5.4. Comparison of the modified coefficient of efficiency (E_1) obtained for each simulation comparing the data set to the 1:1 line.

	Depth [m]	No inflow	Inflow	Inflow & turbidity
LAG02	Surface	0.11	0.22	0.27
	12	0.05	0.25	0.3
	16	0.02	0.25	0.31
	22	0	0.23	0.31
	28	-0.02	0.26	0.37
	32	-0.05	0.27	0.39
	40	-0.26	0.14	0.26
	All depths	**0.04**	**0.27**	**0.35**
LAG01	Surface	0.03	0.27	0.24
	16	-0.09	0.26	0.2
	22	-0.06	0.34	0.29
	28	-0.03	0.33	0.32
	32	0.01	0.23	0.26
	40	-0.04	0.12	0.17
	Bottom (79)	0	0.08	0.29
	All depths	**0.21**	**0.41**	**0.42**
LAG03	16	0	0.38	0.42
	26	0	0.29	0.27
	36	0.14	0.17	0.13
	All depths	**0.08**	**0.31**	**0.3**

Table 5.4 suggests that the simple setup with no inflow produces results that are at best as good as a mean value for most of the thermistors. The introduction of the inflow improves significantly these results since they are at all stations and depths better than a mean value guess. The addition of the turbidity ameliorates the performances of the model for the deeper layers at stations LAG02 and LAG03. The worse coefficients are found at 40 m depth at LAG02 (-0.26) for the no inflow setup, at 79 m depth (bottom) at LAG01 (0.08) for the setup with inflow and at 36m depth at LAG03 (0.13) for the more complex setup with both inflow and turbidity.

Plots of the simulated data against observed data (Figures 5.6, 5.7 and 5.8) give us a more visual image of the goodness-of-fit of the simulation results according to the model setup. Figure 5.6 show that this setup results in a poor fit at station LAG02 both with the 1:1 line and the least-square fit line. The data is spread on either side of the 1:1 line, with a limited amount of scatters actually on the line. The general tendency is for the model to underestimate the lower temperatures and overestimate the higher temperatures. Outliers are numerous and temperature underestimations exceeding 4°C are observed. The results are of better quality at LAG01 and LAG03; the least-square fit lines are quasi parallel to the 1:1 line, however the scatters are still relatively spread on both sides of the 1:1 line.

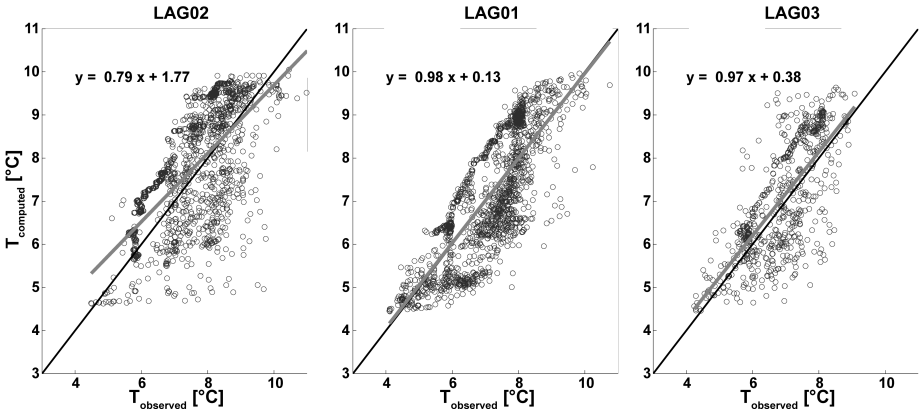

Figure 5.6. Computed (y-axis) versus observed (x-axis) temperatures at all depths for stations LAG02, LAG01 and LAG03 for setup 1 (no inflow). The black solid line has a 1:1 slope and represents complete agreement between the model and observations. The red line is the least-square fit line associated with that data set. The equation of this line appears on the graph.

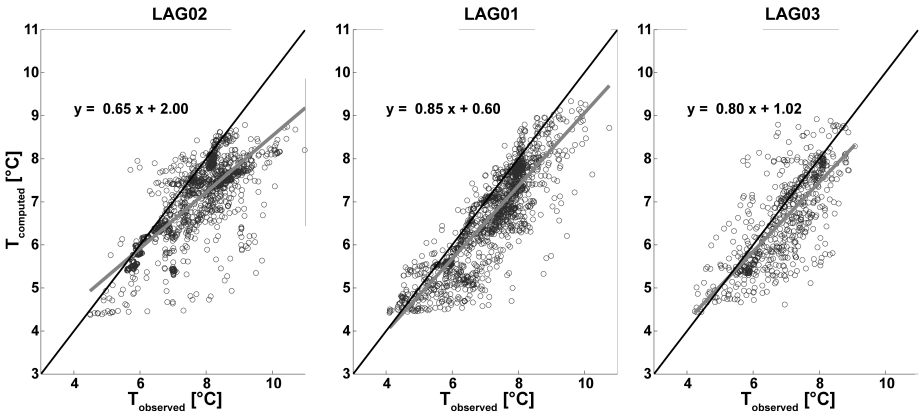

Figure 5.7. Computed (y-axis) versus observed (x-axis) temperatures at all depths for stations LAG02, LAG01 and LAG03 for setup 2 (inflow). The black solid line has a 1:1 slope and represents complete agreement between the model and observations. The red line is the least-square fit line associated with that data set. The equation of this line appears on the graph.

With the addition of the inflow in the model (Figure 5.7), the scatter clouds get tighter and more scatters are actually on the 1:1 line. However, this model setup shows a strong tendency to underestimate the temperatures in the water column. The simulation results are similar with the addition of the suspended sediments (Figure 5.8), the scatter clouds get slightly tighter and elongated along the 1:1 line.

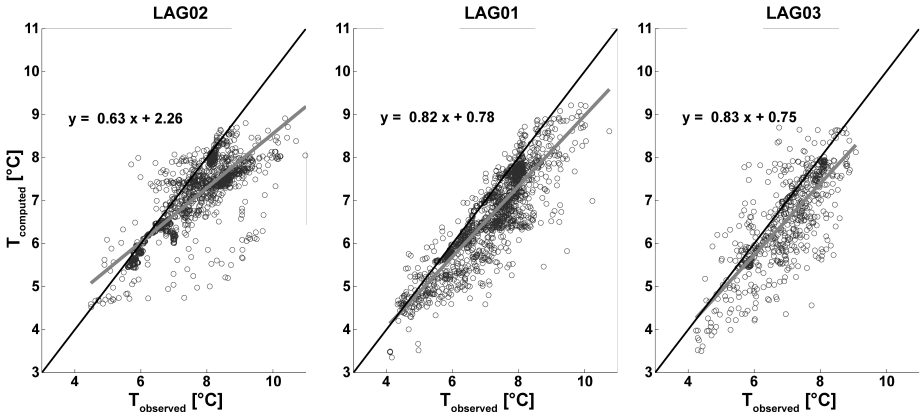

Figure 5.8. Computed (y-axis) versus observed (x-axis) temperatures at all depths for stations LAG02, LAG01 and LAG03 for setup 3 (inflow and turbidity). The black solid line has a 1:1 slope and represents complete agreement between the model and observations. The red line is the least-square fit line associated with that data set. The equation of this line appears on the graph.

Stratification and heat transfer The observed stratification periods ($\Delta \geq 0.5$°C) are evaluated to be 126 days at LAG02, 100.6 days at LAG01 and 110.6 days at LAG03. The comparison of the three main setups for the definition of the stratification (strength and period) (Table 5.5) shows that the inclusion of the inflow improves the stratification in terms of strength. The addition of the suspended sediment in the model decreases slightly the quality of the results (slightly larger rms values), this can be observed on Figures 5.3, 5.4 and 5.5 with a tendency of that setup to underestimate The stratification period is not properly simulated at station LAG02 by the three setups. The period discrepancy seems to be shorter with the first setup (no inflow), however getting back to Figure 5.4, it appears that this difference is artificially created by a stratification season that lasts artificially longer with this model setup.

Table 5.5. Comparison of the representation of the stratification by the different simulations for the station LAG02, LAG01 and LAG03.

	LAG02			LAG01			LAG03		
	Strength rms	Period [days]	Δ [days]	Strength rms	Period [days]	Δ [days]	Strength rms	Period [days]	Δ [days]
No inflow	1.69	112.1	-13.9	1.22	107.5	6.9	0.94	108.1	-2.5
Inflow	0.94	92.9	-33.2	0.75	99.0	-1.6	0.73	101.2	-9.5
Inflow & turbidity	0.97	87.4	-38.7	0.79	97.6	-2.9	0.76	109.7	-1.0

In order to compare how well the different setups are able to simulate the stratification and heat transfer throughout the water column, average water temperature profiles are computed for the three stations and at different periods and compared to the observed average profiles at the same location.

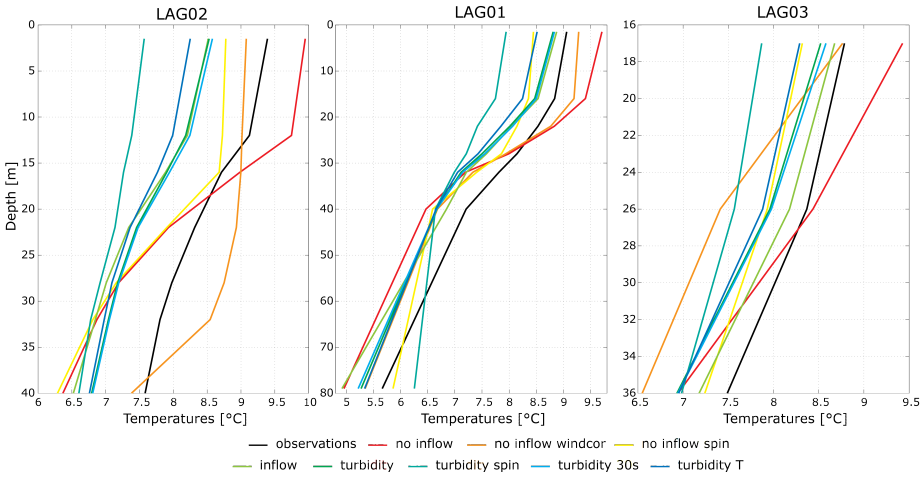

Figure 5.9. Comparison of average temperatures in the water column at LAG01 for DOY 232 to 234 included for the different model setups used.

Figure 5.9 shows that the omission of the inflow results in profiles that are rather far from the observed profiles. The increase of the spin-up time corrects that discrepancy a little. The addition of the inflow improves significantly the shape of the profiles but results in a overall underestimation of temperatures in the water column. The worse performances of the model are observed at LAG02.

The evolution of the profiles over the summer season give us some pieces of information about the heat transfer throughout the water column in the different setup. At station LAG01 (Figure 5.10), with no inflow, the model progressively develops a two layer system with a 20-10 m large thermocline between 20 and 40 m depth that sharpens artificially as the stratification period progresses. At the start of the stratification period,

the upper layer's temperatures are underestimated while the bottom temperatures are slightly overestimated. At DOY 263-265, close to the end of the stratification period, the model overestimates by slightly more than a degree the water temperature in the upper layer while underestimating by more than a degree the deepest layer.

The addition of the inflow improves the general shape of the profiles at station LAG01, with a simulated profile for DOY 232-234 very similar to the one observed but with an approximately 0.5°C underestimation of the temperatures. While that shift almost disappears a month later (DOY 263-265) in the upper layer of the water column, it worsens below 30 m depth. The further addition of the suspended sediments (turbidity) does not present much improvement compared to the sole addition of the inflow. While it improves the temperatures at the bottom of the lake it results in an artificially sharp thermocline at the end of the summer season.

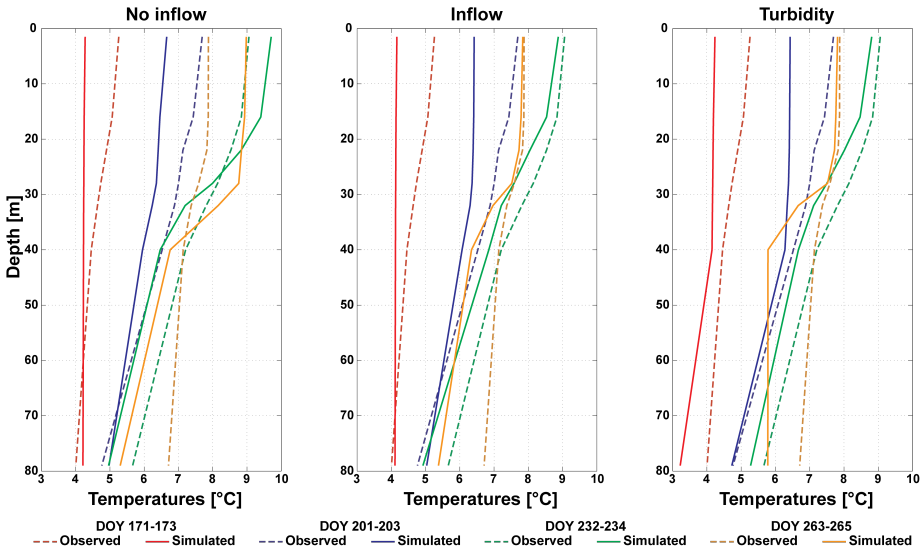

Figure 5.10. Comparison of average observed and computed temperatures in the water column at LAG01 for DOY 171-173, 201-203, 232-234 and 263-265 for the three main setups : no inflow, inflow, inflow and turbidity from left to right.

At station LAG02 (Figure 5.11), the model, without inflow, overestimates the temperatures in the 20 to 30 m upper layer while underestimating the temperatures below. The addition of the inflow once again improves drastically the shape of the profiles, despite a general underestimation of the temperatures.

Similar observations can be made at LAG03 (Figure 5.11), where the slopes of the simulated profiles are opposite to the observed slopes for almost every periods considered. At DOY 263-265, a difference of almost 2°C can be observed at 26 m depth. The addition of the inflow improves once again the profile shapes, nonetheless the profiles for DOY 263-265 have quite dissimilar slopes as well.

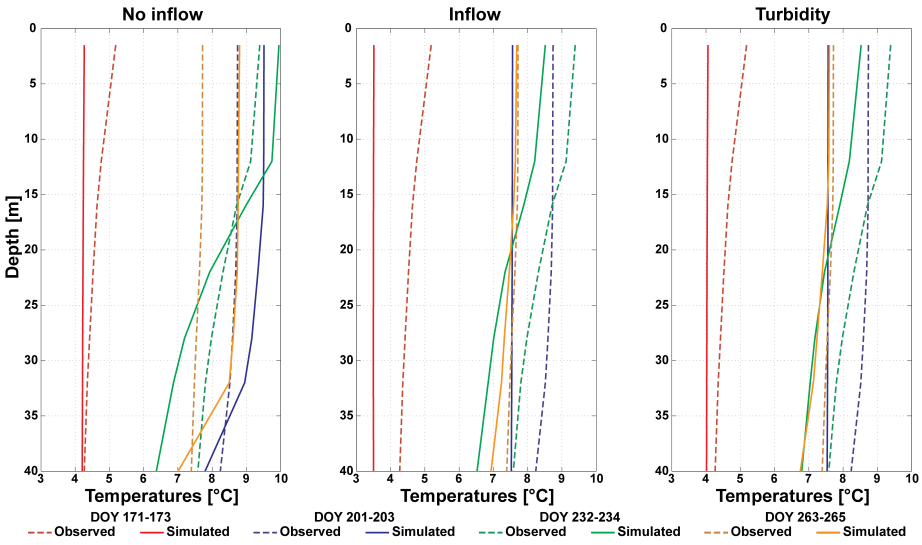

Figure 5.11. Comparison of average observed and computed temperatures in the water column at LAG02 for DOY 171-173, 201-203, 232-234 and 263-265 for the three main setups : no inflow, inflow, inflow and turbidity from left to right.

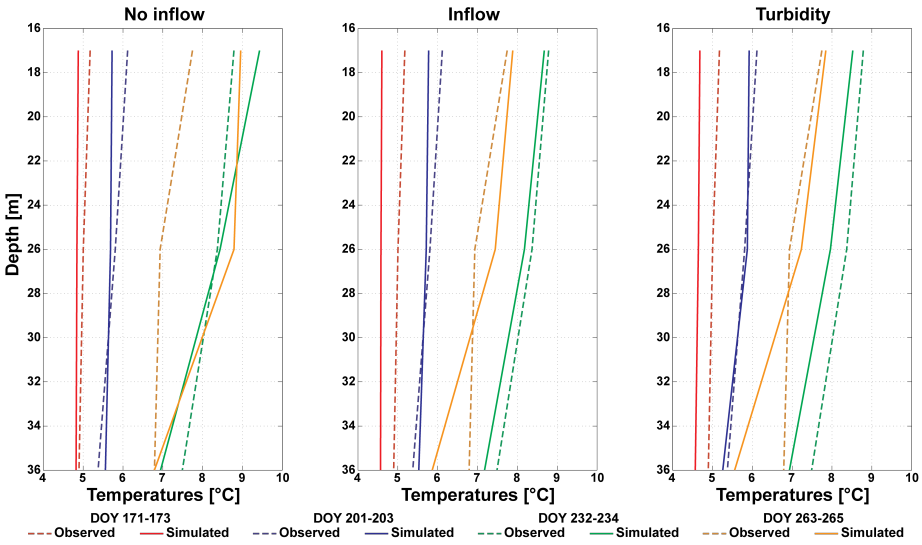

Figure 5.12. Comparison of average observed and computed temperatures in the water column at LAG03 for DOY 171-173, 201-203, 232-234 and 263-265 for the three main setups : no inflow, inflow, inflow and turbidity from left to right.

The introduction of the inflow in the model is essential in order to obtain a good representation of the stratification in the lake. The addition of the suspended sediments

improves generally the deeper layer but can increase slightly the underestimation of the temperatures.

Internal waves Internal wave periods are analyzed for the model setup including both the river inflow and the suspended sediments and compared to the observations at LAG01 (Figure 5.13) and LAG03 (Figure 5.14). Spectral analyses show a generally better agreement between the observed and simulated periods for the month of July.

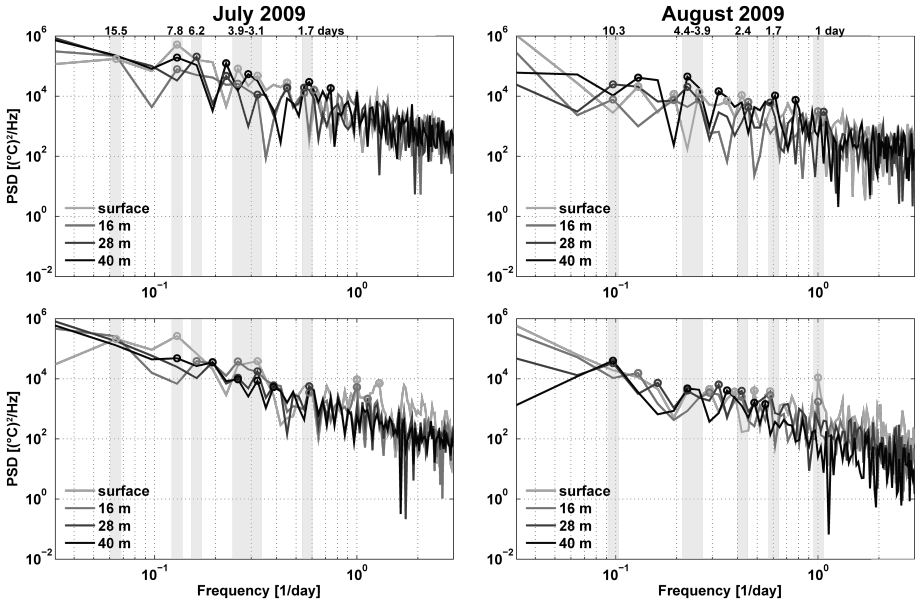

Figure 5.13. Spectral analyses of the water temperature variations at LAG01 in July and August 2009 for observed data and the simulated results (inflow and turbidity).

As shown in Figures 5.13 and 5.14, the model is able to reproduce appropriately both the main oscillation frequencies of the internal waves and their spectral power density. This is particularly clear for LAG03 where the signal is cleaner, despite a slight underestimation of the energy associated with the main observed oscillation periods.

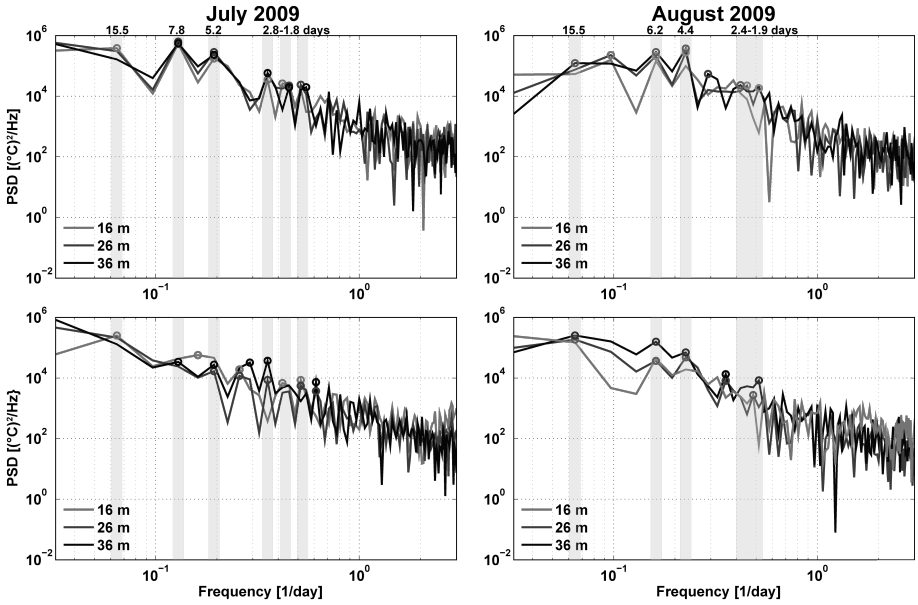

Figure 5.14. Spectral analyses of the water temperature variations at LAG03 in July and August 2009 for observed data and the simulated results (inflow and turbidity).

Turbidity A major of interest of this model is to understand the intrusion impact of the glacial river on the internal motions of the lake. This is especially crucial as it is heavily loaded with suspended sediments which can have a significant impact on the ecology of the lake when injected in the water column.

In order to identify if the model is able to simulate properly the river intrusion and suspended sediment load, comparison methods are rather limited, however the field campaign carried out on the 30^{th} of July 2009 by Hrund Ólöf Andradóttir with a Ysi multi-parameter sonde allows us to compare the results of the model along the lake basins as much for the temperature as for the turbidity.

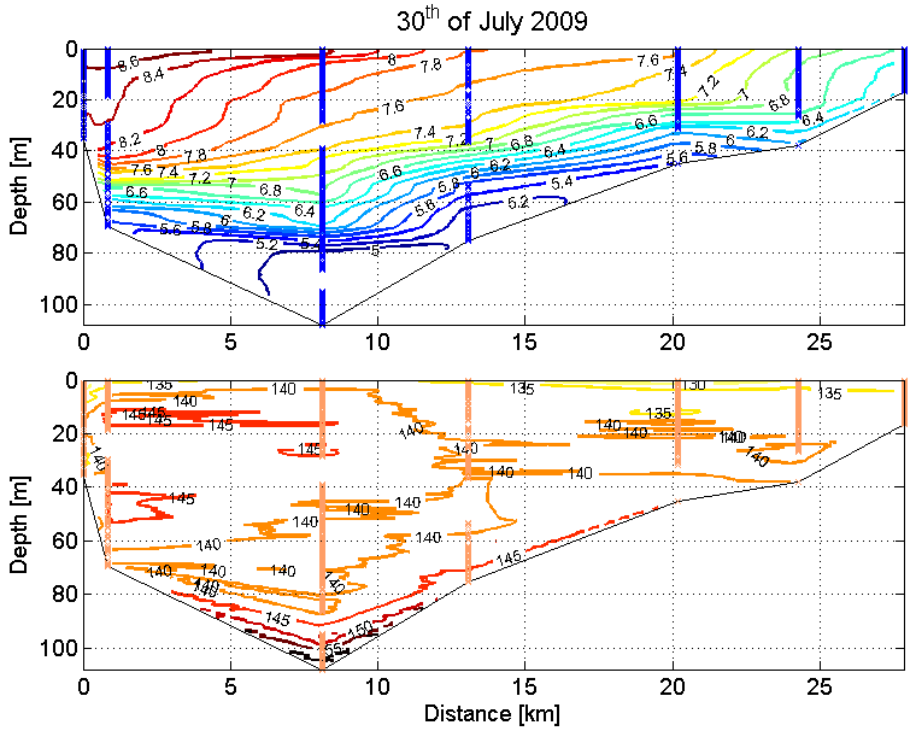

Figure 5.15. Longitudinal cross-section (SW end to NE end) of the temperatures in °C (up) and of the turbidity in NTU in Lake Lagarfljót recorded with a Ysi multi-parameter sonde on the 30th of July 2009. The blue crosses represent the location of the actual measurements. The temperature and turbidity values are displayed on their associated isolines.

Despite the sparsity of the measurements, some characteristic features are revealed. Figure 5.15 shows that on the 30th of July 2009 the thermal structure in the lake was rather simple with some upwelling at the northern end of the lake and downwelling at its southern end resulting in a horizontal gradient of temperatures. The turbidity longitudinal cross-section presented some high level of turbidity ($\geq$ 145 NTU) at the bottom of the lake in the main basin almost all the way to the northern shallower basin. In addition, high NTU values were measured at about 30 m depth at Hafursá (about 8 km from the southern end on the plot).

Comparing these observations with the results obtained from the model for the 30th of July 2009 (Figure 5.16), it is striking to see how well it is able to reproduce the thermal structure in the lake, despite some underestimation of the water temperatures. Some discrepancy appears at the northern end of the lake with some unobserved warm temperatures in the upper layer of the water column. The turbidity level can be directly connected to the concentration in suspended sediments (cf. relationship TSS and NTU): the higher the concentration, the higher the turbidity. Just as in the observations, the

modeling results show higher level of suspended sediments at the bottom of the main basin extending almost to the northern secondary basin and a high peak of turbidity between 20 and 60 m depth at about 8 km from the southern end of the lake.

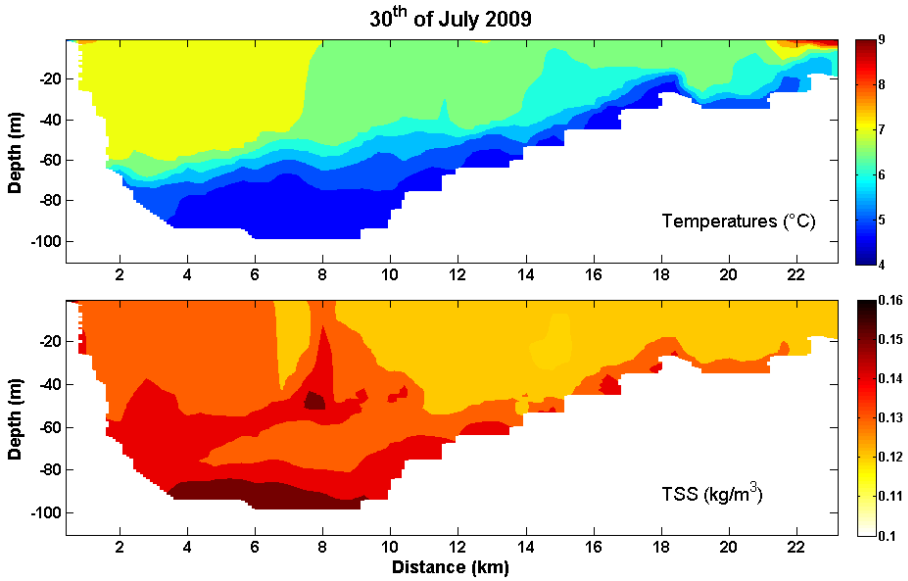

Figure 5.16. Longitudinal cross-section (SW end to NE end) of the temperatures in °C (up) and of the suspended sediments in kg/m^3 in Lake Lagarfljót on the 30th of July 2009 at 12.00 as computed by the model (model setup 3 : inflow and turbidity).

These good results are obtained after almost two months from the start of the simulation and suggest that the model is performing well both for the thermal and the suspended sediments distribution.

5.2.2 Contributions of the model on the study of internal waves in Lake Lagarfljót

In the previous section, it is shown that the model is able to simulate quite closely the internal behaviors of the lake without requiring any change of the source code (apart from the introduction of turbidity in the equation of state) nor any tweaking of the input parameters. The validation of the simulation makes it possible to use the information from the model to investigate further the dynamics of lake Lagarfljót.

Effect of external forcing on internal waves In Chapter 4, it is shown that the periodicity of the wind at Egilsstaðir airport is really close to the natural periods in the lake basin found by the 2D Münnich model. In addition the in-situ measurements performed in the lake waters show similar results. In order to examine the role of wind in the onset and feeding of internal waves.

As easily expected lake numbers for Lake Lagarfljót are low and lake numbers below 1 are frequent through out the stratification season (Figure **??**).

In order to investigate the effect of wind on the internal wave regime, wind speed events are identified and synchronous as well as subsequent possible changes in the water column examined (Figure 5.17). To isolate the wind events the threshold of 10 m/s is arbitrarily defined (Figure 5.1): all wind events with speeds exceeding that threshold are looked into. A simple color coding is used in order to simplify the reading : blue for northern winds, red for southern wind, and the events with LN$<$1 are emphasized with a gray shadow.

Northern winds The first wind event (DOY 199) is associated with a cooling of the surface temperatures but also a warming up of the bottom temperatures (downwelling). As the wind speed subsides abruptly just before DOY 200, surface temperatures rise again temporarily. The middle layer with temperature around 6°C progressively occupies most of the water column until the wind event subsides at around DOY 205. The 30 upper meters warms up suddenly as the surface layer pushed to the southern end of the lake comes back.

The second event is much shorter (in the order of one day), no significant event are identified in the water column.

For the third wind event (DOY 275) no significant change of the surface layer characteristic can be observed on the temperature contour plot, however as the event finishes we can observe that the concentration in suspended sediment of the surface layer increases suddenly. In the bottom layer, a temperature inversion appears associated with a high suspended sediment concentration.

The fourth and last northern wind event (DOY 281) lasts about 2 days and wind speeds reaching 15 m/s (hourly mean). The temperature contour plots suggests a mixing of the water column, however the contour plot showing the suspended sediment concentration indicates otherwise. As the lake surface cools down the interlayer/middle layer reaches the surface (upwelling), simultaneously the bottom temperatures increases (downwelling). Mixing of the water column happens about 5 days later if we consider the sediment distribution in the water column as well as the temperatures.

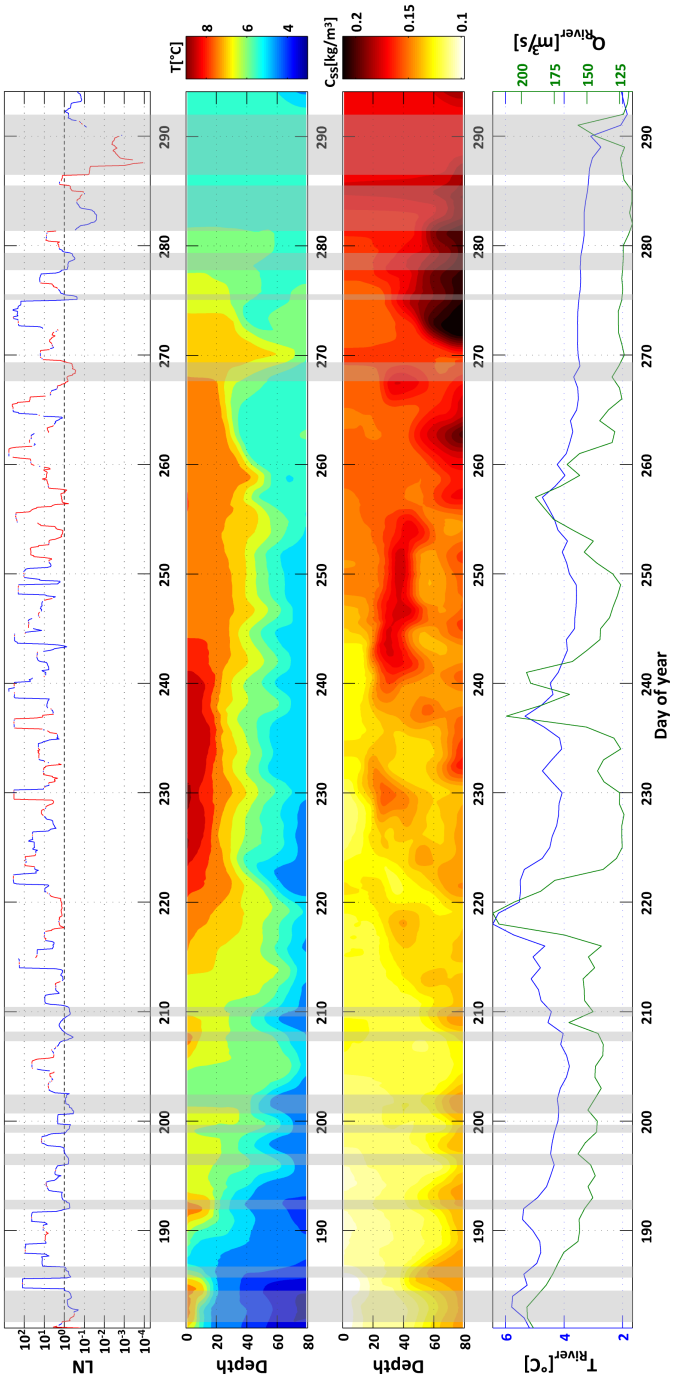

Figure 5.17. SI3D model results for LAG01. a) Water column stability, represented by lake number. Red represents wind from south, blue from north). b) Water temperature c) and suspended sediment concentration d) southern inflow discharge and temperature of the southern inflow. Gray shadows underline episodes with LN<1. Data are smoothed based on a first mode (H1V1) period (Ti) estimated to be 4 days.

Southern winds The first event isolated (DOY 232) is very short, we can observe some slight warming of the surface which could also be attributed to solar heating, at the bottom we observe upwelling associated with higher suspended sediment concentration.

The next event happens at about DOY 251 and lasts (discontinuously) about 3 days. Some downwelling can be observed which can also be attributed to the high suspended sediment intrusion at 40-50 m depth which is associated to the high river discharge event that occurred between DOY 237 and DOY 241.

The third southern wind events starts about a day after the previous one finished and lasts about 4 days. The surface layer gets warmers and deepens, however the bottom experience upwelling (high Css) which results in the apparition of the sharp thermocline oscillating between 40 and 60 m depth.

The fourth event lasts about 4 days between DOY 266 and 270, wind speeds reach 15 m/s at DOY 267. The surface temperature drops at DOY 268: the station LAG01 is not located the northern end of the basin, the surface water is blown north passed the station, possibly into the southern basin. The water column is almost fully mixed at DOY 270. As the wind speed drops upwelling occurs in association with a sudden increase of the suspended sediments at the bottom of the water column.

From DOY 282, the water column is thermally mixed however density gradients are still existing due to higher suspended sediment concentration at the bottom of the water column. As a result of the short wind event from DOY 284, further mixing happens in the upper part of the water column and upwelling is observed at the bottom.

The sixth and last southern wind event identified happens shortly after the fifth one and lasts about 4 days. It results in the full mixing of the water column.

Large discharge events from the glacial river Four major discharge events can be isolated (DOY 183, DOY 219, DOY 237, the fourth one reaches a peak at DOY 257 and is synchronous to a large wind event from the South, Figure 5.17). Following these events, peaks of high suspended sediments concentrations are observed at LAG01 at varying depths (30 to 50 m depths or at the bottom). The interflow intrusions are associated with lower concentrations of suspended sediments than those found at the bottom; they are associated to stretching and deepening of the isotherms (see temperature contour plot in Figure 5.17). The sudden suspended concentration peaks occurring at the bottom of the water column after these large events are on the other end associated with inverse stratification and upwelling.

While large wind events appear to be forcing the wave climate and particularly the upper layers, the large discharges from the glacial river influence the layers below 30 m and particularly the bottom where sudden large upwelling are associated with a rise in the suspended sediment concentration.

Drivers for internal wave periodicity Figure 5.18 presents the progression of energy associated with different wind and lake temperature periodicities during the stratification period. The comparison of the wavelet analysis of internal oscillations at LAG01 to that of the wind identifies three episodes, noted as A, B and C on the Figure.

Episode A occurs at the start of the stratification season (DOY 174-178). A strong northerly wind signal then is detected at about 7 days in panel a and less prominently in panel b.

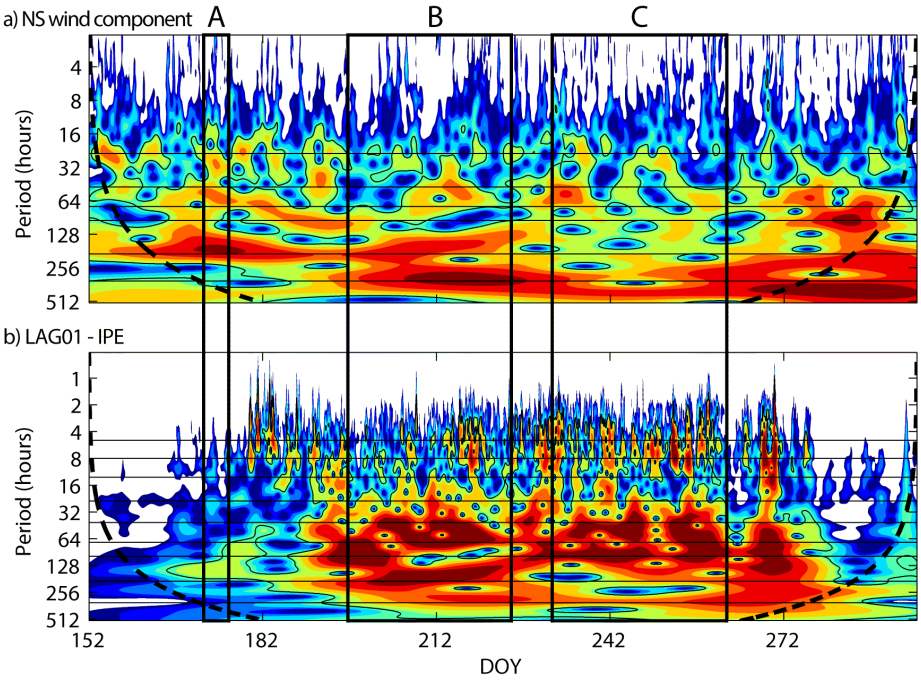

Figure 5.18. Wavelet power spectrum of the NS wind component (panel a) and the IPE at LAG01 (panel b).

Episode B (DOY 199-228) is dominated by northerly winds. The wind oscillation signal seems reproduced in the temperature signal (Figure 5.19B), with a different distribution of the associated energy. Peaks are observed at roughly 13, 7 and 2 days, the wind presenting more energy in the longer periods unlike the IPE showing larger amplitudes at 7 and 2 days than at 13 days. The wind seems to be able to force the oscillations in the basin, the response of the basin being stronger as the stratification develops.

Episode C is associated with a weaker wind signal in the NS direction, the isotherms start oscillating with a shorter periodicity, roughly 2 and 4 days, irrespective of the wind signal.

The oscillations of the IPE at LAG01 presenting the largest energy have periods very close to the main natural periods found by the Münnich model, supporting the idea that these oscillations predominate due to some phenomena of resonance of the basin.

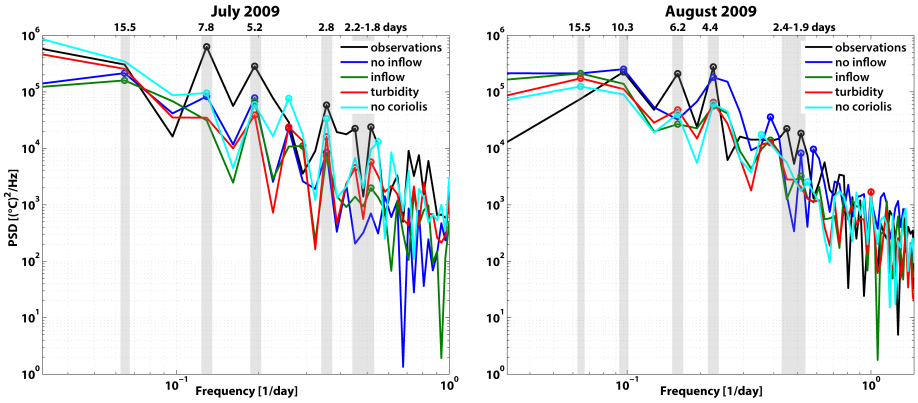

Figure 5.19. Spectral analysis of observed and simulated water temperatures at LAG03 in July and August 2009 at 22 m depth.

Effect of Earth rotation on internal waves It is shown in Thermal stratification and internal dynamics in Lake Lagarfljót (section 2) that the Coriolis forces are able to act on the lake and are generating Kelvin waves, however the field measurements did not allow us to identify them precisely. In order to analyze the Coriolis forcing effects in the lake, some additional simulations were performed, using the optimal setup (inflow and turbidity) and with a larger number of time series recorded along the lake (Figure 5.2).

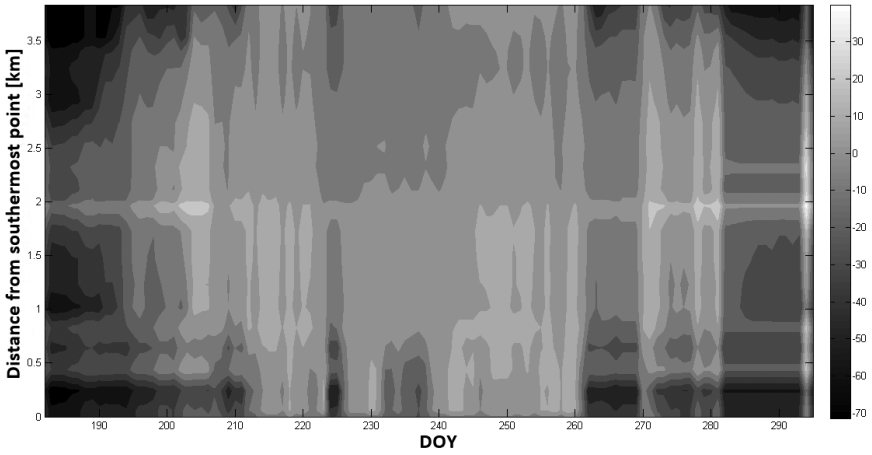

Figure 5.20. Tilt displacement of the thermocline along the shore of the southern basin of Lake Lagarfljót. The thermocline depth (in meter) is represented by the gray scale. The distances from southermost station E1 and circularly counterclockwise to northermost station E10 and back (Figure 5.2).

The analysis of the tilt displacement along the main basin shores (Figure 5.20) is not very clear and does not allow us to draw any definite conclusion as for the

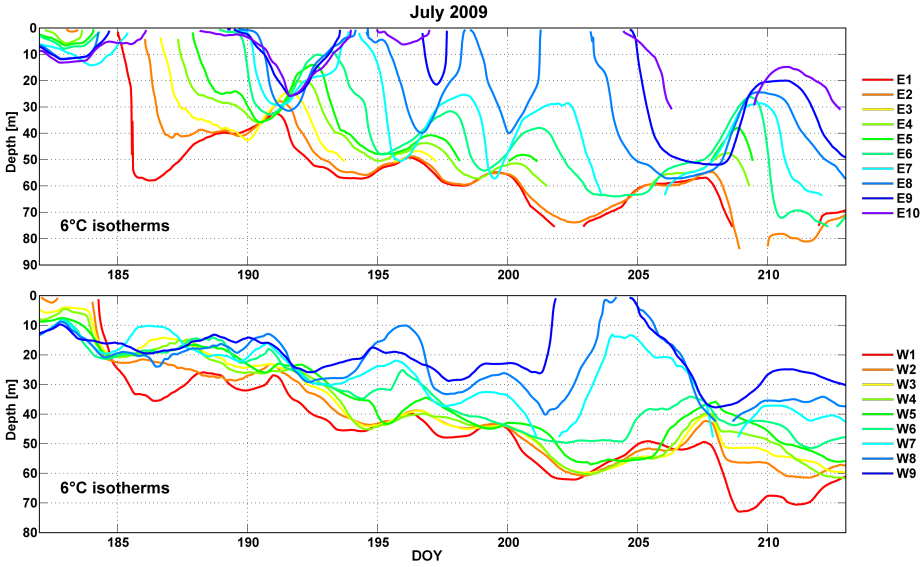

Figure 5.21. Modeled depth of 6°C isotherm in the southern basin at the stations in Figure 5.2 during the month of July 2009.

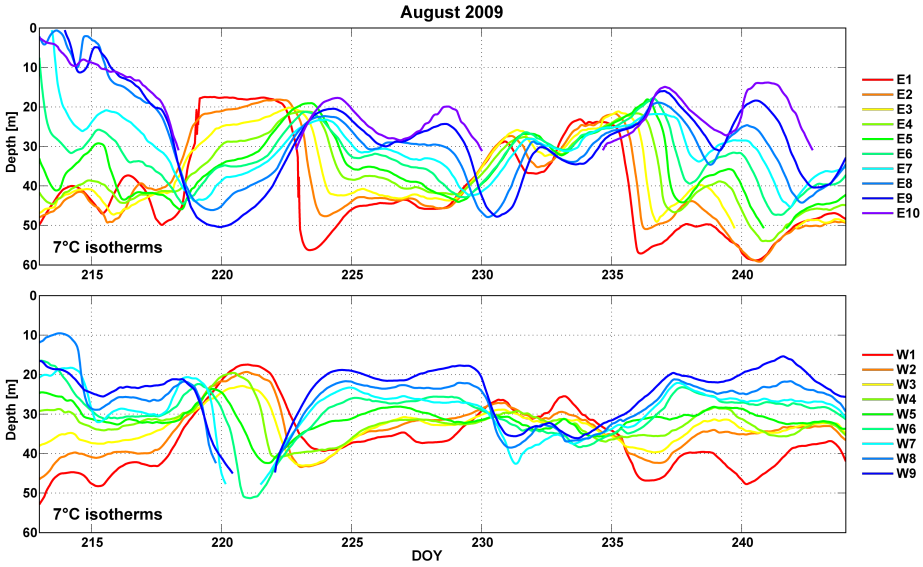

Figure 5.22. Modeled depth of 7°C isotherms in the southern basin at the stations in Figure 5.2 during the month of August 2009.

presence of Kelvin waves in the basin. However, a seasonality in the wave propagation seems to exist, with a symmetry at the start of the summer until late July (DOY 210)

and again later from DOY 262, interrupted with an asymmetrical episode (tilt of the thermocline laterally across the basin). In addition, looking at 6°C and 7°C isotherms (these isotherms are selected as they are the least interrupted during the summer season (Figure 5.21 and 5.22)), clear phase shifts appear between the isotherm depths at the different stations, with a time lead for the eastern stations from south to north and a time lag for the western stations in the same direction. This phase shifts suggest a counter-clockwise rotation of the internal wave with period around 5 days in July 2009 and closer to 6-7 days in August 2009.

5.3 Summary

The 3D hydrodynamic model is shown to represent reasonably well the internal waves in a weakly stratified lake and hence can contribute to the investigation of hydrodynamics in this type of lake. These simulations demonstrate the importance of the quality of the input information on the results. The introduction of the inflow corrects significantly the representation of the stratification by the model. However the internal waves periods do not seem to be affected by the modification, which suggests that the bathymetry is the prime controlling factor of the oscillations in the basin.

Wind is the main stimulus of internal waves and in these simulations the wind field was assumed to be homogeneous over the whole basin, however the recent measurements by a weather station set at the southern end of the basin shows that there is a non negligible difference between the wind speed and direction at the northern and southern ends of the lake. The introduction of a spatially heterogeneous wind field in the model could be introduced in order to investigate its effect on the internal waves.

5.3.1 Sources of errors

The different validation tests show that the model is an adequate tool to simulate the internal motions in lake Lagarfljót. These analyses emphasize the importance of the quality of the input data in order to get accurate results. Some sources of error, inherent to the model or to the input data, can be pinpointed.

The initial conditions in the model are assumed to be homogeneous throughout the lake, however Figures 5.3, 5.4 and 5.5 indicate that there is a significant difference in stratification level between the three stations at the start of the simulation period, with a more developed stratification at LAG02. By assuming homogeneous conditions at the starting date, errors are introduced that the model needs to correct and overcome, this can in part explain the poorer results at station LAG02.

The surface boundary conditions (weather input) are simplified and partly extrapolated. Two stations are monitoring the weather close to the lake, one at its northern end (Egilsstaðir Airport) and one at Hallormsstaðir, close to the Hallormsstaðir forest (hence partly sheltered) and at 60 m above the sea level, to wit about 30 m above the lake level. A quick comparison of the data collected at both stations shows that there is a difference between both the air temperatures, generally warmer at Hallormsstaður, and the wind speeds and directions. In addition, the comparison with a temporary station placed at the

southern end of Lake Lagarfljót in an open field (Appendix A) shows some significant discrepancies in the wind velocities along the lake axis, suggesting that the wind speeds recorded at Hallormsstaður are strongly underestimating the wind conditions at the lake level. However a simple correction and transformation of the wind speeds and directions into velocities along the lake (setup wind cor) is insufficient and does not manage to improve significantly results and rather worsen them at some stations. This stresses how crucial that is for the wind input variable to be correct. The importance of the spin-up period is highlighted by the setup "Spin up". The lake stratifies weakly and its internal motions are slow (long internal wave periods), it is therefore reasonable to estimate that a longer spin up period could help the model minimize the effects of simplified initial conditions.

Furthermore, the addition of the inflow suffers from a couple of simplifications. The water temperatures in Grimsá are obtained from corrected and extrapolated data. Grímsá is, however, thought to affect mostly the circulation in the secondary basin but there was no measuring station in that basin in 2009, there is therefore no clear estimation of the effect of this simplification.

The inflow at the southern end is a combination of three types of rivers, two glacial rivers Jökulsá í Fljótsdal and the discharge from the Kárahnjúkar power station and a freshwater river Kelduá. In order to simplify the inflow characteristics it is assumed that the waters from these rivers mix fully before entering the lake, however composite satellite images of the southern end of the lake suggest that the different rivers and in particular Kelduá do not mix fully before entering the lake.

Finally, the suspended sediment load or concentration (C_{SS}) is added to the model using a simple relationship with the discharge of the inflow (cf. p.48), however as it is pointed out in this same section,this relationship suffers from a problem of non-stationarity.

5.3.2 Complex interplay of the external forcings

The role of the wind in the forcing of internal wave is confirmed for this low lake number. The model brings in addition some important insights on the role of the glacial river inflow and explains why the glacial inflow can not be omitted when studying the circulation within lake Lagarfljót as it is participating to the renewal of the cold water trapped at the bottom of the lake forcing further the oscillation occurring at the bottom due to internal waves and allowing the water to pass the sill threshold, to the thermal mixing of water as it drags warmer water down the water column and to the internal waves themselves when intruding in the mid layers (stretching the isotherms).

A simple consideration of the isotherms during the two months of the summer season suggest that the southern basin experiences oscillations forced by the Coriolis force, resulting in Kelvin waves with oscillation period around 4 to 5 days in July and 6 to 7 days in August 2009. These findings are confirmed by the additional analyses presented in Priet-Mahéo et al. (2019), in addition the presence of super-inertial Poincaré waves is also demonstrated.

6 The fate of the southern glacial river inflow in Lake Lagarfljót

Chapters 3 and 5 emphasize the necessity to include the inflow of the main tributaries in the study of the internal dynamics of Lake Lagarfljót. The 3D hydrodynamic model Si3D has shown to successfully reproduce the features observed in the lake such as turbidity peaks and thermal stratification inversions, allowing us to use the results the model to analyze and understand the pathways of the inflow.

This final chapter builds on the findings of the previous chapters. The results from the model and observations are used to support the analysis of the fate of the glacial inflow in the lake. The circulation between the two basins of the lake is also investigated and a conceptual model is proposed.

6.1 Method

The 3D model Si3D results are used primarily to investigate the river fate in the lake; field measurements are then scrutinized and used to validate the results from the model.

6.1.1 Tracer study

The model is run with inflows and outflow as described in Chapter 5. Tracers analyses can be simulated within the model using the transport equation for non-active scalar, unlike the suspended sediments, it will not contribute to the equation of state.

Twelve tracer experiments were run in the Si3D model and the concentration in space and time simulated with the model. The tracer is defined as conservative and does not affect the equation of state. It allows us to track the water particles that entered the lake simultaneously. Three different output files were produced: a section file (or vertical cross-section) following the thalweg of the lake and plane files (different depths) recording velocities, temperatures and suspended sediment concentrations and a tracer file where the 3D path of a conservative tracer injected by pulse in the glacial inflow is saved. Time series of tracer mass present in the basin were determined for different spatial extent: total tracer, tracer above 50 m depth, tracer below 50 m depth, tracer in the surface layer (in the 10 m layer below the surface), tracer at the bottom of the water column (in the 10 m layer above the bottom), tracer in the southern basin and tracer in the northern basin.

6.1.2 Field evidences

Field measurements are considered in light of the new findings, made possible by the tracer experiments. Sonde profiles, which combine both temperature and turbidity measurements are of great importance to validate the theory developed based on findings from simulations. In addition, the thermistors chains (LAG03 and LAG04) placed during summer 2011 on either side of the sill are in a key position to record the exchanges between the two basins. The temperature changes across depth will be considered at both location synchronously in order to discern large water exchange events occurring during the period of measurements.

6.2 Results

The residence time in the lake is estimated to have reduced to approximately half a year since the outflow from the hydropower plant was added to the glacial inflow upstream from the lake. The signal of the river inflow is clearly observed not only at LAG02 but also at LAG01 a station located on the northern side of the lake, about 13.5 km from the river mouth (see 3.3). Finally as shown in validation of the model results (see 5.2.1), the inclusion of the river inflow improves significantly the model results. We can therefore infer that the glacial inflow has a non negligible influence on the circulation in the lake.

To investigate further the fate of the river in the lake, a tracer study is conducted. Twelve release experiments are performed : from DOY 181 and every 5 days until DOY 221 (included), some conservative tracer is released in the glacial river inflow. The presence of tracer is then studied for each release to determine the specificities and similarities.

6.2.1 Pathways of the river inflow

It is difficult to discuss timeseries of 3D datasets, so to simplify the analysis, the tracer mass present in the basin is classified in categories or spatially discriminated, hence the categories are defined as follow : total tracer, tracer above 50 m depth, tracer below 50 m depth, tracer in the surface layer (in the 10 m layer below the surface), tracer at the bottom of the water column (in the 10 m layer above the bottom), tracer in the southern basin and tracer in the northern basin.

Release 1 (Figure 6.1) is synchronous to a large discharge event. The river enters the lake as an underflow : more than 90% is classified as below 50 m depth and 30 to 40% as in the bottom layer. The tracer concentration in the northern basin increases by "‘jumps"’. The river water is ejected out of the southern basin/bottom layer by cycles. By DOY 280 30% of the water that came in with the river exited the lake.

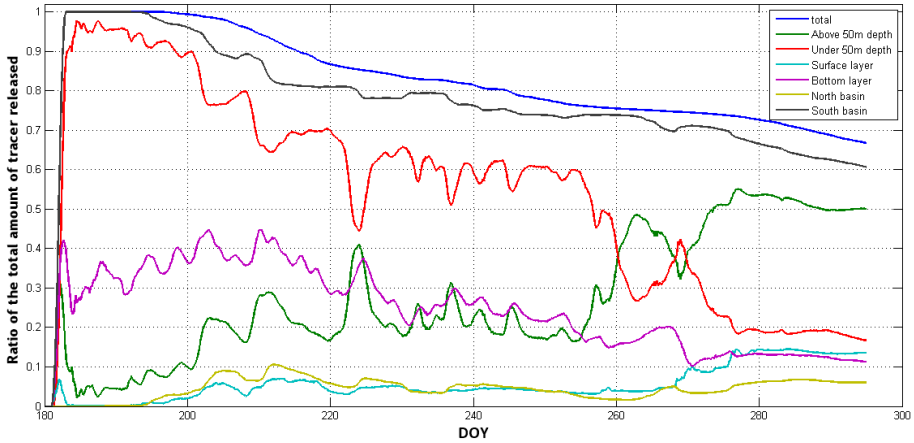

Figure 6.1. Tracer pathways for the first release.

Looking in details at the flushing events, it appears that they follow closely large discharges from the glacial river. The river water flows down the southern slope and as it has acquired kinetic energy continues up the northern slope flushing part of it water in the northern basin, it then continues oscillating in the southern basin (as the oscillation of the curve of tracer above and below 50 m indicates) until another major discharge comes to give an extra push to the older water mass. The more the river water oscillates and the more it mixes. These flushing events are resulting in upwelling event as the curves of tracer in the surface water and above 50 m indicate.

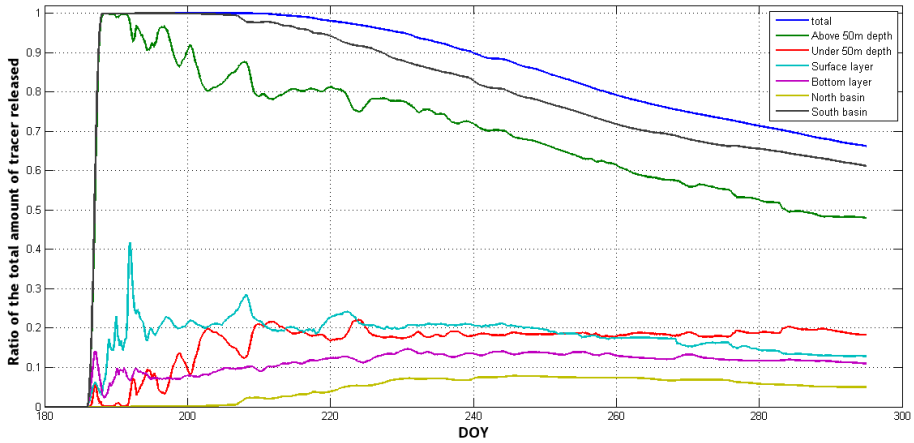

Figure 6.2. Tracer pathways for the second release.

The second release (Figure 6.2) occurs just 5 days later however the fate of the water is very different. Most of the river water intrudes above 50 m. The tracer mixes relatively rapidly (as the fading of oscillations in Figure 6.2) and passes slowly but

continuously through the southern basin to the northern basin.

This shows the importance of the intrusion depth in the fate of the river water.

6.2.2 Variability of the intrusion depth

At the start of the summer season, the glacial river enters the lake as an underflow trapping warmer water under the colder bottom water and episodically flushing the cold water out of the main basin in the secondary basin. By the end of July, the river intrudes the lake as an interflow at about 30 to 60 m depth, the depth increasing slowly with time. Underflows and density currents persist as well, trapping colder, heavier water at the bottom of the main basin.

Figure 6.3 presents several interesting situations. Release 1, 10 and 12 are associated with large discharge and enter the lake as underflow, however while release 1 flows "freely" to the bottom, release 10 and even more release 12 appear to present some increasing resistance from the water already present at the bottom of the lake. Releases 2, 8 and 11 are on the other hand intruding the lake as interflow between 30 to 60 m depth. The interflow of release 2 is entering the lake with an angle characteristic of the downwelling episode happening in the South. The river intrusion associated with release 8 seems to get confined to the southern end of the lake and get split and dragged towards the bottom as the next large discharge (release 10) enters the basin.

In the first tracer release, occurring shortly after the onset of continuous thermal stratification, the glacial river enters the lake as an underflow (Table 6.1). Releases 2-4, the river enters the lake at mid depth, from 30-50 m. Releases 5-10 intrude deeper in the lake than the shallow northern shelf of the lake (depth <45 m), which could inherently be trapped in the deep section of the lake unless large scale motions help moving it upwards. The last three releases during high discharge events in August either enter at mid depth, or as bed intrusions.

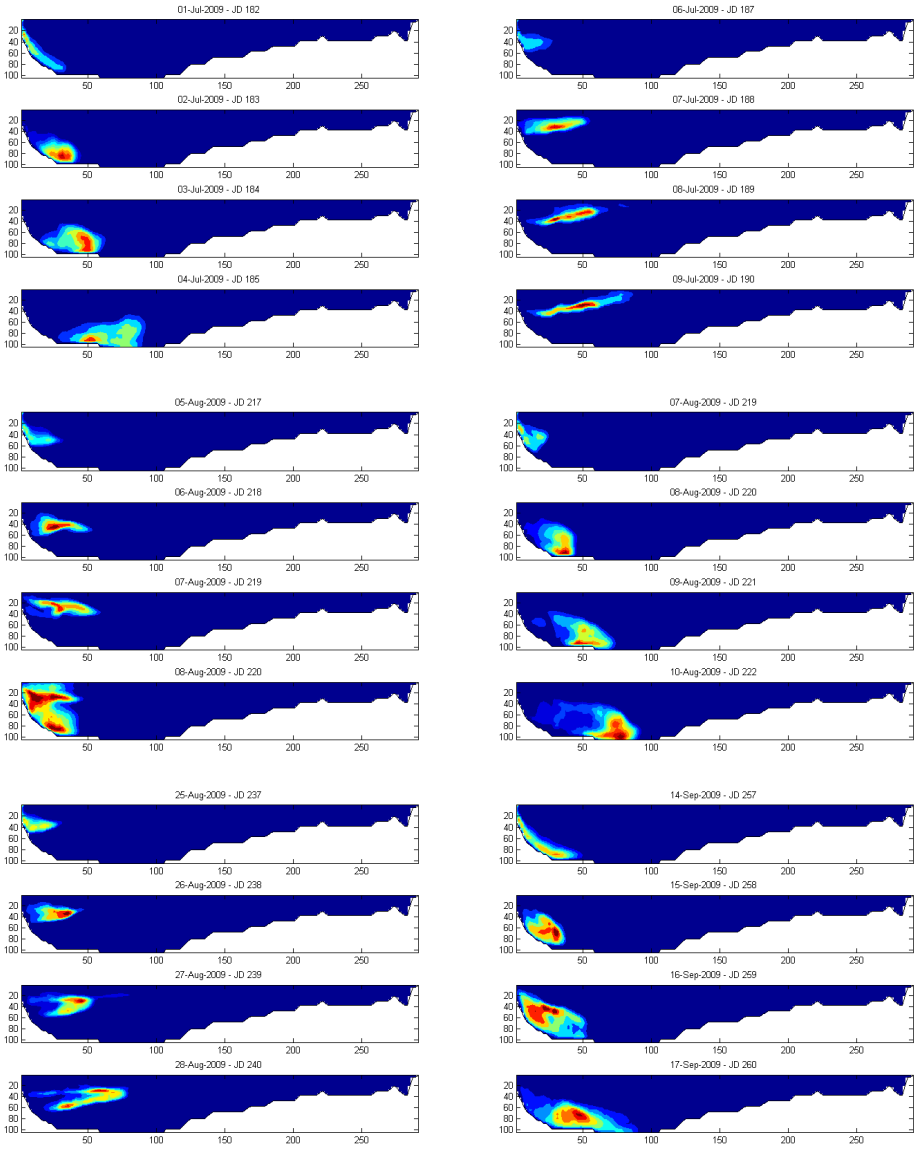

Figure 6.3. Tracer content along the thalweg of Lake Lagarfljót for releases 1, 2, 8, 10, 11 and 12. Each grid cell of the tracer file is projected on the axis of the thalweg and the tracer content values is integrated across the lake width to represent the entire 3D tracer field.

Table 6.1 suggests that deep intrusions typically occur when the internal wave field near the river mouth is upwelling, whereas shallow intrusion occur during downwelling, or a visible vertical mode expanding the hypolimnion near the inlet. A simple regression

Table 6.1. Initial riverine and internal wave conditions during Si3D tracer releases and simulated initial intrusion depth in 2009.

Nr.	DOY	T_{river} [°C]	Q_{river} [m^3/s]	$C_{ss,river}$ [mg/L]	Internal wave tilt near inlet	Initial intrusion depth (m)
1	182	5.4	195	260	V1 upwelling	80 m (bed)
2	187	4.9	172	280	V1 downwelling	30 m
3	192	5.4	152	220	V2	30-40 m
4	197	4.5	157	220	V2	30-40 m
5	202	4.2	144	225	V1 downwelling	50-60 m
6	207	4.1	138	230	V2	40-50 m
7	212	4.9	152	200	V1 downwelling	60-70 m
8	217	5.7	167	220	V1 downwelling	60 m
9	222	5.5	174	360	V1 upwelling	80 m
10	219	6.2	222	430	V1 upwelling	50-60 m & 80 m
11	237	5.3	211	350	V1 downwelling	30-40 m
12	257	4.7	189	460	?	80 & 40-60 m

analysis, giving upwelling the value of 1, vertical mode a value zero, and downwelling the value of -1, gives the highest correlation of the three parameters shown in table, that is R2 = 0.6. This suggests that in a weakly stratified lake receiving largely regulated glacial river water, the internal wave structure in the lake is important, if not dominant in determining the initial fate.

6.2.3 Flushing time

The flushing time is the time taken for a mass to exit a system. The tracer study allows us to get an estimation of the flushing time of the river water for the different releases.

The shape of the curve of releases 2 and 3, releases 4 and 5 and finally releases 6 and 7 are very similar results (Figure 6.4). Releases 8 and 9 are also showing similarities with a slight shift in time.

Release 11 is the fastest to reach the outflowing river as the first 0.1% of the tracer evacuated the basin after solely 15.5 days and 5% after 23.3 days, comparatively release 10 is taking the longest time with 65.2 days for the flushing of 5%of the total amount of tracer (Table 6.2). These two releases are associated with high discharges. However while most of release 10 is intruding the lake below 50 m and hence is separated/isolated from the northern basin, release 11 is intruding the lake as an interflow at about 40 m depth (Figure 6.3).

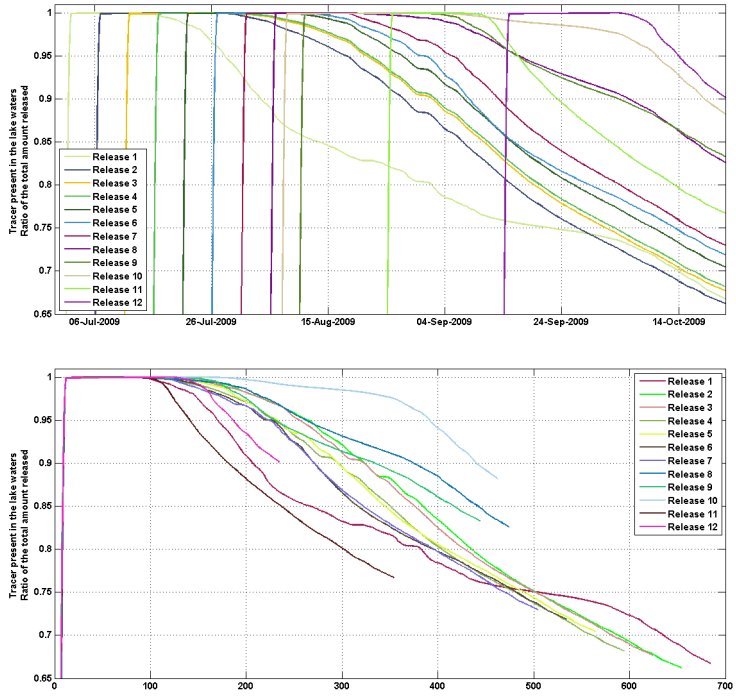

Figure 6.4. Tracer releases from 1 to 12, in chronological order (up) and from time of release (down).

Table 6.2. Number of days passed before the flushing of part of the tracer initially released in the lake by the southern inflow for each tracer experiment.

		Number of days before the exit of % of $C_{Tracer,initial}$			
Nr.	Release date (DOY)	0.1	5%	25%	30%
1	181	16.0	28.2	84.0	105.8
2	186	24.5	44.0	83.5	97.8
3	191	21	42.5	83.5	96.8
4	196	16.7	38.0	80.0	93.3
5	201	19.5	38.7	81.5	
6	206	18.2	37.2	80.2	
7	211	19.7	37.3	78.3	
8	216	17.5	43.7		
9	221	24.5	38.3		
10	218	31.0	65.2		
11	236	15.5	23.3		
12	256	21.8	31.0		

However while the tracer of release 1 starts exiting the lake after only 16 days (28.2 days for 5%), it takes 84 days for 25% and 105.8 days for 30% of the total amount of the tracer released to leave the basins, which is longer than any of the other following releases (Table 6.2). Releases 4 to 7 present very similar results when it comes to figures.

6.2.4 Transport between the two basins

While interflows are exiting the southern basin and lake in a steady, continuous manner (Figure 4.19 and 4.2), underflows show more complicated patterns.

As discussed earlier (see Pathways of river inflow), the water present at the bottom of the southern basin is sometimes suddenly flushed into the northern basin. In Figures 6.5 and 6.7, this is illustrated by the sudden drops and peaks of the tracer ratio curves. However, it appears that the water that enters the northern basin does not necessarily stay in the northern basin to be then conducted towards the outflow, but can be recirculated in the southern basin : the tracer ratio drops to then increase slightly again, this is clearly happening for release 1, 6, 10 and 11.

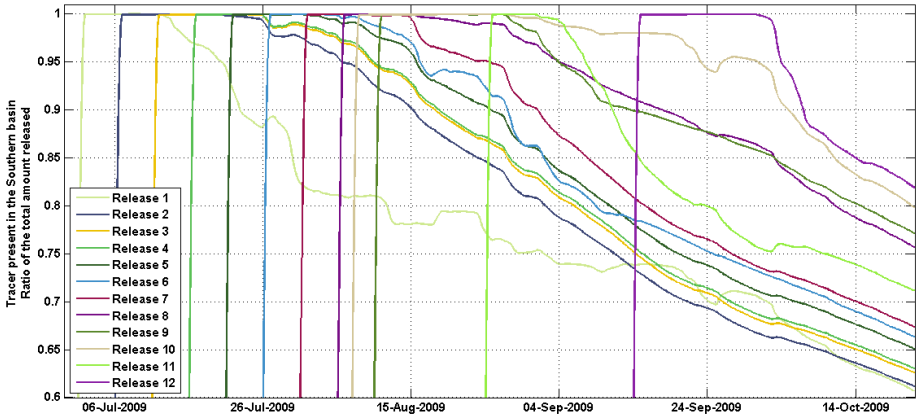

Figure 6.5. Ratio of tracer present in the southern basin to total amount released.

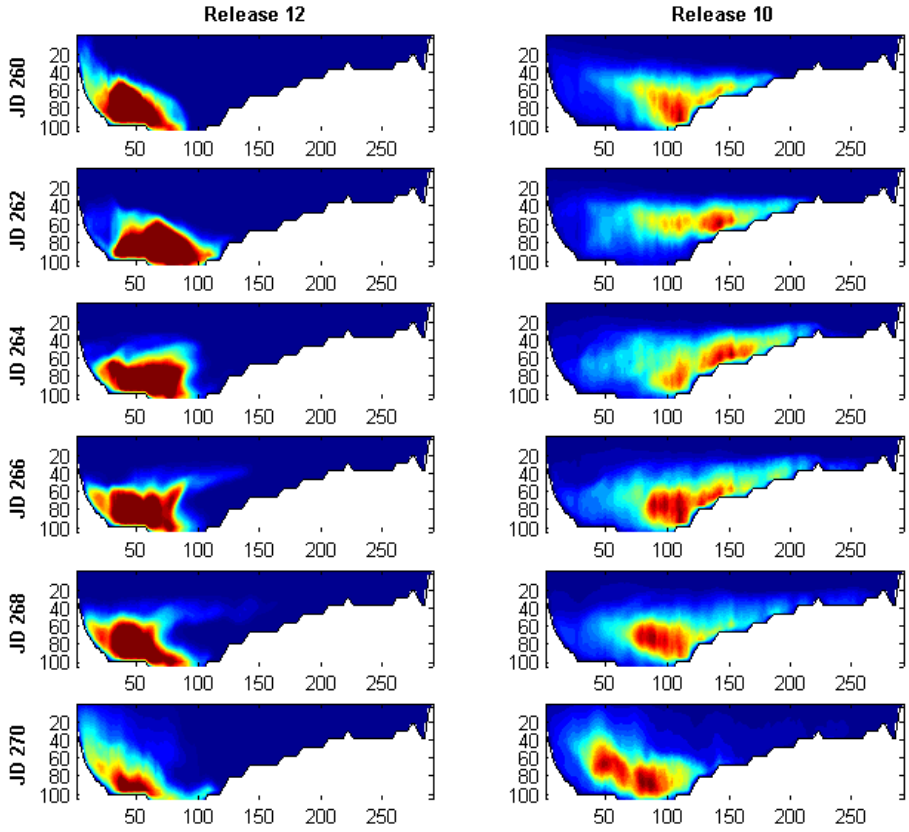

Figure 6.6. Example of tracer transfer between the southern and northern basins - Releases 10 and 12. Tracer content has been integrated across the width of the lake.

Figure 6.6 illustrates the basic steps of the transfer of water from the bottom of the main basin to the northern basin. A large underflow (release 12) is flowing down the bottom of the lake and pushes the river water already present at the bottom (release 10). The bottom water receives enough energy to go up the northern slope of the main basin and part of the water flows passed the sill into the smaller northern basin. Then potential energy drags the water of release 10 back down, squeezing the newly arrived water at the southern end of the main basin.

At DOY 260 (24th of September), the northern basin experiences a sudden increase in tracer from releases 1, 8 and 12 and simultaneously a sudden drop in tracer from releases 2, 3, 4, 5, 7 and 11 (Figure 6.7).

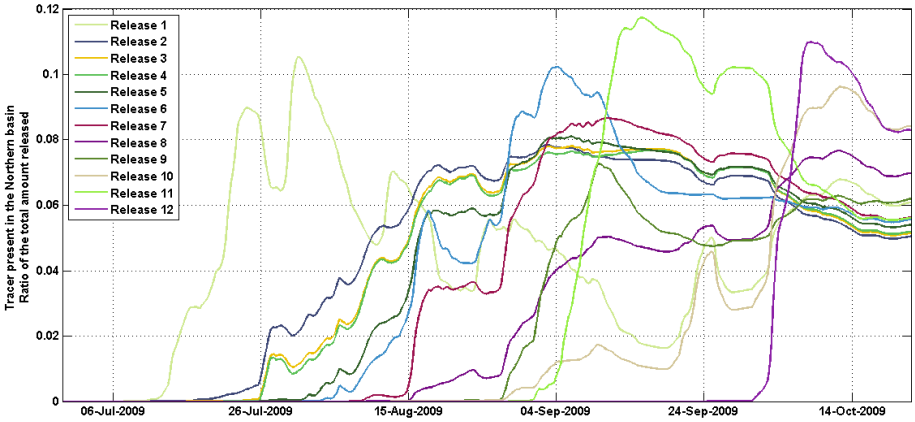

Figure 6.7. Ratio of tracer present in the northern basin to total amount released.

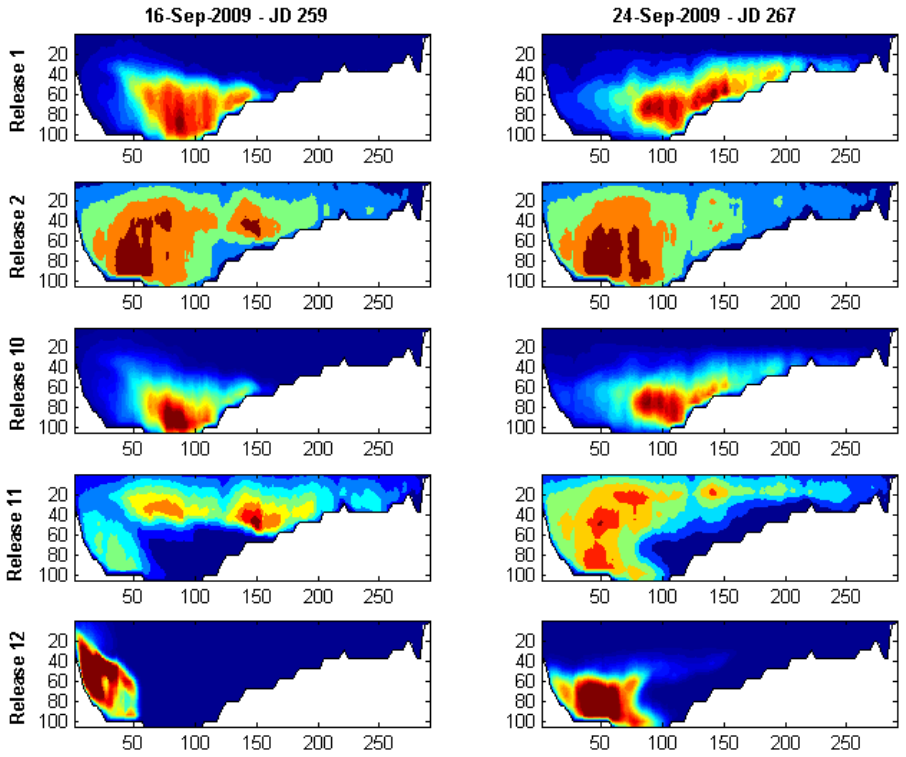

Figure 6.8. Spatial distribution of tracer at day 259 (left) and 267 (right) for releases 1, 2, 10, 11 and 12.

Figure 6.8 described very well the story. DOY 257 is the peak of a large discharge event whose waters are partly identified by the tracer of release 12. The inflow enters

the basin as an underflow or density current that is pushing the water trapped earlier in the bottom (releases 1 and 10 for example) up the northern slope of the southern basin up to the northern basin. Releases 2 and 11 that entered the basin as interflow in the upper layer and is present in both the southern and the northern basin. Following the underflow and as the bottom water is being pushed out of the southern basin, the water from these releases gather in the southern end of the main basin and seem partly squeezed out of northern basin (probably mostly in the outflowing river).

In addition in Figure 6.8 , it appears that the river water does not mix very fast as the high concentrations of tracer from release 1 shows. This can be effectively explained by the large differences in suspended sediments concentration in these different releases.

6.2.5 Coriolis effects

Model results were analyzed on horizontal planes extracted at 10, 30 and 50 m depth. In addition, a second simulation was performed with a Coriolis factor f set to 0 s^{-1}, in order to identify how the Coriolis forcing affects the circulation in the lake.

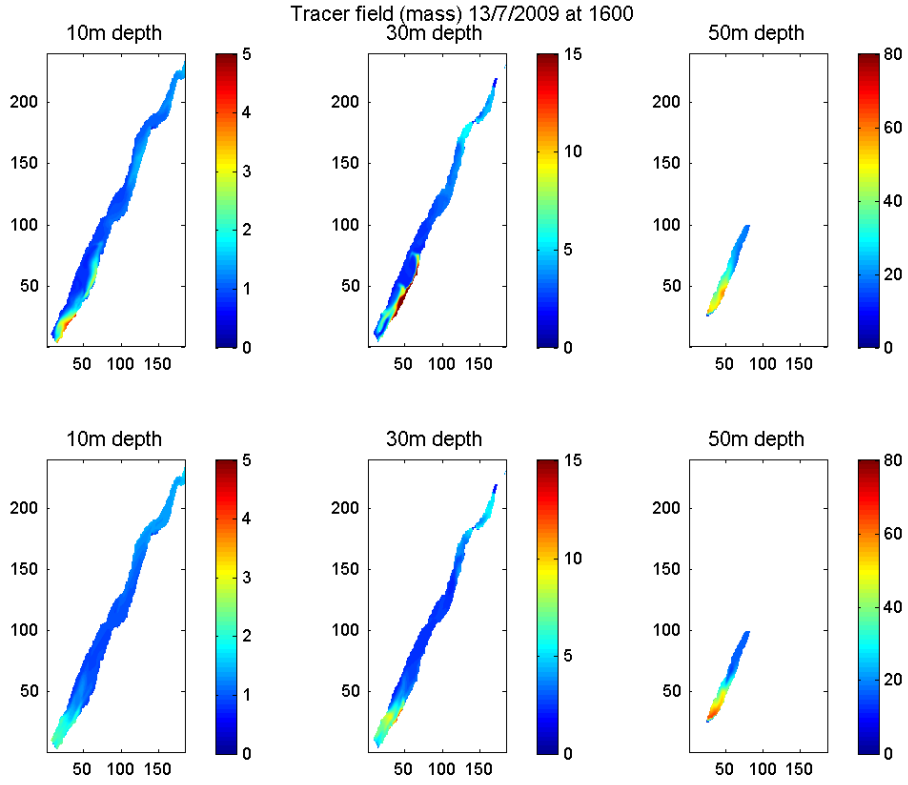

Figure 6.9. Tracer concentrations in the lake waters at 10, 30 and 50 m depth on the 13th of July 2009 under normal Coriolis forcing condition (up) and without Coriolis forcing (down).

Without Coriolis rotational effects the tracer is taking about 11 days to propagate all the way to the northern secondary basin while with the rotational effects it is detected approximately 1 day and a half later. The tracer study show that the Coriolis forces deflect the glacial river inflow to the east of the lake when it enters the lake, the flow spirals then anticlockwise (Figure 6.9).

6.2.6 Conceptual model

The process of trapping and flushing identified from the tracer study is simplified and summarize into a conceptual model of the two large deep discharges (Figures 6.10 and 6.11).

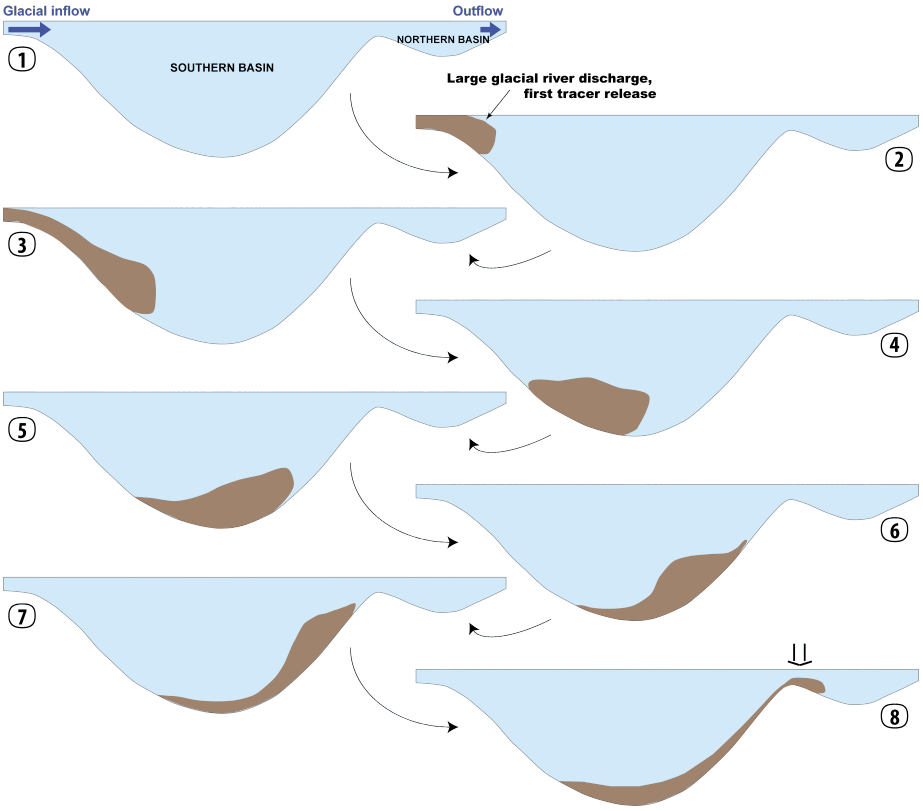

Figure 6.10. Flushing between basins associated with wind driven basin scale motions.

The first large discharge event, loaded with suspended sediments, enters the southern basin (2), it sinks to the bottom of the lake (3-4) and gains kinetic energy, it continues its trip up the northern end of the basin (5-6-7) but slowly looses speed. Part of the river discharge (8) is exiting the southern basin, while most of it sinks back to the bottom (Figure 6.10).

As the river discharges settles in the southern and northern basins (1), part of its

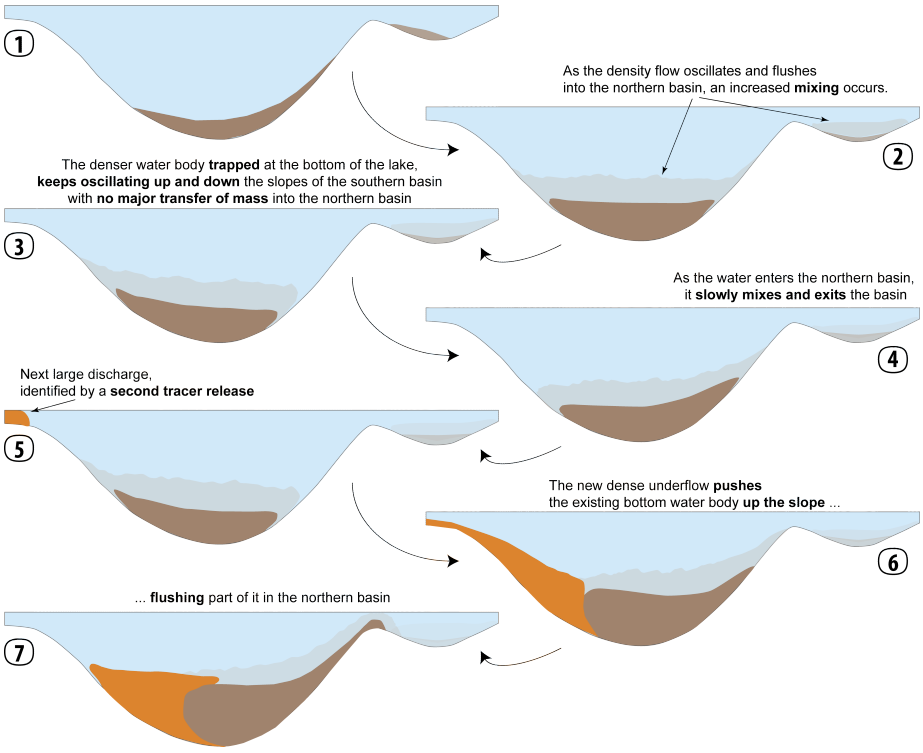

Figure 6.11. Exchanges between basins associated with deep river intrusions.

water slowly mixes with the lake's waters (2), enhanced with the oscillations of the mass (3). The river waters that entered the northern basin mixes and exits the lake basin. When the next large discharge enters the lake as an underflow (5), it meets the older one that had settled at the bottom of the lake (6) and pushes it up the northern slope of the basin, flushing part of it into the northern basin (7) (Figure 6.11).

6.2.7 Validation from the field measurements

During summer 2011, sonde profiles were taken in the lake during 4 days, 2 in July (10^{th} of July and 12^{th} of July) and 2 in August (10^{th} and 11^{th} of August) (see 3.3).

The first measurements in July occurs after northernly winds with hourly mean reaching 7.8 m/s on the 9^{th} and 9.5 m/s on the 8^{th}. On the 4^{th} of July the discharge of Jökulsá í Fljótsdal suddenly increases from a low 10 m^3/s to over 70 m^3/s, the discharge returns to 10 m^3/s or less in the evening of the 8^{th} of July. This relatively small peak of discharge is associated with water temperatures around 5°C while the lower discharge of the following days is associated with slightly higher temperatures due to a fast increase of temperatures observed in particular in Jökulsá í Fljótsdal and Keldúa.

These two measurements days illustrate what is observed in the simulations. A warmer, sediment-rich underflow (Figure 6.12 A-C) enters the lake following the

discharge peak pushing the older, colder bottom water (underline by the purple line in Figure 6.12 A) up towards the warmer northern basin. The turbidity associated to the underflow is exceeding 150 NTU while the older deep water's maximum turbidity is around 120-125 NTU. At the southern end of the basin, the isotherms show a large downwelling with the 4.6°C isotherm plunging to 70 m depth while present above 10 m 13 km into the basin. The isotherm is then plunging down again towards the sill.

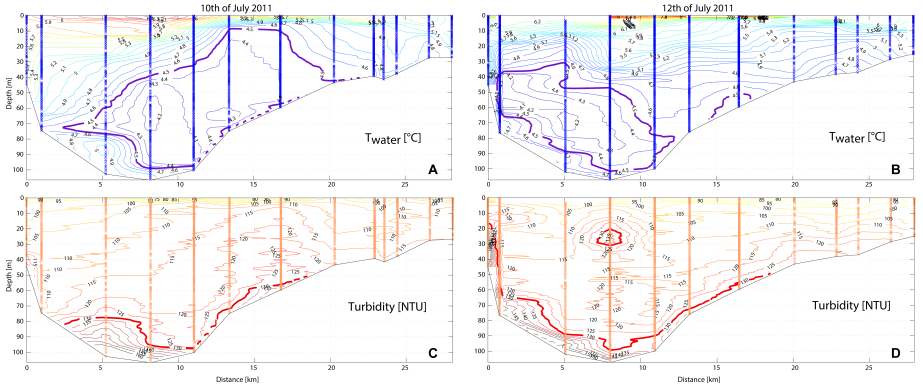

Figure 6.12. River signals captured by the temperature (A-B) and turbidity (C-D) measurements performed with a multi-parameter sonde the 10th (A-C) and 12th (B-D) of July 2011.

Two days later, the colder water has oscillated back down the southern basin and partly up, over the heavier and warmer underflow (Figure 6.12 B). The northern basin bottom turbidity has increased (>120 NTU) . A new peak of turbidity (>130 NTU) has appeared at the center of the southern basin at 25 m depth (Figure 6.12 D). This peak of turbidity can be associated to the warmer lower discharge of the river entering the lake and deflected by Coriolis, at least in part, to the East bank of the lake and back in the center of the lake (in a counterclockwise manner) 7-8 km away from the mouth of the river. This interflow influenced by Coriolis is observed by the model and illustrated by Figure 6.9. This intrusion of the river inflow in the water column is reflected by a stretching of the isotherms between 5.4 and 5.7°C.

Figure 6.13 shows thermistor chain measurements on either side of the sill at LAG03 in the southern deeper basin and at LAG04 in the northern shallower basin. In 2011, northerly winds were preponderant and large northerly wind episodes result in large upwellings in the northern end of the basin. However, sudden cooling of the bottom of the lake at LAG03 then in LAG04 is observed while average wind speeds are below 5 m/s and shortly after a large discharge event peaking on day 186. The cold water mass oscillates back and forth on the northern bottom slope of the southern basin, with some small spilling detected at LAG04 on the other side of the sill. Larger flushing of this cold bottom water occurs when upwelling resulting from stronger northerly winds helps push it up the slope.

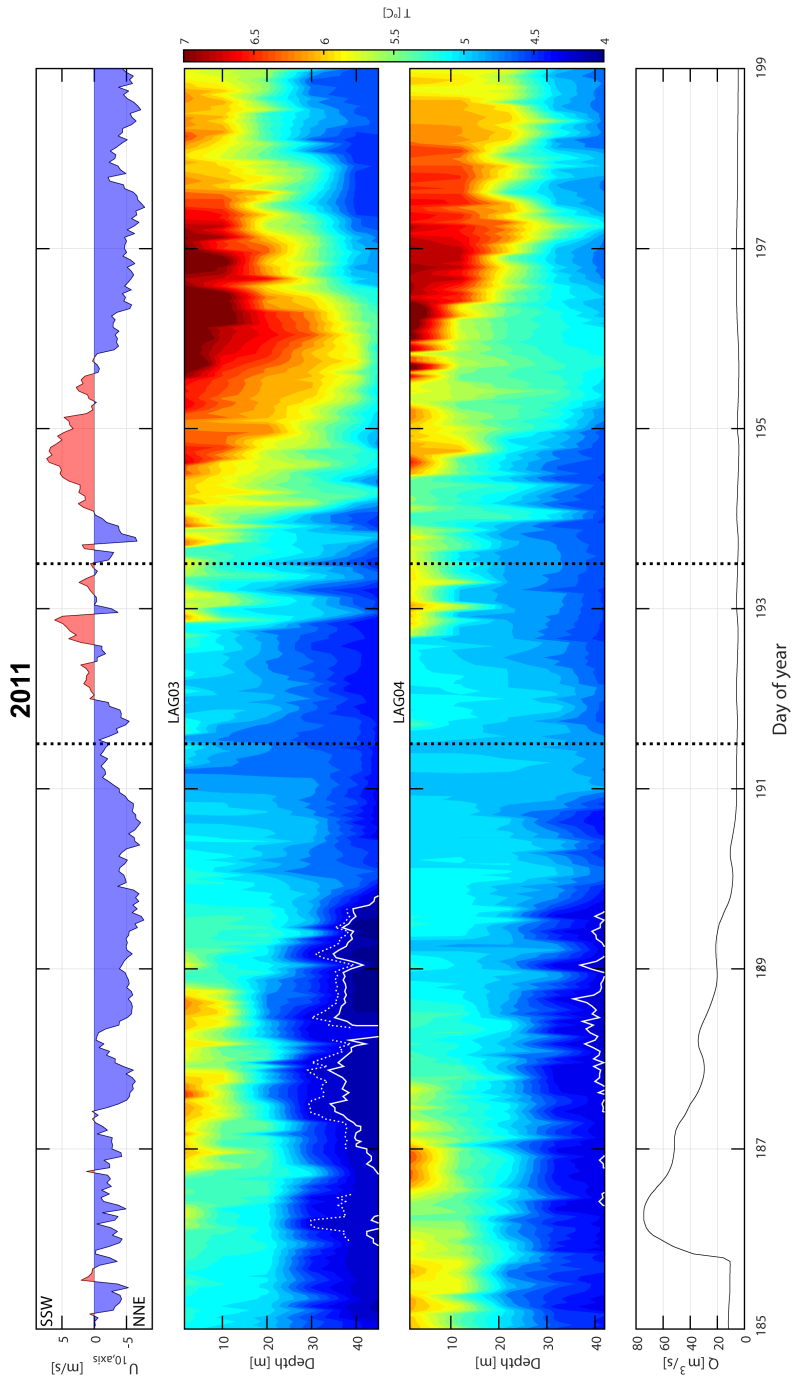

Figure 6.13. Transfer of deep bottom waters from the southern basin to the northern basin following a large glacial discharge event at the southern end of lake evidenced by the sudden apparition of water with temperature close to maximum density (outlined in white) in the northern basin in July 2011.

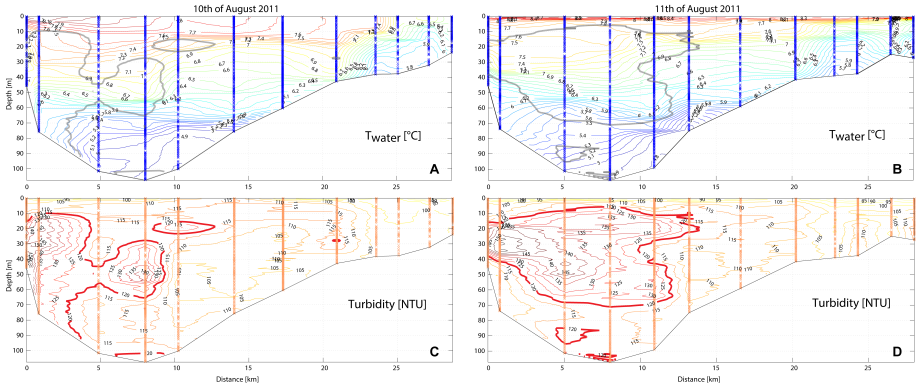

Figure 6.14. River signals captured by the temperature (A-B) and turbidity (C-D) measurements performed with a multiparameter sonde the 10^{th} (A-C) and 11^{th} (B-D) of August 2011.

In August 2011, the measurements days are preceded by a northernly wind episode with a maximum hourly mean reaching 9.4 m/s at 11.00 on the 6^{th} of August. On the 10^{th} of August, the river inflow signal is visible in the turbidity plot (Figure 6.14 C) at the southern end of the lake between 20 and 50 m depth3.20 but also at 50 m about 8 km away from the river mouth and possibly at 20 m depth 10 km away. These peaks of turbidity are associated with a stretching of the isotherms between 6.7 and 7.4 °C. These peaks in the water column are associated to low discharge of river inflow deflected to the East side of the lake by Coriolis. The difference of trajectory and final intrusion depth can be explained by the variation of inflow temperature: during this period, hourly means of the river water temperature is observed to vary by up to 4°C.

On the next day (11^{th} of August), the more turbid river signal is observed along the thalweg of the lake (see red lines in Figure 3.20 D), the river intrudes the lake as an interflow at 15 to 40 m depth and the plumes stretches down to 70m depth. The isotherms (see gray lines in Figure 3.20B delineating the turbidity plume) are spreading downward as the warm(er) river water is denser due to the suspended sediments.

6.3 Summary

The river inflow has very large impact on the lake's stratification. During the summer season, both interflows and underflows are observed both in the field data and in model simulations. The underflows occur when the gradient between the concentration in suspended sediment in the river and the lake is the highest: in particular at the start of the stratification when the concentration in sediment in the lake is lowest and at the end of the summer season when the sediment load in the river discharge is at its highest.

The pathway of the river will influence the flushing time. Interflows will pass through the basins steadily, mixing with the lake waters. The underflows will sink at the bottom of the lake after having run up and down the slopes of the southern basin; they will be flushed out by pulse when internal waves and new discharges from the river

combine to push the older bottom water out of the basin. The Earth's rotational effects deflect the river waters towards the eastern bank of the lake; they will intrude toward the center of the lake about 7 km away from the mouth. According to model simulation without Coriolis, the Coriolis force results in a longer flushing time as it maintains the river inflow a bit longer in the southern main basin and mixes its waters.

The conceptual model explains simply the mechanisms that are expected to participate to the transfer of bottom waters from the deep southern basin and the shallower northern basin. The presence of suspended sediments, in higher concentration in the new inflow, contributes to the renewal of the deeper, possibly colder, layers. Field measurements support this interpretation.

7 Conclusion

This doctoral research project is the first of its kind in Iceland. The research used methods and approaches, field measurements, data analysis and numerical modeling, to improve the general understanding of subarctic weakly stratified water bodies. Lake Lagarfljót, an Icelandic fjord lake with glacial inflow, was selected as example, as some data were readily available. From a general need of understanding these weakly stratified water bodies in the subarctic lake, several key questions arose and were investigated: what is the internal wave regime of the lake? What are the key forcing of these internal waves? Can numerical models reproduce these processes in weakly stratified water bodies and help us understand the mechanism? What is the fate of the glacial inflow? The key findings are as follow:

1. Lake Lagarfljót is a weakly stratified lake that undergoes two overturning episodes (mixing periods), in spring and in fall when heat fluxes become negative. The thermal stratification period is short ($\approx$ 100 days). The internal waves have periods of 0.5 to 14 days and the oscillations can exceed 30 m in the southern basin. Higher vertical modes as well as lateral modes are observed both in the thermistor and the sonde measurements. There is a clear connection between the wind and the internal wave periods but the field data does not allow us to say if the waves are strictly forced by the wind or in resonance. Similarly we observe oscillations in the transverse and cross-spectra of the thermistor measurements around the lake suggesting counter-clockwise rotation of the waves with periods consistent with Kelvin waves.

2. After the construction of the Kárahnjúkar power installation, the lake residence time is estimated to be half what it used to be, showing the importance of the southern glacial inflow in the lake circulation. The river inflow is complex, with a southern inflow exhibiting both a nival and glacial regime. It is shown that the sediment in suspension in the river are particularly fine and is likely to stay in suspension for most part once in the lake during the ice-free season. Results from the sonde measurement campaigns show some temperature inversions that are associated with increased turbidity. These peaks of suspended sediment are associated to the glacial river inflow. The intrusion depth of the river is typically controlled by temperatures, however these field measurements suggest that the role of suspended sediment is not negligible and it can affect the intrusion depth. Measurements show that the river is deflected to the east side of the lake upon arrival and it penetrates towards the center of the lake at the level of Hafursá, in a counter clockwise rotational movement. This rotational effect can be attributed to Coriolis forces on the inflowing river.

3. The Münnich model was modified in order to compute eigenmodes in complex basins. The model shows that the bathymetry affects the internal wave field of Lake Lagarfljót. Most energetic modes are higher modes, either horizontally and/or vertically. The results of the model demonstrate that the natural oscillations of the lake basin are close to the oscillation period of the wind. As the lake stratifies, the dominant mode and periodicity evolve and enter into resonance with the forcing wind, giving rise to more energetic waves.

4. The 3D hydrodynamic model Si3D has been adapted to account for the suspended sediment load and successfully reproduced the motions observed in the lake, showing that it can reliably be used for the study of weakly-stratified lakes. The model results suggest that wind is the main driver of internal waves in the lake but the river influences the stratification and it can not be ignored when studying the circulation in the lake. Kelvin waves can be identified in the basin (Priet-Mahéo et al., 2019).

5. Tracer studies helped us analyze the pathways of the river and its fate. During the summer stratification, the river intrusion takes the form of interflows or underflows, which will affect the residence time of the water. Coriolis forces acting on the river inflow deflect it to the East, keeping it longer on higher grounds, before directing it back towards the center of the lake in an anti-clockwise motion. These rotational effects result in an increase of the flushing time of the river waters. Waters flowing as underflow can become trapped at the bottom of the deepest southern basin. The oscillating water will be flushed episodically in the northern basin when the next large river discharge enters the lake as an underflow, pushing the older river water up the sill. The water entering the lake as interflow gets mixed more easily and is flushed quasi continuously out of the basin.

This research demonstrates the complexity of circulation and the sensitivity of these weakly stratified subarctic lakes. Lake Lagarfljót, with temperatures close to the temperature of maximum density, is expected be particularly responsive to any change in the external forcings of heat, wind and river inflow. These three forcings are anticipated to change radically with global warming and therefore will impact the internal lake dynamics. In the case of increased heat fluxes, for example, stratification would strengthen, resulting in the trapping of the deepest layer of the southern basin. River inflow would be expected to enter the lake more frequently as interflow as the river water temperature would rise and the contribution of suspended sediment would not be as relevant due to the greater temperature gradient in the water column. We could also expect an increase of the temperatures in the northern basin as bottom waters from the southern basin would no longer transfer.

Further investigation of the lake processes could include the use of heterogeneous wind field in the 3D hydrodynamic model. Secondly, the inflowing southern river should be studied to appreciate better the importance of mixing prior to the intrusion in the lake. Additionally, the hydrodynamic behavior of the lake prior to the damming of Jökulsá á Dal should be investigated. Lastly, the effects of climate change on Lake Lagarfljót require further evaluation.

References

Aðalsteinsson, H. (2010). Grugg og gegnsæi í Lagarfljóti fyrir og eftir gangsetningu Kárahnjúkavirkjunar. Technical Report LV-2010-123, Landsvirkjun. (In Icelandic).

Acosta, M., Anguita, M., Rueda, F., and Fernández-Baldomero, F. (2010). Parallel implementation of a semi-implicit 3-d lake hydrodynamic model. In *Proceedings of the 2010 International Conference on Computer and Mathematics. Methods in Science and Engineering.(CMMSE) IV*, pages 1026–1037.

Adalsteinsson, H., Jónasson, P. M., and Rist, S. (1992). Physical characteristics of thingvallavatn, iceland. *Oikos*, pages 121–135.

Adrian, R., O'Reilly, C. M., Zagarese, H., Baines, S. B., Hessen, D. O., Keller, W., Livingstone, D. M., Sommaruga, R., Straile, D., Van Donk, E., et al. (2009). Lakes as sentinels of climate change. *Limnology and Oceanography*, 54(6):2283.

Aija-Riitta, E. et al. (2007). The energy balance and vertical thermal structure of two small boreal lakes in summer. *Boreal environment research*, 12(5):585–600.

Alavian, V., Jirka, G. H., Denton, R. A., Johnson, M. C., and Stefan, H. G. (1992). Density currents entering lakes and reservoirs. *Journal of Hydraulic Engineering*, 118(11):1464–1489.

Andradóttir, H. (2008). Thermal dynamics of sub-arctic lake lagarfljót. *Nordic Hydrology and its global role*, 1:82–93.

Andradóttir, H. (2008). Thermal dynamics of sub-arctic lake lagarfljót. *Earth and Planetary Science Letters*, 272(1-2):78–88.

Andradóttir, H. Ó. (2012). Icelandic lakes, physical characteristics. In *Encyclopedia of Lakes and Reservoirs*, pages 362–368. Springer.

Antenucci, J. (2009). Currents in stratified water bodies 3: Effects of rotation. In Likens, G. E., editor, *Encyclopedia of Inland Waters*, pages 559–567. Elsevier.

Antenucci, J. P. and Imberger, J. (2001). Energetics of long internal gravity waves in large lakes. *Limnology and oceanography*, 46(7):1760–1773.

Antenucci, J. P. and Imberger, J. (2003). The seasonal evolution of wind/internal wave resonance in lake kinneret. *Limnology and oceanography*, 48(5):2055–2061.

Assel, R., Cronk, K., and Norton, D. (2003). Recent trends in laurentian great lakes ice cover. *Climatic Change*, 57(1-2):185–204.

Austin, J. and Atkinson, S. (2004). The design and testing of small, low-cost gps-tracked surface drifters. *Estuaries and Coasts*, 27(6):1026–1029.

Barry, R. G. and Chorley, R. J. (2009). *Atmosphere, weather and climate*. Routledge.

Blöndal, J., Birgisson, T., Björnsson, H., Jónasson, K., and Petersen, G. N. (2011). Vindhraðamælingar og dambreytni vinds. Technical Report VÍ 2011-014, Icelandic Meteorological Office. (In Icelandic).

Boegman, L. (2009). *Encyclopedia of Inland Waters*, volume 1, chapter Currents in

Stratified Water Bodies 2: Internal waves., pages 539–558. Oxford: Elsevier, gene e. likens edition.

Boehrer, B., Herzsprung, P., Schultze, M., and Millero, F. J. (2010). Calculating density of water in geochemical lake stratification models. *Limnology and Oceanography: Methods*, 8(11):567–574.

Boehrer, B. and Schultze, M. (2008). Stratification of lakes. *Reviews of Geophysics*, 46(2):RG2005.

Bras, R. L. (1990). *Hydrology: an introduction to hydrologic science*. Addison-Wesley Reading.

Callaghan, T. V., Bergholm, F., Christensen, T. R., Jonasson, C., Kokfelt, U., and Johansson, M. (2010). A new climate era in the sub-arctic: Accelerating climate changes and multiple impacts. *Geophysical Research Letters*, 37(14).

Carey, S. K., Boucher, J. L., and Duarte, C. M. (2013). Inferring groundwater contributions and pathways to streamflow during snowmelt over multiple years in a discontinuous permafrost subarctic environment (yukon, canada). *Hydrogeology Journal*, 21(1):67–77.

Carson, C. E. and Hussey, K. M. (1960). Hydrodynamics in three arctic lakes. *The Journal of Geology*, 68(6):pp. 585–600.

Chung, S., Hipsey, M., and Imberger, J. (2009). Modelling the propagation of turbid density inflows into a stratified lake: Daecheong reservoir, korea. *Environmental Modelling & Software*, 24(12):1467–1482.

Clifford, N., Richards, K., Brown, R., and Lane, S. (1995). Scales of variation of suspended sediment concentration and turbidity in a glacial meltwater stream. *Geografiska Annaler. Series A. Physical Geography*, pages 45–65.

Critchfield, H. J. (1974). *General climatology*. Prentice-Hall.

Davies-Colley, R. and Smith, D. (2001). Turbidity, suspended sediment, and water clarity: a review. *Journal of the American Water Resources Association*, 37(5):1085–1101.

De Cesare, G., Boillat, J.-L., and Schleiss, A. J. (2006). Circulation in stratified lakes due to flood-induced turbidity currents. *Journal of Environmental Engineering*, 132(11):1508–1517.

Denman, K. and Gargett, A. (1983). Time and space scales of vertical mixing and advection of'phytoplankton in the upper ocean. *OCEANOGRAPHY*, 28(5).

Downing, J. A., Prairie, Y., Cole, J., Duarte, C., Tranvik, L., Striegl, R. G., McDowell, W., Kortelainen, P., Caraco, N., Melack, J., et al. (2006). The global abundance and size distribution of lakes, ponds, and impoundments. *Limnology and Oceanography*, 51(5):2388–2397.

Durran, D. R. (1999). *Numerical methods for wave equations in geophysical fluid dynamics*. Springer Science & Business Media.

Einarsson, A. (1982). The palaeolimnology of lake mỳvatn, northern iceland: plant and animal microfossils in the sediment. *Freshwater Biology*, 12(1):63–82.

Einarsson, A., Stefánsdóttir, G., Jóhannesson, H., Ólafsson, J. S., Gíslason, G. M., Wakana, I., Gudbergsson, G., and Gardarsson, A. (2004). The ecology of lake myvatn and the river laxá: variation in space and time. *Aquatic Ecology*, 38(2):317–348.

Engineers, U. A. C. O. (1984). Shore protection manual. *Army Engineer Waterways Experiment Station, Vicksburg, MS. 2v*, pages 37–53.

Farmer, D. M. (1978). Observations of long nonlinear internal waves in a lake. *Journal of Physical Oceanography*, 8(1):63–73.

Fischer, H. B., List, E. J., Koh, R. C., and Imberger, J. (1979). *Mixing in inland and coastal waters*. Academic Press (New York).

Foley, B., Jones, I. D., Maberly, S. C., and Rippey, B. (2012). Long-term changes in oxygen depletion in a small temperate lake: effects of climate change and eutrophication. *Freshwater Biology*, 57(2):278–289.

Forbes, B. C., Ebersole, J. J., and Strandberg, B. (2001). Anthropogenic disturbance and patch dynamics in circumpolar arctic ecosystems. *Conservation Biology*, 15(4):954–969.

Ford, D. E. and Johnson, M. C. (1983). An assessment of reservoir density currents and inflow processes. Technical report, DTIC Document.

GARMIN (2003). Garmin, rino series specifications - the convenience of gps with a 2-way radio.

Gibbs, R. J., Matthews, M. D., and Link, D. A. (1971). The relationship between sphere size and settling velocity. *Journal of Sedimentary Research*, 41(1):7–18.

Gislason, S. R., Oelkers, E. H., Eiriksdottir, E. S., Kardjilov, M. I., Gisladottir, G., Sigfusson, B., Snorrason, A., Elefsen, S., Hardardottir, J., Torssander, P., et al. (2009). Direct evidence of the feedback between climate and weathering. *Earth and Planetary Science Letters*, 277(1):213–222.

Gislason, S. R., Oelkers, E. H., and Snorrason, Á. (2006). Role of river-suspended material in the global carbon cycle. *Geology*, 34(1):49–52.

Gleick, P. H. (1996). Water resources. In Schneider, S. H., editor, *Encyclopedia of Climate and Weather*, volume 2, pages 817 – 823. Oxford University Press, New York.

Gloor, M., Wüest, A., and Münnich, M. (1994). Benthic boundary mixing and resuspension induced by internal seiches. *Hydrobiologia*, 284(1):59–68.

Gómez-Giraldo, A., Imberger, J., and Antenucci, J. P. (2006). Spatial structure of the dominant basin-scale internal waves in lake kinneret. *Limnology and oceanography*, 51(1):229–246.

Gorham, E. (1991). Northern peatlands: role in the carbon cycle and probable responses to climatic warming. *Ecological applications*, 1(2):182–195.

Gray, J. R., Glysson, G. D., Turcios, L. M., and Schwarz, G. E. (2000). *Comparability of suspended-sediment concentration and total suspended solids data*. US Department of the Interior, US Geological Survey.

Haflidason, H., Larsen, G., and Olafsson, G. (1992). The recent sedimentation history of thingvallavatn, iceland. *Oikos*, pages 80–95.

Hamelin, L. E. (1978). *Canadian nordicity: it's your north too*. Harvest House Montreal.

Harðardóttir, J. and Þorláksdóttir, S. B. (2004). Niðurstöður aurburðarmælinga í jökulsá í fljótsdal árið 2003. Technical report, Reykjavík:Orkustofnun. (In Icelandic).

Hemond, H. F. and Fechner-Levy, E. J. (2000). *Chemical fate and transport in the environment*. Academic Press.

Hinzman, L. D., Bettez, N. D., Bolton, W. R., Chapin, F. S., Dyurgerov, M. B., Fastie, C. L., Griffith, B., Hollister, R. D., Hope, A., Huntington, H. P., et al. (2005). Evidence and implications of recent climate change in northern alaska and other arctic regions. *Climatic Change*, 72(3):251–298.

Hodges, B., Imberger, J., Saggio, A., and Winters, K. (2000). Modeling basin-scale internal waves in a stratified lake. *Limnology and Oceanography*, pages 1603–1620.

Holtmeier, F.-K. and Broll, G. (2010). Wind as an ecological agent at treelines in north america, the alps, and the european subarctic. *Physical Geography*, 31(3):203–233.

Hopping, P. N. and Smith, B. T. (2002). Measurement of flow patterns using gps drogues. In *Hydraulic Measurements and Experimental Methods 2002*, pages 1–10.

Hughes, M. and Cassano, J. J. (2015). The climatological distribution of extreme arctic winds and implications for ocean and sea ice processes. *Journal of Geophysical Research: Atmospheres*, 120(15):7358–7377.

Hughes, S. A. (2002). Estimating surface currents near coastal structures using dye and drogues. *ERDC/CHL CHETN-VI-37,U.S. Army Engineer Research and Development Center, Vicksburg, MS.*

Hutchinson, G. and Löffler, H. (1956). The thermal classification of lakes. *Proceedings of the National Academy of Sciences of the United States of America*, 42(2):84.

Hutter, K. (2012). *Nonlinear internal waves in lakes*. Springer.

Hutter, K., Wang, Y., and Chubarenko, I. P. (2011). *Physics of lakes*, volume 2. Springer.

Imberger, J. and Hamblin, P. (1982). Dynamics of lakes, reservoirs, and cooling ponds. *Annual Review of Fluid Mechanics*, 14(1):153–187.

IMO (2010a). Meterorological data from hallormsstaðir and egilsstaðir airport. Technical report, Iceland Meteorological Office, Reykjavík.

IMO (2010b). Water level and flow rates in selected locations near lake lagarfljót eastern iceland. Technical Report IMO database deliveries nr. 2010-02-08/01 and 2010-02-02/01., Iceland Meteorological Office, Reykjavík.

IMO (2011). River flowrates, water level and water temperatures for jökulsá í fljótsdal, grímsá, kelduá, fellsá, lagarfljótsvirkjun and lagarfell. Technical Report Delivery of data from the Hydrological database, no. 2011-04-26/01., Iceland Meteorological Office, Reykjavík.

IMO (2012). River flow rates, water level and water temperatures at hafursá, grimsá, gilsá, jökulsá í fljótsdal, fellsá and lagarfell. Technical Report Deliveries of data from the Hydrological database, no. 2012-02-02/02 and nr. 2012-05-10/01., Iceland Meteorological Office, Reykjavík.

Intergovernmental Panel on Climate Change, I. (2014). *Climate Change 2014–Impacts, Adaptation and Vulnerability: Regional Aspects*. Cambridge University Press.

Johnson, D., Stocker, R., Head, R., Imberger, J., and Pattiaratchi, C. (2003). A compact, low-cost gps drifter for use in the oceanic nearshore zone, lakes, and estuaries. *Journal of atmospheric and oceanic technology*, 20(12):1880–1884.

Johnson, H. K. (1999). Simple expressions for correcting wind speed data for elevation. *Coastal Engineering*, 36(3):263–269.

Jónasson, P. M. (1979). The lake mỳvatn ecosystem, iceland. *Oikos*, pages 289–305.

Jónasson, P. M. (1992). The ecosystem of thingvallavatn: a synthesis. *Oikos*, pages 405–434.

Jónasson, P. M., Adalsteinsson, H., and St. Jónsson, G. (1992). Production and nutrient supply of phytoplankton in subarctic, dimictic thingvallavatn, iceland. *Oikos*, pages 162–187.

Kamphuis, J. W. (2000). *Introduction to Coastal Engineering and Management*. World Scientific.

King, A., Rueda, F., Tinoco, R., and Cowen, E. (2009). Modeling flow and transport through aquatic vegetation in natural water bodies. In *Proceedings of the 33rd IAHR Congress. Vancouver BC, Canada*.

Kottek, M., Grieser, J., Beck, C., Rudolf, B., and Rubel, F. (2006). World map of the köppen-geiger climate classification updated. *Meteorologische Zeitschrift*, 15(3):259–263.

Krause, P., Boyle, D., and Bäse, F. (2005). Comparison of different efficiency criteria for hydrological model assessment. *Advances in Geosciences*, 5:89–97.

Kristmannsdóttir, H. and Ármannsson, H. (2004). Groundwater in the lake myvatn area, northern iceland: Chemistry, origin and interaction. *Aquatic Ecology*, 38(2):115–128.

Laborde, S., Antenucci, J., Copetti, D., and Imberger, J. (2010). Inflow intrusions at multiple scales in a large temperate lake. *Limnology and Oceanography*, 55(3):1301–1312.

Larsen, J. N. and Fondahl, G. (2015). *Arctic human development report: Regional processes and global linkages*. Nordic Council of Ministers.

Laval, B., Imberger, J., Hodges, B., and Stocker, R. (2003). Modeling circulation in lakes: Spatial and temporal variations. *Limnology and Oceanography*, pages 983–994.

Lawler, D., Dolan, M., Tomasson, H., and Zophoniasson, S. (1992). Temporal variability of suspended sediment flux from a subarctic glacial river, southern iceland. In *Erosion and Sediment Transport Monitoring Programs in River Basins. Proc. Oslo Symp. IAHS Publ*, volume 210, pages 233–243.

Legates, D. R. and McCabe, G. J. (1999). Evaluating the use of "goodness-of-fit" measures in hydrologic and hydroclimatic model validation. *Water resources research*, 35(1):233–241.

Lehner, B. and Döll, P. (2004). Development and validation of a global database of lakes, reservoirs and wetlands. *Journal of Hydrology*, 296(1):1–22.

Lemmin, U., Mortimer, C., and Bäuerle, E. (2005). Internal seiche dynamics in lake geneva. *Limnology and oceanography*, pages 207–216.

León, L., Imberger, J., Smith, R., Hecky, R., Lam, D., and Schertzer, W. (2005). Modeling as a tool for nutrient management in lake erie: A hydrodynamics study. *Journal of Great Lakes Research*, 31(2):309–318.

León, L., Lam, D., Schertzer, W., Swayne, D., and Imberger, J. (2007). Towards coupling a 3d hydrodynamic lake model with the canadian regional climate model: simulation on great slave lake. *Environmental Modelling & Software*, 22(6):787–796.

Leon, L. F., Lam, D. C., Schertzer, W. M., Swayne, D. A., and Imberger, J. (2008). Lake and climate models : interactions in small and large lakes. In *Parametrization of lakes in NWP and Climate Modelling*, St. Petersburg (Zelenogorsk), Russia.

Lewis Jr, W. (1983). A revised classification of lakes based on mixing. *Canadian Journal of Fisheries and Aquatic Sciences*, 40(10):1779–1787.

Lindegaard, C. and Jónasson, P. M. (1979). Abundance, population dynamics and production of zoobenthos in lake mỳvatn, iceland. *Oikos*, pages 202–227.

Liu, Q., Babanin, A. V., Zieger, S., Young, I. R., and Guan, C. (2016). Wind and wave climate in the arctic ocean as observed by altimeters. *Journal of Climate*, 29(22):7957–7975.

Lutgens, F., Tarbuck, E., and Tasa, D. (2013). *The Atmosphere: An Introduction to*

Meteorology. Pearson.
MacIntyre, S. and Melack, M. (2009). *Encyclopedia of Inland Waters*, volume 1, chapter Mixing Dynamics in Lakes across Climatic Zones., pages 603–612. Oxford: Elsevier, gene e. likens edition.
Manley, T. O. (2010). Drifters, drogues, and circulation. *Oceanography*, 23(4):165–172.
Martin, J. L. and McCutcheon, S. C. (1998). *Hydrodynamics and transport for water quality modeling*. CRC Press.
Mellor, G. L. and Yamada, T. (1974). A hierarchy of turbulence closure models for planetary boundary layers. *Journal of the Atmospheric Sciences*, 31(7):1791–1806.
Mueller, D. R., Van Hove, P., Antoniades, D., Jeffries, M. O., and Vincent, W. F. (2009). High arctic lakes as sentinel ecosystems: Cascading regime shifts in climate, ice cover, and mixing. *Limnology and Oceanography*, 54(6part2):2371–2385.
Münnich, M. (1996). The influence of bottom topography on internal seiches in stratified media. *Dynamics of atmospheres and oceans*, 23(1):257–266.
MÜnnich, M., WÜest, A., and Imboden, D. M. (1992). Observations of the second vertical mode of the internal seiche in an alpine lake. *Limnology and oceanography*, 37(8):1705–1719.
Naithani, J., Deleersnijder, E., and Plisnier, P. (2003). Analysis of wind-induced thermocline oscillations of lake tanganyika. *Environmental Fluid Mechanics*, 3(1):23–39.
Norton, M. P. and Karczub, D. G. (2003). *Fundamentals of noise and vibration analysis for engineers*. Cambridge university press.
Ólafsson, J. (1979a). The chemistry of lake mỳvatn and river laxá. *Oikos*, pages 82–112.
Ólafsson, J. (1979b). Physical characteristics of lake mỳvatn and river laxá. *Oikos*, pages 38–66.
O'Reilly, C. M., Sharma, S., Gray, D. K., Hampton, S. E., Read, J. S., Rowley, R. J., Schneider, P., Lenters, J. D., McIntyre, P. B., Kraemer, B. M., et al. (2015). Rapid and highly variable warming of lake surface waters around the globe. *Geophysical Research Letters*, 42(24):10–773.
Þorláksdóttir, S. B. and Harðardóttir, J. (2013). Overview of suspended sediment measurements conducted according to traditional contract with landsvirkjun for year 2012. Technical Report SBTh/JHa/2013-01, Iceland Meteorological Office. (In Icelandic: Yfirlit yfir svifaursmælingar sem gerðar voru samkvæmt hefðbundnum svifaurssamningum við Landsvirkjun árið 2012).
Þorláksdóttir, S. B., Óskarsdóttir, S. M., and Harðardóttir, J. (2014). Niðurstöður greininga á styrk og kornastærð svifaurssýna frá austurlandi árin 1998-2013. Technical Report SBTh/SMÓ/JHa/2014-1, Veðurstofa Íslands.
Oswald, C. and Rouse, W. (2004). Thermal characteristics and energy balance of various-size canadian shield lakes in the mackenzie river basin. *Journal of Hydrometeorology*, 5(1):129–144.
Pálsson, S., Harðardóttir, J., Vigfússon, G., and Snorrason, A. (2000). Reassessment of suspended sediment load of river jökulsá á dal at hjarðarhagi. Technical Report OS-2000/070, Orkustofnun – Vatnamælingar. (In Icelandic).
Pálsson, S. and Vilmundardóttir, E. G. (1983). Bergflokkun og eðismassi aurs. Technical Report OS-83016/VOD-01, Orkustofnun - Vatnsorkudeild. (In Icelandic).
Pálsson, S. and Vilmundardóttir, E. G. (2003). Bergflokkun og eðismassi svifaurs.

Technical Report OS-2003/059, Orkustofnun - Vatnamæ lingar. (In Icelandic).
Patterson, J., Hamblin, P., and Imberger, J. (1984). Classification and dynamic simulation of the vertical density structure of lakes. *Limnology and Oceanography*, 29(4):845–861.
Peel, M. C., Finlayson, B. L., and McMahon, T. A. (2007). Updated world map of the köppen-geiger climate classification. *Hydrology and earth system sciences discussions*, 4(2):439–473.
Pickard, G. L. and Emery, W. J. (1990). *Descriptive physical oceanography*. Pergamon Press Oxford.
Pivovarov, A. A. (1973). *Thermal conditions in freezing lakes and rivers*. John Wiley & Sons.
Pond, S. (1975). The exchanges of momentum, heat and moisture at the ocean-atmosphere interface. In *Numerical Models of Ocean Circulation. Proceedings of the Symposium. National Academy of Sciences, Washington DC*, pages 26–28.
Priet-Mahéo, M., Ramón, C., Rueda, F., and Andradóttir, H. (2019). Mixing and internal dynamics of a medium-size and deep lake near the arctic circle. *Limnology and Oceanography*, 64(1):61–80.
Prowse, T. D. and Ommanney, C. S. L. (1990). Northern hydrology: Canadian perspectives. *NHRI science report*.
Rawson, D. (1954). Limnology in the north american arctic and subarctic. *Arctic*, 7(3 and 4):206–212.
Res, B. (2010). Simulation of temperate freezing lakes by one-dimensional lake models: Performance assessment for interactive coupling with regional climate models. *Boreal environment research*, 15:143–164.
Riordan, B., Verbyla, D., and McGuire, A. D. (2006). Shrinking ponds in subarctic alaska based on 1950–2002 remotely sensed images. *Journal of Geophysical Research: Biogeosciences (2005–2012)*, 111(G4).
Roe, P. (1984). Generalized formulation of tvd lax-wendroff schemes. Technical report, NASA Langley Research Center; Hampton, VA, United States.
Rouse, W., Douglas, M., Hecky, R., Hershey, A., Kling, G., Lesack, L., Marsh, P., McDonald, M., Nicholson, B., Roulet, N., et al. (1997). Effects of climate change on the freshwaters of arctic and subarctic north america. *Hydrological Processes*, 11(8):873–902.
Rueda, F. (2001). *A three-dimensional hydrodynamic and transport model for lake environments*. PhD thesis, PhD thesis, University of California, Davis.
Rueda, F. and Cowen, E. (2005). Residence time of a freshwater embayment connected to a large lake. *Limnology and Oceanography*, pages 1638–1653.
Rueda, F. and MacIntyre, S. (2009). Flow paths and spatial heterogeneity of stream inflows in a small multibasin lake. *Limnology and Oceanography*, 54(6):2041–2057.
Rueda, F., Schladow, S., and Clark, J. (2008). Mechanisms of contaminant transport in a multi-basin lake. *Ecological Applications*, 18(sp8):72–88.
Rueda, F. and Schladow, S. G. (2003). Dynamics of large polymictic lake. ii: Numerical simulations. *Journal of Hydraulic Engineering*, 129:92.
Rueda, F. J. and Schladow, S. G. (2002). Quantitative comparison of models for barotropic response of homogeneous basins. *Journal of Hydraulic Engineering*, 128(2):201–213.

Rueda, F. J., Schladow, S. G., and Pálmarsson, S. Ó. (2003). Basin-scale internal wave dynamics during a winter cooling period in a large lake. *Journal of Geophysical Research: Oceans (1978–2012)*, 108(C3).

Rydberg, J., Klaminder, J., Rosén, P., and Bindler, R. (2010). Climate driven release of carbon and mercury from permafrost mires increases mercury loading to sub-arctic lakes. *Science of the total environment*, 408(20):4778–4783.

Sabet, B. and Barani, G. (2010). Design of small gps drifters for current measurements in the coastal zone. *Ocean & Coastal Management*.

Sakai, T. and Redekopp, L. G. (2010). A parametric study of the generation and degeneration of wind-forced long internal waves in narrow lakes. *Journal of Fluid Mechanics*, 645:315–344. Copyright - Copyright © Cambridge University Press 2010; Document feature - ; Last updated - 2011-10-24.

Schindler, D. W. and Smol, J. P. (2006). Cumulative effects of climate warming and other human activities on freshwaters of arctic and subarctic north america. *AMBIO: a Journal of the Human Environment*, 35(4):160–168.

Seppälä, M. (2004). *Wind as a geomorphic agent in cold climates*. Cambridge University Press.

Sheng, Y. P. and Villaret, C. (1989). Modeling the effect of suspended sediment stratification on bottom exchange processes. *Journal of Geophysical Research: Oceans (1978–2012)*, 94(C10):14429–14444.

Shulman, M. and Bryson, R. (1961). The vertical variation of wind-driven currents in lake mendota. *Limnology and Oceanography*, pages 347–355.

Smith, L., Sheng, Y., MacDonald, G., and Hinzman, L. (2005). Disappearing arctic lakes. *Science*, 308(5727):1429–1429.

Smith, P. (2006). Semi-implicit, three-dimensional model for estuarine circulation. Technical report, United States Geological Survey.

Snorrason, S. S., Malmquist, H. J., Ingólfsdóttir, H. B., Ingimundardóttir, Þ., and Ólafsson, J. S. (2011). Effects of geothermal effluents on macrobenthic communities in a pristine sub-arctic lake. *Inland Waters*, 1(3):146–157.

Stefan, H., Hondzo, M., Fang, X., Eaton, J., and McCormick, J. (1996). Simulated long term temperature and dissolved oxygen characteristics of lakes in the north-central united states and associated fish habitat limits. *Limnology and Oceanography*, 41(5):1124–1135.

Stevens, C. and Imberger, J. (1996). The initial response of a stratified lake to a surface shear stress. *Journal of Fluid Mechanics*, 312:39–66.

Striberger, J., Björck, S., Ingolfsson, O., Kjaer, K. H., Snowball, I., and Uvo, C. B. (2011). Climate variability and glacial processes in eastern iceland during the past 700 years based on varved lake sediments. *Boreas*, 40(1):28–45.

Tolmazin, D., Waslenchuk, D., and Herring, J. (1982). Dynamical characteristics from a lagrangian study. In *OCEANS 82*, pages 322–326. IEEE.

Tolvanen, A. and Kangas, K. (2016). Tourism, biodiversity and protected areas–review from northern fennoscandia. *Journal of environmental management*, 169:58–66.

Tómasson, G.G.and Harðardóttir, J. (2001). Kárahnjúkavirkjun: Áhrif á lit lagarfljóts. niðurstöður tilrauna. Technical Report LV-2001/012, VST-2000-0304/08, OS-2001/016, Landsvirkjun, VST, Orkustofnun. (In Icelandic).

Touchart, L. (2005). Typologie des lacs polaires. une démarche de géographie lim-

nologique. *Norois. Environnement, aménagement, société*, 2005/1(194):97–107.

Valerio, G., Pilotti, M., Marti, C. L., and Imberger, J. r. (2012). The structure of basin-scale internal waves in a stratified lake in response to lake bathymetry and wind spatial and temporal distribution: Lake iseo, italy. *Limnology and Oceanography*, 57(3):772–786.

Vidal, J. and Casamitjana, X. (2008). Forced resonant oscillations as a response to periodic winds in a stratified reservoir. *Journal of Hydraulic Engineering*, 134(4):416–425.

Vidal, J., Casamitjana, X., Colomer, J., and Serra, T. (2005). The internal wave field in Sau reservoir: Observation and modeling of a third vertical mode. *Limnology and Oceanography*, pages 1326–1333.

Vidal, J., Rueda, F., and Casamitjana, X. (2007). The seasonal evolution of high vertical-mode internal waves in a deep reservoir. *Limnology and Oceanography*, pages 2656–2667.

Vidal Hurtado, J. et al. (2007). *Basin-scale hydrodynamics in a Mediterranean reservoir. Implications for the phytoplankton dynamics*. PhD thesis, Universitat de Girona.

Vincent, W., Hobbie, J., and Laybourn-Parry, J. (2008a). Introduction to the limnology of high-latitude lake and river ecosystems. In Vincent, W. and Laybourn-Parry, J., editors, *Polar lakes and Rivers: Limnology of Arctic and Antarctic Aquatic Ecosystems*, volume 1st, pages 1 – 18. Oxford University Press.

Vincent, W. F., MacIntyre, S., Spigel, R. H., and Laurion, I. (2008b). The physical limnology of high-latitude lakes. In Vincent, W. F. and Laybourn-Parry, J., editors, *Polar Lakes and Rivers. Oxford University Press, New York, NY*, pages 65–81. Oxford University Press, New York.

VST (2001). Kárahnjúkar hydropower station - temperatures of lake lagarfljót. Technical Report LV-2001/011, Landsvirkjun. (In Icelandic).

Wain, D. J., Gall, M. P., Cooper, M. J., Payet, J. P., Maher, D., Galí, M., Robins, P. E., Pace, M. L., Ryan-Keogh, T. J., Ochs, C. A., et al. (2013). Internal wave-driven transport of fluid away from the boundary of a lake. *Limnology and Oceanography*, 58(2):429–442.

Walling, D. and Webb, B. (1986). Solutes in river systems. *Solute processes*, pages 251–327.

Watson, R. T., Zinyowera, M. C., and Moss, R. H. (1996). Ipcc second assessment report: Climate change 1995. impacts, adaptations and mitigation of climate change:scientific-technical analyses. contribution of working group ii to the second assessment report of the intergovernmental panel on climate change. Technical report, IPCC.

Watson, R. T., Zinyowera, M. C., and Moss, R. H. (1998). *The regional impacts of climate change: an assessment of vulnerability*. Cambridge University Press.

Wetzel, R. (1983). *Limnology*, volume 767. Saunders Philadelphia.

Wiegand, R. C. and Carmack, E. C. (1986). The climatology of internal waves in a deep temperate lake. *Journal of Geophysical Research: Oceans (1978–2012)*, 91(C3):3951–3958.

Williamson, C. E., Saros, J. E., Vincent, W. F., and Smol, J. P. (2009). Lakes and reservoirs as sentinels, integrators, and regulators of climate change. *Limnology and Oceanography*, 54(6):2273–2282.

Winterwerp, J. (2001). Stratification effects by cohesive and noncohesive sediment. *Journal of Geophysical Research: Oceans (1978–2012)*, 106(C10):22559–22574.

Woo, M.-K. and Winter, T. C. (1993). The role of permafrost and seasonal frost in the hydrology of northern wetlands in north america. *Journal of hydrology*, 141(1-4):5–31.

Wüest, A. and Lorke, A. (2003). Small-scale hydrodynamics in lakes. *Annu. Rev. Fluid Mech*, 35:373–412.

Yoshimura, S. (1936). A contribution to the knowledge of deep water temperatures of japanese lakes. part i. summer temperatures. *Jap. J. Astr. Geophys*, 13:61–120.

A Comparison of the meteorological forcing measured along the lake

Hallormsstaður weather station is the weather station closest to the southern end of the lake. However, its location in the heights and close to a forest, suggests that the wind and temperature measurements are not the most appropriate to describe the conditions at the lake level. A weather station was installed at the southern end of Lake Lagarfljót (Figure A.1) in August 2011 at (UTM 28 W - 507509, 7216375) and was retrieved the summer after in August 2012 measuring weather data during almost an entire year.

A.1 Summary of the data collected

The weather station measured different parameters at a 10 min interval : precipitation (mm), air temperature (°C), humidity (%), wind speed (m/s) and direction (°) and the atmospheric pressure (mbar). It recorded in addition the voltage of the battery.

Using software Hoboware pro, the dataset is filtered to obtain hourly averages in order to compare it with the data from the weather stations at Egilsstaðir Airport and Hallormsstaður delivered by the Icelandic Meteorological Office.

The wind speed was collected at 3 m height hence in order to compare it appropriately with the other data set, the wind speed needs to be corrected. The general relationship that is considered valid up to 20 m height

$$\frac{U_{10}}{U_z} = (\frac{10}{z})^{1/7}$$

as described in Engineers (1984) and Johnson (1999). The 1/7 power expression was tested and its use is considered appropriate in Iceland for this kind of elevation differences (Blöndal et al., 2011).

A.2 Comparison with station at Hallormsstaður

Figure A.2 shows a really good linear relation between the temperature recorded at the new station called Brú and the station at Hallormsstaður. The correlation coefficient is very high (R=0.9863). The temperatures at Hallormsstaður are about 0.25 °C colder which is coherent with the altitude of the station (60 m above the sea level) while the station at Brú is approximately at 28 m above the sea level (GPS estimate).

Figure A.3 presents the relationship between the wind speed at Hallormsstaður

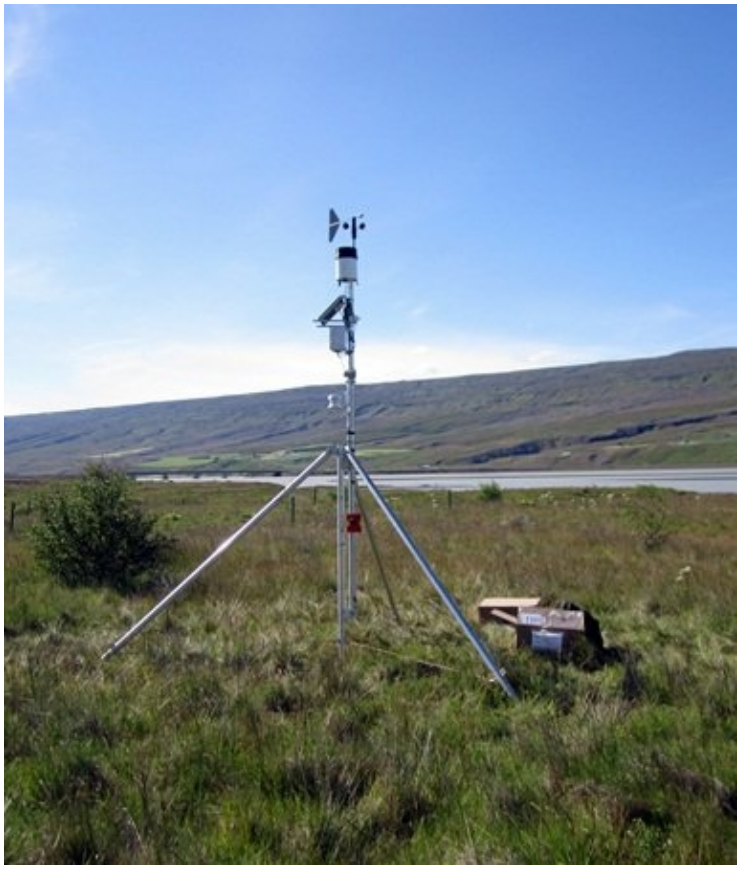

Figure A.1. Temporary weather station installed close to the southern end of the lake from August 2011 to August 2012

and Brú. It appears that the wind speed at Hallormsstaður is significantly lower (by a coefficient of 0.41) than at Brú, the correlation coefficient is rather low (R=0.6420). Correcting the data in order to have the wind speed along the main axis of the lake (Figure A.4) , we obtain a simpler linear relationship which can be approximated to y=0.41x and much better correlation of the data (R=0.8302), suggesting that the shift in wind direction at Hallormsstaður is significant.

A.3 Comparison with station at Egilsstaðir Airport

Figure A.5 shows that the temperature at Egilsstaðir airport are almost half a degree colder than at Brú (R=0.9755). The station being at approximately at the same altitude (23 m above sea level), the main explanations for this shift can be the location further south of the station and the Foehn effect.

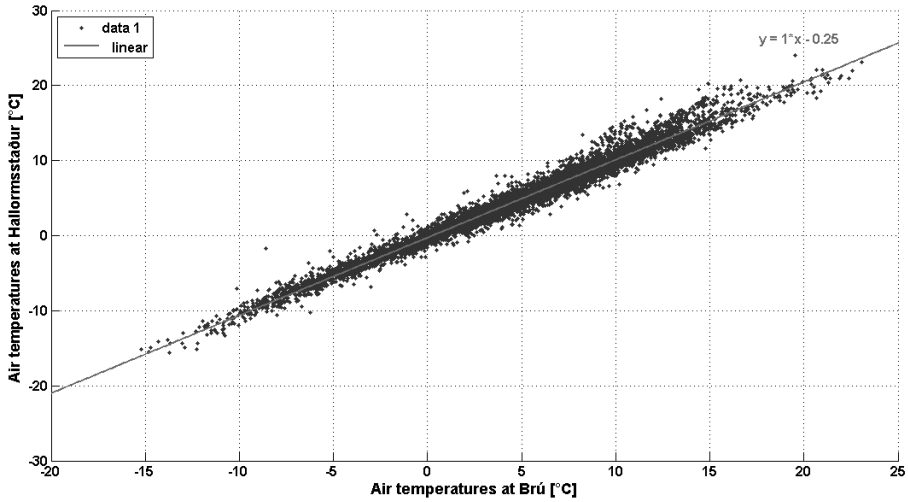

Figure A.2. Air temperatures measured at Hallormsstaður against the air temperature measured by the station at Brú.

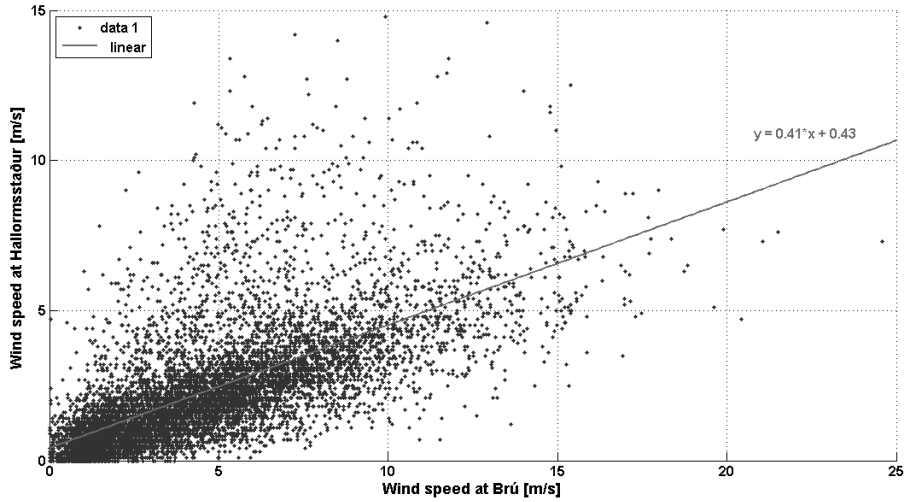

Figure A.3. Wind speed measured at Hallormsstaður against the wind speed measured by the station at Brú.

Figure A.6 presents the relationship between the wind speed at Egilsstaðir airport and Brú. The correlation coefficient is rather low (R=0.6493) and the y-intercept value is high, meaning that the relationship between the two locations is complex. It is however still possible to say that the wind speed is lower at Egilsstaðir airport than at Brú.

Correcting the wind speed with the wind direction in order to get the wind speed

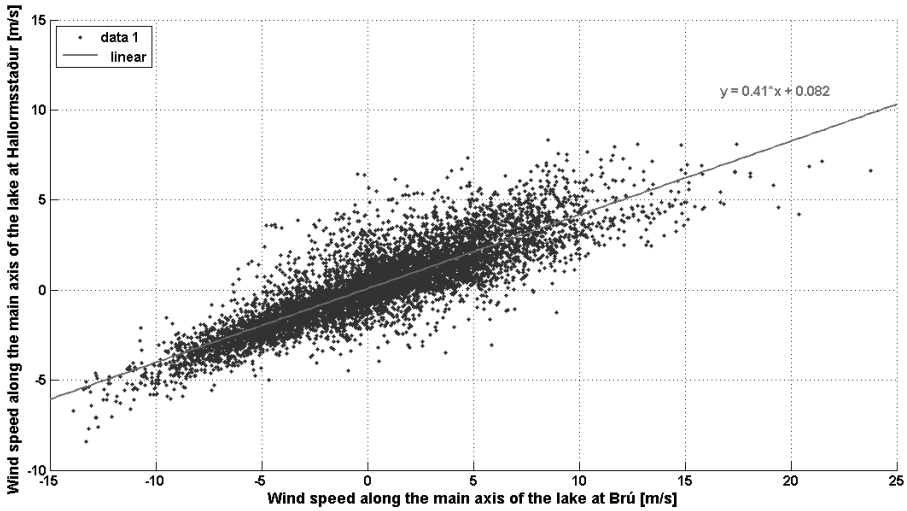

Figure A.4. Wind velocity along the main lake axis at Hallormsstaður against the wind velocity along the main lake axis at Brú.

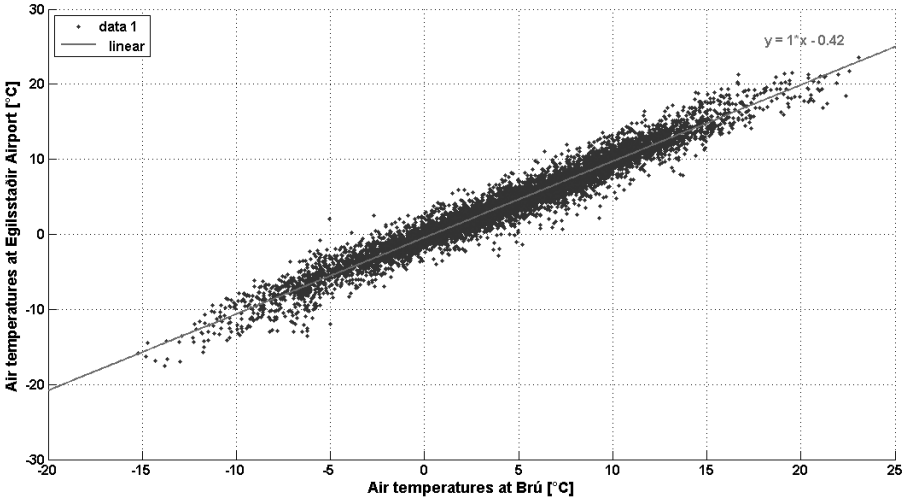

Figure A.5. Air temperatures measured at Egilsstaðir airport against the air temperature measured by the station at Brú.

along the lake, we obtain a better linear relationship between the measurements at the two stations (R=0.7527) with a lower value, yet still significant, for the y-intercept.

These comparisons shows that the weather station at Hallormsstaður underestimates the temperatures (slightly) and the wind speed over the lake basin. It also shows that Egilsstaðir is not representative of the weather over the entire lake.

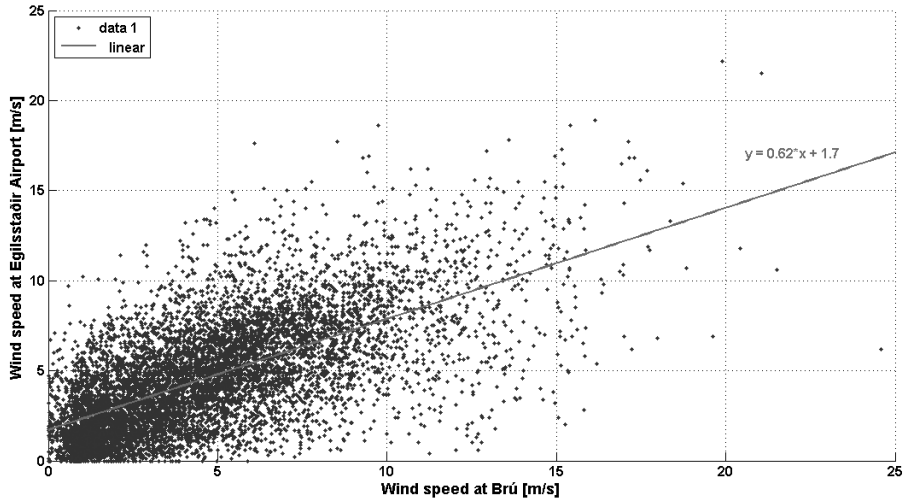

Figure A.6. Wind speed measured at Egilsstaðir airport against the wind speed measured by the station at Brú

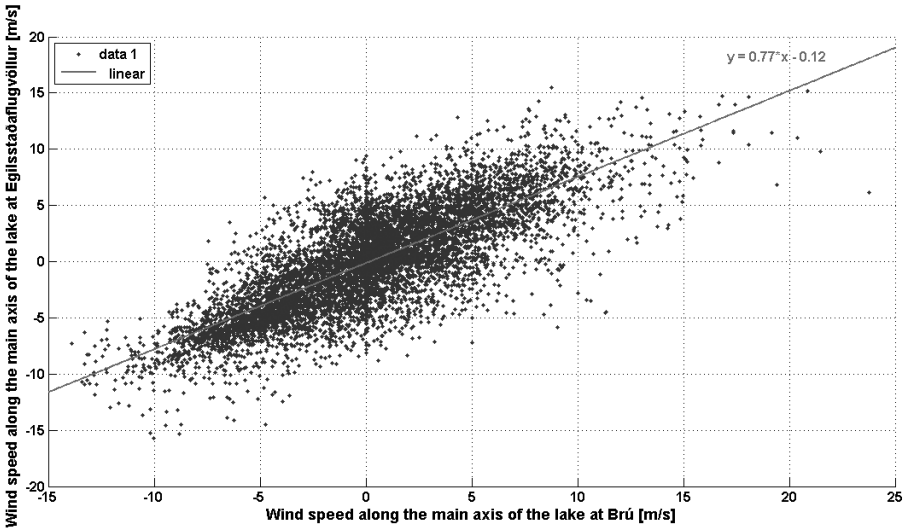

Figure A.7. Wind velocity along the lake main axis at Egilsstaðir airport against the wind velocity along the main at Brú.

B ADCP measurements and drogue studies

Current measurements can provide precious information on the internal circulation of the lake, traditional current profiler measurements were performed to see what we can learn from them. However Lake Lagarfljót's waters are so turbid that measurements with a traditional current profiler are limited. For that reason an additional unattended drogue experiment was also Carried out (see C) during summer 2011. The results for both procedures are presented in this Appendix.

B.1 Bottom currents

Near-bed current velocities were measured with a Nortek Aquadopp Current Profiler (ADCP) in the shallower northern basin. Due to the high turbidity of the lake waters, the ADCP was operated in high resolution mode (1–5 cm vertical resolution). This instrument measured 3D velocity profiles within the first 3 meters above the bed (with an accuracy of 1% of the value for a product of the profiling range and velocities inferior to $5 m^2/s$) as well as water temperature, pressure, tilt, and compass information for 4 weeks at a time. The instrument was attached on a three-footed Y-shaped platform designed to stay as close to the bottom as possible without sinking into the mud. For retrieval purposes, two surface floating lines with buoys were connected.

A first deployment took place the 10^{th} of July 2010 ; the second deployment was organized the 9^{th} of August, both nearby LAG03 station. In summer 2011, the ADCP was deployed during the month of August nearby LAG04 thermistor chain.

Bottom water currents - results

Figure B.8A presents the angle histograms of water currents measured within the first three meters above the bottom during August 2010 (left panel) and 2011 (right panel). Both measurement sessions were taken in the shallow northern basin at 42 and 39 meters depth. In 2010, the ADCP was deployed at LAG03, station located on the edge of the sill. In 2011, however, it was located at LAG04, further away from the sill in the smallest basin (2.1). In both deployments, the majority of the currents aligned with the lake axis (240°and 195°).

For analysis purposes, velocities and speeds of the bottom current along the lake axis will be considered from now on. Figure B.8B shows the time-averaged speeds within the bottom 3 meters. The thickness of the bottom boundary layer is on the order

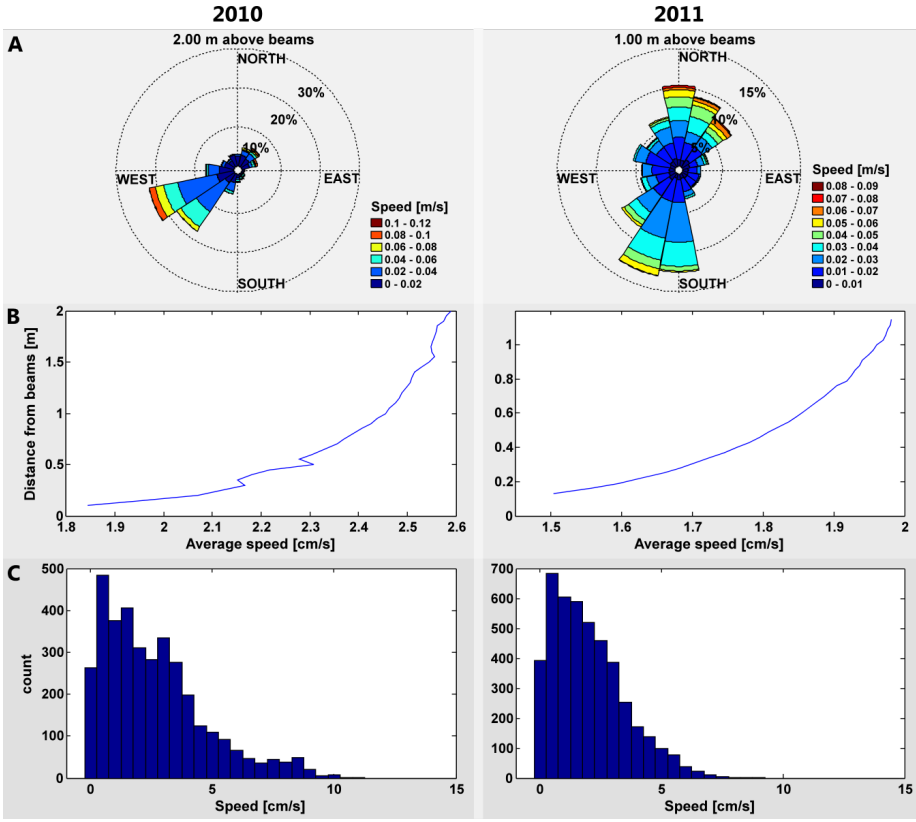

Figure B.8. Analyses of the current measurements by the ADCP in August 2010 (left) and 2011 (right) : A) angle histograms of water currents, B) time-averaged speeds within the bottom 3 meters and C) distribution of current speeds at 2 m above the bottom

of 2 m. Figure B.8C shows that the near-bottom speeds at 2 m above bottom (outside the boundary layer) have a log-normal distribution with a mode around 0.5 cm/s. In 2010, few occurrences of speeds exceeding 10 cm/s per second were observed, in 2011 none of the speeds recorded exceeded 9 cm/s.

In Figure B.9 A to C, the longitudinal and lateral bottom current velocities are plotted along with the longitudinal wind velocities and the water temperatures measured at the nearest station, LAG03 in 2010 and LAG04 in 2011. The longitudinal component of the current velocity is positive when going S-SW and oscillates from positive 5 cm/s to negative 4.6 cm/s in 2010, and slightly lower in 2011, which was a less stratified season (Figure 2.8). The range of the lateral component of the current velocity was not negligible, it was from 1.6 to -3.6 cm/s in 2010 and 1.9 to -2 cm/s in 2011, positive when going W-NW. While in 2010 the longitudinal and lateral component of the bottom current were fairly in-phase, in 2011, at LAG04, they are almost exactly 180°out-of-phase and with similar amplitudes.

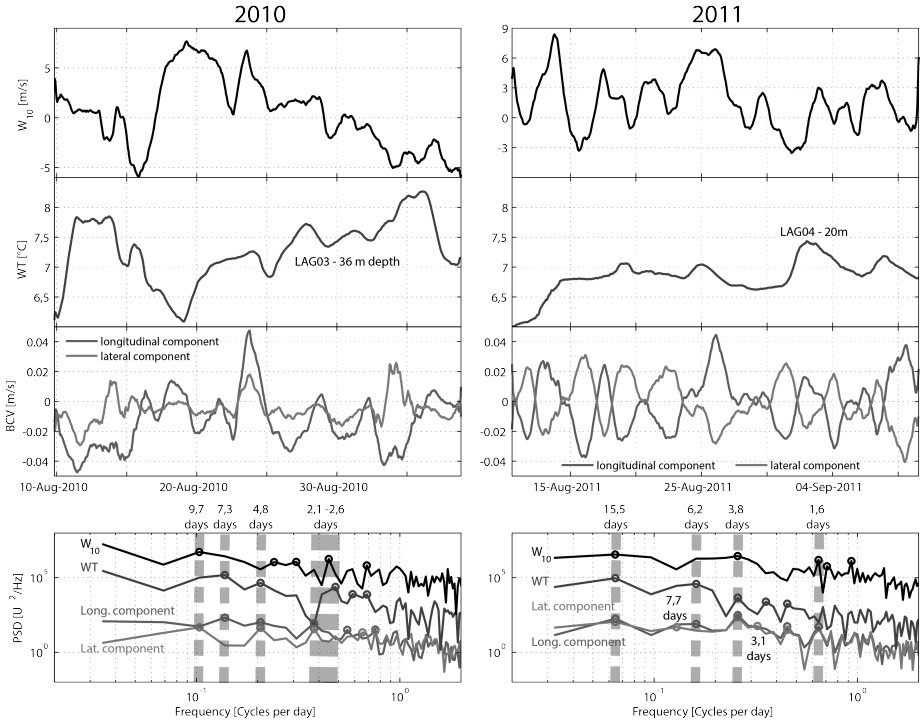

Figure B.9. Time series of synchronous A) longitudinal wind velocities (W_{10}), B) water temperatures (WT) and C) bottom current velocities (BCV) with D) associated spectral plots in 2010 (left) and 2011 (right).

The spectral analysis of these four variables (Figure B.9D) suggests that, in 2010, the main modes of oscillations of the bottom currents and water temperatures had periods of 7.3 and 4.8 days corresponding to the previously mentioned modes calculated for the entire season on Figure 2.12A. The main mode for the wind for August only is 9.6 days which corresponds to the main oscillation period of the lateral component of the current and is twice the time of the second main mode of oscillation of the other variables. The third mode of oscillation of the bottom velocities had a period of 2.6 days, matching closely the 2.1 and 2.2 days periods of the temperature and wind respectively. A good match is observed for higher order modes as well.

The spectral analysis for 2011 shows generally also a good match between the four variables. However, the main peaks of oscillations are slightly different, in particular most energy was associated with synoptic 15 days period. Subharmonics of the main periods are found for the four variables.

The spectra of the lateral current are very similar to the ones of the longitudinal current, particularly in 2011, supporting the observations made from Figure B.9C and suggesting that internal waves do not necessarily travel straight up and down the long axis of the basin.

In August 2010, lags between the wind and the current signals were estimated to be

around 2 days while the lag between the current and the water temperature signal were found to be around 0.6 and 1.3 days, the later corresponds to a fourth of the second and third modes of oscillations, as theory would predict. In 2011, the time lag between the wind and the current signals were slightly shorter, from 1 to 2 days. The time delay between the current and the water temperature were longer, from 2.5 to 3 days, corresponding to the strong synoptic signal.

Overall, the good correspondence between wind, water temperatures and bottom currents are evidence that wind-driven internal waves in weakly stratified lakes generate substantial bottom currents.To give an idea, the near bottom longitudinal displacements can be on the order of 15 km over a time-span of 5 days. The mean residence time of the lake, however, is 0.5 year. Hence it is clear that internal waves dominate the circulation in the lower portion of the lake, and that the lake is much more dynamic than just considering through-flows.

B.2 Drogue study

Tests were made to use drogues to track currents in the lake epilimnion (within the 15 m top meters) to complement the measurements made at the bottom by the ADCP. The methodology employed is described in appendix C. Measurements were performed on day 222 and 223 (August 2011), over period of 8 hours. The three drogues (two with sail at 5 m and one at 15 m depth) were released in the two basins, on either side of the sill : near station LAG03, on the northern end of the deepest southern basin on day 222 and near station LAG04, on the southern end of the northern basin on day 223 (Figure C.11). The sail at 15 m and a sail at 5m were released near the thermistor stations in the center, while a sail at 5 m depth was released further towards the western edge of the basins.

The patterns appearing from these measurements are very different in the two basins. While in the northern basin the trajectories are parallel and follow the lake axis toward the North East, in the southern basin the sails at 5m depth are dragged towards the south in a counterclockwise-like motion, while the sails at 15 m is traveling shortly towards the north.

C Use of the new technology in the field : new perspectives introduced by the android technology

Limnology is heavily based on field work which is a very costly part of the research. It is costly in time but also costly in terms of equipment. When preparing the field season the cost and the use of the instruments are taken into account. Can the budget afford a tool, very specialized but that might be used only over a season or even a field trip?

To study currents in lakes, several methods have been developed. Point (Eulerian) measurements are most commonly performed with Acoustic Doppler Current Profiler (ADCP), current meters and high frequency radars. These methods allow continuous measurements. The ADCP can measure current speed and direction at many depths simultaneously, while the current meter and the high frequency radar can only measure them respectively at a specific depth and at the surface. These measurements require expensive equipments. Path (Lagrangian) measurements are cheaper and more flexible. Tracers (for example dyes) are sometimes used to define the flow path, observations and water analyses help quantifying the diffusion and advection processes. Surface or subsurface drogues/drifters which follow the flow are also used to characterize lakes' circulation. Different setups have been tested to determine the location of the drogues over time and facilitate their retrieval.

The earliest drogues studies were relying on observations with a compass and taffrail log (Shulman and Bryson, 1961), sextants (Tolmazin et al., 1982) or a simple stopwatch and visual estimations Hughes (2002). Recent works have been focusing on developing the tracking system and facilitating the retrieving process in order to reduce the time spent during these operations as well as the cost linked to the loss of the equipment. GPS drogues (GPS combined with a logging system) are now widely used (Hopping and Smith, 2002; Sabet and Barani, 2010). Radio transmitters (Austin and Atkinson, 2004; Johnson et al., 2003; Manley, 2010) are used to ease the retrieving process. GPS technology is improving rapidly. Small, low-cost devices are now available, however their applications are often intended for touring purposes and lack flexibility (recording frequency, variable recorded). Radio transmitters present also some limitations in terms of range of transmission, hence an antenna 3 m above the water level allows a 10 km range of transmission (Johnson et al., 2003) while a simple wind wave can disturbed the communication with a normal antenna, and the radio unit integrated in the Garmin Rino 110 has a range limited to 0,75 miles (approximately 1,2 km) (Austin and Atkinson, 2004). The cost for the drifters equipped with both a logging system and a transceiver have a cost superior in all cases to $ 200 and in the case of a good radio transmission it exceeds $ 600.

The GPS technology is now spreading in everyday accessories such as hand-held cellular phones. With the development of the android operating system, gadget phones can be turned into real field equipment and open new perspectives of communication and transmission, replacing all at once the GPS receiver, the data logger and the transceiver.

In this paper, we describe how we used some LG Optimus One phones in a project of unattended drogue study in a first part, in a second part, we discuss the first results obtained and present possible improvements.

C.1 Methods

The ANDROID operating system has been developed for mobile devices such as mobile phones. This operating system is open source (as opposed to the Iphone operating system iOS) allowing users to create their own programs using the functionalities of the phone, including various captors such as GPS, pressure sensors, thermometers, etc. . Many fully functional programs are available though Google Market, many of them free. Some of these ready-made programs have features which are usable for field work but most have additional features that are, in the best case, left unused and, in the worst case, put unnecessary load on the operating system and the phones resources. The access to the source code of the operating system makes it possible to create programs that respond directly and only to our needs, limiting the memory use and battery consumption. Softwares are programmed in Java using the Android Software Development Kit but also in C/C^{++} language with the Native Development Kit. The Google App Inventor can be used by novice programmers.

Three Android phones LG Optimus One, chosen for their light weight (129 gr), battery life (700 h at rest, 8h in use), operating system (Android O.S. 2.2 - Froyo , then one of the newest version), their memory (built-in memory 170 MB and 2 GB memory card) and of course moderate cost (about US$ 200 at the time of this article), were selected for that purpose. A fourth (android) phone is used to communicate with these three phones.

Two programs were made and one acquired from the Android Market. The main program was designed in order to record the time, the coordinates of the location, the accuracy of the measurement at regular predefined intervals and write to a file on the SD-card. In order to save battery the phone is programmed to hibernate in between the measuring periods.

A second program is monitoring the state of the phone battery and sends an alarm message via SMS if the battery level goes below a predefined level to make sure that the phones are retrieved before they go out of battery. The program also answers to a predefined keyword sent to the phone via SMS and responds with another SMS containing the battery level.

Finally a third program from the Android Market (Where is my Droid) allows communication between the deployed phones and the fourth android phone for retrieving purposes; it answers to a keyword sent by SMS and sends back the current location coordinates as well as a link to Google Maps. The two last programs use the mobile phone network (GSM) to communicate with the outside world using ordinary SMS

messages.

Before using the phones on the field their battery life and GPS accuracy are tested. The hibernation system enabled the phones to record data over 24 hours without getting out of battery. The phones were placed in their compartments on a rooftop to decrease shadowing as much as possible during the 3h long recording. The UTM coordinates of the precise location is subtracted from the location measured by the phones, in order to see better the accuracy given by the gps unit.Figure C.10a shows all the fixes with the best accuracy for each measuring sequences, Figure C.10b shows what the programs keeps and write on the file, the first fix with the best accuracy. By taking around 9 GPS measurements at each measuring period and keeping the one with the best accuracy, we succeeded to get a good approximation of the location: in fact, location accuracies (Circular Error Probable) were found to be systematically inferior to 7m, with most of the time a value of 5m and down to 3m . As a matter of comparison, Garmin announces an accuracy for its Rino Series inferior to 15 m 95% of the times (GARMIN, 2003), which corresponds to an accuracy (CEP) equal to 6,25m .

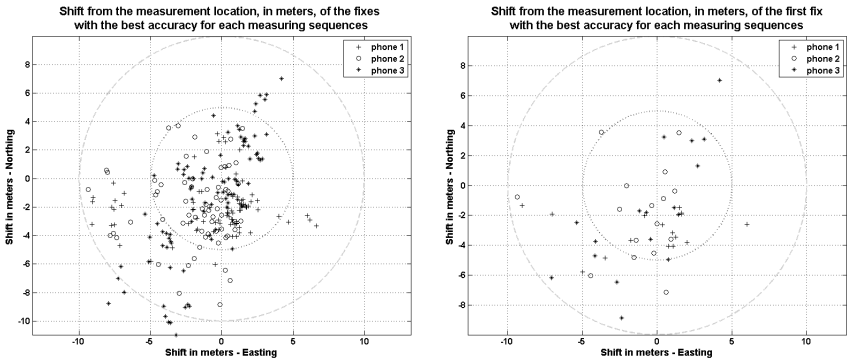

(a) Fixes with best accuracy *(b) Fixes selected by the program*

Figure C.10. Test runs of the phone to estimate the accuracy of the instruments. The inner circle corresponds to the CEP for 5m accuracy

All non-essential features, programs and services are turned of, such as back-lighting for the screen, Internet access etc. to extend the lifetime of the battery. The three phones were set in waterproof compartments on top of the buoys connected to the drogues sails. At the deployment the logging software is started. Distance monitoring through the fourth phone allowed to keep track of those throughout the measurement days. The phones are retrieved very simply thanks to a direct link to Google map locating them on the lake.

C.2 Results and discussion

This use of android phones on drogues was tested two days in a row during summer 2011 at two different locations in lake Lagarfljót, NE Iceland.

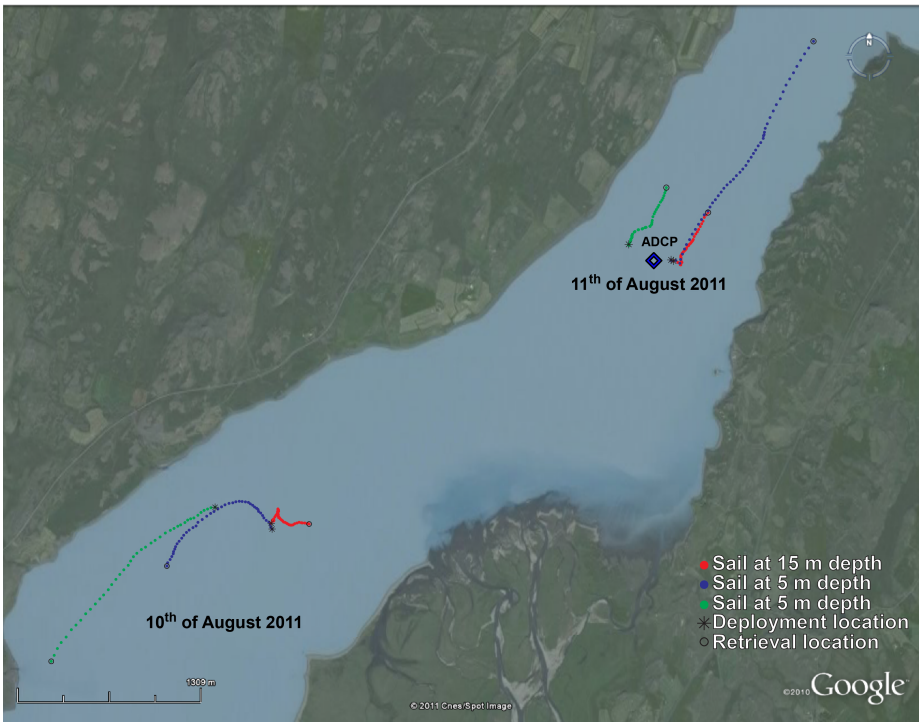

Figure C.11. Trajectories of the sails during the two measurement days

Two sails at 5m and 15m were released at a central location, while a third sail at 5 m was released on the side of the lake. It was possible to keep tracks of them through out our day of measurements. The second day, the sails were deployed near by the Acoustic Doppler Current Profiler (ADCP) measuring currents at the bottom of the lake (40 m depth at that location).

After about 8 hours on the water the phones have their battery 81 to 87 % full. The three phones gave really good results with a recording approximately every 10 minutes, and a accuracy of $\pm$ 5 m.

Comparing the speeds (Figure C.12) recorded by the phones (mean speeds 0,0186 m/s at 15m depth and 0,0538m/s at 5m depth) to the speed recorded by the ADCP at the bottom of the lake (mean speed 0,0239m/s), we can see that the results are in the same order of magnitude.

The operation was a success. This method provides results with an as good accuracy as other methods using low-cost GPS. It uses unspecific tools and is therefore inexpensive, since the receiver can be a personal phone and these phones can later on be used

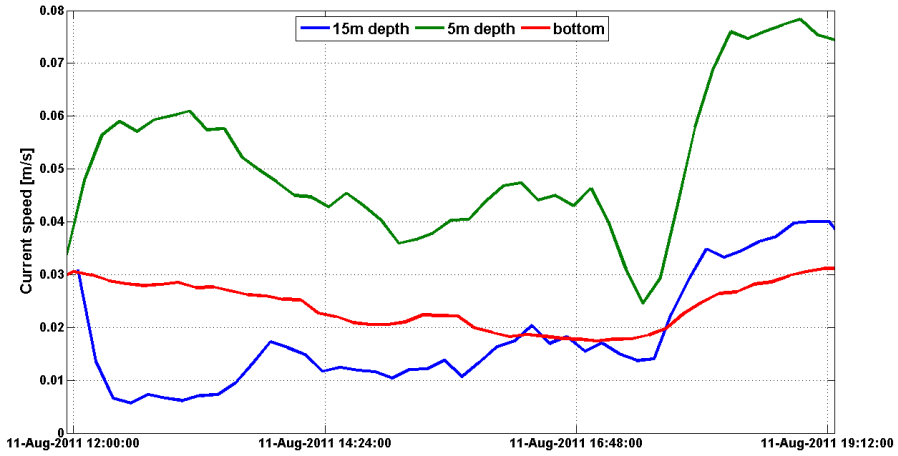

Figure C.12. Comparison of the speeds recorded by the phones and the ADCP the 11th of August 2011

for other projects. The flexibility of their operating system enables the programmer to limit the battery use by suppressing all superficial functionalities and limit the programs to strictly necessary operations, hence it has appeared that measurements could be taken over more than 24 hours. With sizes of file of the order of few kilobytes, the memory (>2 gigabytes) is not an issue.

However, it requires a sufficient phone network coverage and the phones needs to be able to send sms, so some additional subscription costs may have to be considered. In our case, the phones could communicate for free between each others, having a sim card from the same phone company.

Other improvements could be implemented for next deployment, such as a alarm system if the drogue approach a delimited area (for example the outflowing river) or if it gets stranded. These implementations would allow a longer unattended measurement period.

In the case where battery life is not a problem and in an area with good mobile network coverage, it could be feasible to use the Internet connection of the phones to send the location and other data as a life stream to a central computer.

C.3 Conclusion

The use of Android phone to track drogues has proven to be a very efficient low-cost solution. The accuracy of data collected is in the same order as the accuracy for low-cost GPS, such as the GARMIN Rino. The transmission range is not limited as long as the GSM network is decent. Future developments could permit longer unattended recording periods.

D Field measurements: photographs

Figure D.13. Preparation of the Niskin for deep water sample collection - January 2011

Figure D.14. Water samples collected in August 2011.

Figure D.15. Tributaries of Lake Lagarfljót - July 2011

Figure D.16. Drogues, deployment and retrieval - summer 2011